Asymmetries in top quark pair production at hadron colliders

J.A. Aguilar-Saavedra

Departamento de Física Teórica y del Cosmos,
Universidad de Granada,
E-18071 Granada,
Spain.
PH-TH Department, CERN,
CH-1211 Geneva 23,
Switzerland.

D. Amidei

Department of Physics,
University of Michigan,
Ann Arbor, MI 48109,
USA.

A. Juste

Institució Catalana de Recerca i Estudis Avançats (ICREA),
E-08010 Barcelona,
Spain.
Institut de Física d'Altes Energies (IFAE),
E-08193 Bellaterra, Barcelona,
Spain.

M. Pérez-Victoria

Departamento de Física Teórica y del Cosmos and CAFPE,
Universidad de Granada,
E-18071 Granada,
Spain.

We review the asymmetries in top quark pair production at the Tevatron and the LHC. We summarize the experimental measurements and the interpretations of a possible excess in terms of new physics. We also review other top quark properties—emphasizing effects related to the $t\bar{t}$ asymmetries—as well as other collider signals.

CONTENTS

I. INTRODUCTION

Precision tests of the production and decay modes of elementary particles have proved to be of great help to extend our knowledge of the forces that govern their interactions, and search for new physics. The role of e^+e^- colliders, such as the CERN Large Electron Positron (LEP) collider, has been fundamental in this task (Schael *et al.*, 2006). Hadron colliders, which are usually regarded as discovery machines, offer complementary precision measurements that further test the standard model (SM) of elementary particle interactions. This is indeed the case for the physics of the top quark, which was discovered at the Fermilab Tevatron $p\bar{p}$ collider (Abachi *et al.*, 1995; Abe *et al.*, 1995). The relative ease to identify top quarks in a hadronic collider environment and the large samples produced, not only at the Tevatron but also at the CERN Large Hadron Collider (LHC), have allowed to perform several precision measurements of its properties. In most cases a good agreement has been obtained with the predictions of the SM. However, a notable exception has been found in several forward-backward (FB) asymmetries, often also referred to as charge asymmetries, in top quark pair ($t\bar{t}$) production at the Tevatron. Experimentally, these asymmetries are conveniently defined in terms of the rapidities of the top (anti-)quark and their decay products in the laboratory frame, where the rapidity of a particle is given by

$$y = \frac{1}{2} \log \frac{E + p_z}{E - p_z}, \qquad (1.1)$$

with E its energy and p_z the component of its three-momentum in the $\hat{z}$ axis, taken here in the proton direction. The largest deviations were found in the so-called $t\bar{t}$ rest-frame FB asymmetry,

$$A_{FB} = \frac{N(\Delta y > 0) - N(\Delta y < 0)}{N(\Delta y > 0) + N(\Delta y < 0)}, \qquad (1.2)$$

with $\Delta y = y_t - y_{\bar{t}}$ and N standing for the number of events.[1] The discrepancy between experimental data and the SM predictions surpassed three standard deviations in the 2011 CDF measurement of A_{FB} at high $t\bar{t}$ invariant mass $m_{t\bar{t}} \geq 450$ GeV (Aaltonen *et al.*, 2011a), with roughly 5 fb^{-1} of data taken at a centre-of-mass (CM) energy $\sqrt{s} = 1.96$ TeV. Deviations were found in the inclusive asymmetry too, and also by the D0 experiment (Abazov *et al.*, 2011a). This anomaly motivated

intense research in model building—invoking new physics in $t\bar{t}$ production as the explanation for the anomaly—as well as the update of the SM calculations. Since then, it has also fostered the theoretical and experimental search of other anomalies in $t\bar{t}$ production, which might appear if the Tevatron asymmetry were indeed a sign of new physics. Among the latter, the charge asymmetry at the LHC has a prominent role. Close to the end of Tevatron operations, in 2011 the LHC began taking data in pp collisions at $\sqrt{s} = 7$ TeV, quickly producing large $t\bar{t}$ samples. However, in pp collisions a FB asymmetry with a fixed $\hat{z}$ axis, such as the one defined in Eq. (1.2), vanishes due to the symmetry of the initial state. Instead, a "forward-central" charge asymmetry can be defined,

$$A_C = \frac{N(\Delta|y| > 0) - N(\Delta|y| < 0)}{N(\Delta|y| > 0) + N(\Delta|y| < 0)}, \qquad (1.3)$$

with $\Delta|y| = |y_t| - |y_{\bar{t}}|$, which is a complementary probe of asymmetric $t\bar{t}$ production. (The precise meaning of this statement will be clear in the following section.) Noticeably, the measurements of this asymmetry performed by the ATLAS and CMS Collaborations at $\sqrt{s} = 7$, 8 TeV (Aad *et al.*, 2014b; Chatrchyan *et al.*, 2012, 2013b, 2014c; **?**) are in good agreement with the SM predictions. These results, although not conclusive because the measurements refer to an observable that differs from the Tevatron one, call into question the Tevatron excess. Concurrently, when the full Tevatron dataset of around 10 fb^{-1} has been analyzed, the discrepancies have been reduced with respect to previous results. The CDF Collaboration finds a 1.7σ excess over the SM predictions (Aaltonen *et al.*, 2013c) whereas the D0 Collaboration finds agreement within 1σ (Abazov *et al.*, 2014c). Other asymmetries can also be constructed using the momenta of charged leptons ℓ produced in the top quark decay $t \to Wb \to \ell\nu b$. The Tevatron measurements (Aaltonen *et al.*, 2013b, 2014b; Abazov *et al.*, 2013b, 2014b) are above the SM values too, whereas leptonic asymmetries measured at the LHC are consistent with the SM.

This review attempts to provide a self-contained description of the current status of theoretical and experimental research on the subject of the $t\bar{t}$ asymmetries, paying also special attention to other observables that further test the presence of new physics in $t\bar{t}$ production. The $t\bar{t}$ asymmetries, their interrelation and the SM predictions are reviewed in detail in Sec. II. The current experimental status of asymmetry measurements at the Tevatron is presented in Sec. III. Measurements at the LHC are reviewed in Sec. IV, where prospects for the next run with 14 TeV are also discussed. In Sec. V we give an overview of the new physics proposals to address the Tevatron anomaly. We address the correlated effects in $t\bar{t}$ production of these new physics proposals in Sec. VI, and other collider effects are briefly discussed in Sec. VII. Finally, conclusions are outlined in Sec. VIII.

---

[1] The denomination for this asymmetry stands for the fact that A_{FB} is the same when the t and $\bar{t}$ rapidities are taken in the $t\bar{t}$ rest frame, and in this frame $\Delta y = 2y_t$. Therefore, a "forward" event with the top quark following the proton direction in the $t\bar{t}$ rest frame has $\Delta y > 0$ and, conversely, a "backward" event has $\Delta y < 0$.

II. OVERVIEW OF THE ASYMMETRIES

A. The Tevatron $t\bar{t}$ asymmetry

At the Tevatron, top quark pairs are produced mainly in the partonic subprocesses $q\bar{q}, gg \to t\bar{t}X$, with $q = u, d$ and X denoting possible additional jets. (In this section we explicitly indicate with X the possibility of extra jets, to emphasize the different sources of the inclusive asymmetry; this will be omitted for simplicity in the following sections.) Within the SM, the main contribution to the asymmetry (1.2) arises at next-to-leading order (NLO) in QCD due to the interference of order α_s^3 terms in the cross section that are odd under the interchange $t \leftrightarrow \bar{t}$ with the initial quarks fixed—hence the denomination of A_{FB} as "charge asymmetry", despite the fact that it does not have any relation with the charge conjugation symmetry C. The interference of tree-level and one-loop diagrams for $q\bar{q} \to t\bar{t}$, Fig. 1 (a,b), generates a positive asymmetry, while the interference of initial- and final-state radiation in $q\bar{q} \to t\bar{t}g$, for example diagrams (c,d) in Fig. 1, generates a negative asymmetry (Kuhn and Rodrigo, 1998). The relative size of these contributions depends on the transverse momentum of the $t\bar{t}$ pair, $p_T^{t\bar{t}}$, which is zero in $q\bar{q} \to t\bar{t}$ but not in $q\bar{q} \to t\bar{t}g$. It is found that for $p_T^{t\bar{t}} \lesssim 25$ GeV the asymmetry is positive, while for $p_T^{t\bar{t}} \gtrsim 25$ GeV it is negative. When integrated over the full $p_T^{t\bar{t}}$ spectrum, the net contribution to (1.2) is positive. An alternative way of explaining the $p_T^{t\bar{t}}$ dependence involves QCD radiation (Skands *et al.*, 2012). For forward top quarks the color charge is less accelerated, so they are less likely to emit gluons than backward top quarks. Hence, forward top quarks are associated with smaller $p_T^{t\bar{t}}$, and vice versa.
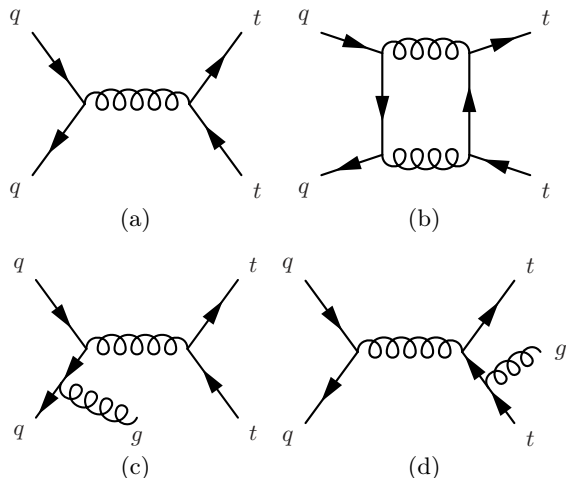

FIG. 1 Sample Feynman diagrams contributing to $q\bar{q} \to t\bar{t}$ at leading order (LO) (a) and NLO in QCD (b,c,d).

The asymmetry generated in $q\bar{q} \to t\bar{t}X$ is diluted by the $gg \to t\bar{t}$ subprocess, which amounts to 10% of the total cross section and does not contribute to the numerator of A_{FB} because of the symmetry of the initial state. Other quark subprocesses like $s\bar{s}$, $c\bar{c}$ do not contribute either because the parton density functions (PDFs) are the same for quarks and antiquarks. They have small cross sections, and do not significantly contribute to the denominator either. For completeness, let us mention that the Tevatron experiments also measure the so-called laboratory-frame asymmetry,

$$A_{FB}^{p\bar{p}} = \frac{N(y_t > 0) - N(y_t < 0)}{N(y_t > 0) + N(y_t < 0)}, \qquad (2.1)$$

which is smaller than the $t\bar{t}$ rest frame asymmetry A_{FB} because of kinematics, and was also found above the SM expectation in earlier measurements. Neither the CDF nor the D0 Collaborations measure this asymmetry in their latest full dataset analyses, however, and we will restrict our discussion to A_{FB}.

The discrepancy found in the 2011 measurements of the asymmetry (Aaltonen *et al.*, 2011a; Abazov *et al.*, 2011a) motivated the refinement of the SM predictions, including weak, mixed QCD-weak and QCD-QED corrections that increase the asymmetry by 25% with respect to the NLO QCD value. Because A_{FB} vanishes at the tree level in the SM, a fixed-order expansion at LO in perturbation theory involves the numerator in Eq. (1.2) at NLO, including $\mathcal{O}(\alpha_s^3)$, $\mathcal{O}(\alpha^2)$ and $\mathcal{O}(\alpha_s^2\alpha)$ terms, and the denominator at LO. Several independent calculations yield similar results, $A_{FB} = 0.089^{+0.008}_{-0.006}$ (Hollik and Pagani, 2011), $A_{FB} = 0.087 \pm 0.010$ (Kuhn and Rodrigo, 2012), and $A_{FB} = 0.088 \pm 0.006$ (Bernreuther and Si, 2012), where the theory uncertainty is due to the variation of the factorization and renormalization scales. The contribution of the different subprocesses can be read in Table I. On the other hand, it has also been suggested that the Tevatron cross section and FB asymmetry can be reproduced with an unconventional choice of renormalization scale for the strong coupling (Brodsky and Wu, 2012), instead of the usual one $\mu_R \sim m_t$. Still, it remains to be shown that the several differential distributions (*e.g.* of $t\bar{t}$ invariant mass, particle transverse momenta and pseudo-rapidities, etc.) that are measured with good accuracy in $t\bar{t}$ production are also well reproduced using this proposal.

Higher-order effects beyond NLO were probed with the inclusion of soft-gluon resummation, with different results depending on the method used: while these effects were found to be rather small by Almeida *et al.* (2008) and Ahrens *et al.* (2011), they were found larger by Kidonakis (2011), and eventually closer to the exact next-to-next-to-leading order (NNLO) calculation. (See Kidonakis (2013) for a comparison between different methods.) Electroweak Sudakov corrections are small, 5% with respect to the NLO QCD value (Manohar and Trott, 2012). Recently, a prediction at NNLO in QCD, with NLO electroweak corrections, has become available (Cza-

TABLE I The contributions to the numerator ΔN of the FB asymmetry (1.2) at NLO for three different scales. The total LO cross sections and the resulting asymmetries are also given. From Bernreuther and Si (2012).

ΔN (pb)		$\mu = m_t/2$	$\mu = m_t$	$\mu = 2m_t$
$O(\alpha_s^3)$	$u\bar{u}$	0.5014	0.3297	0.2251
	$d\bar{d}$	0.0899	0.0582	0.0392
	qg	7.6×10^{-5}	3.4×10^{-5}	2.9×10^{-5}
$O(\alpha^2)$	$u\bar{u}$	1.47×10^{-2}	1.29×10^{-2}	1.15×10^{-2}
	$d\bar{d}$	1.9×10^{-3}	1.6×10^{-3}	1.5×10^{-3}
$O(\alpha\alpha_s^2)_{\text{weak}}$	$u\bar{u}$	10.7×10^{-3}	7.8×10^{-3}	5.8×10^{-3}
	$d\bar{d}$	-3.4×10^{-3}	-2.4×10^{-3}	-1.8×10^{-3}
$O(\alpha\alpha_s^2)_{\text{QED}}$	$u\bar{u}$	0.1047	0.0761	0.0569
	$d\bar{d}$	-9.4×10^{-3}	-6.7×10^{-3}	-4.9×10^{-3}
total ΔN		0.7104	0.4772	0.3332
$\sigma_{\text{QCD}}^{\text{LO}}$		7.618	5.456	4.030
A_{FB} (%)		9.33	8.75	8.27

kon *et al.*, 2014). The full NNLO QCD contribution increases the asymmetry by a factor of 1.13 with respect to the NLO value. Including NLO electroweak corrections, the prediction is $A_{FB} = 0.095 \pm 0.007$. An approximate next-to-next-to-next-to-leading order (aN^{3}LO) calculation in QCD based on soft-gluon resummation, including NLO electroweak corrections, is also available (Kidonakis, 2015), yielding $A_{FB} = 0.100 \pm 0.006$. A summary of some of the results obtained at different orders in perturbation theory is shown in Table II.

TABLE II Summary of selected calculations of the Tevatron $t\bar{t}$ rest-frame asymmetry, at different orders. The label "EW" denotes electroweak (weak, QED and mixed) corrections.

Order	A_{FB}
NLO QCD	0.072 ± 0.009 (Kuhn and Rodrigo, 2012)
NLO QCD + EW	0.088 ± 0.006 (Bernreuther and Si, 2012)
NNLO QCD	0.083 ± 0.003 (Czakon *et al.*, 2014)
NNLO QCD + NLO EW	0.095 ± 0.007 (Czakon *et al.*, 2014)
aN^{3}LO QCD	0.087 ± 0.002 (Kidonakis, 2015)
aN^{3}LO QCD + NLO EW	0.100 ± 0.006 (Kidonakis, 2015)

Finally, let us mention that, alternatively to the NLO predictions with LO denominators discussed above, the asymmetry can be computed using NLO numerator and denominator, and this is the only possibility when using Monte Carlo generators. For example, $A_{FB} = 0.058$ with MCFM (Campbell and Ellis, 1999) and $A_{FB} = 0.05$ with MC@NLO (Frixione and Webber, 2002) for $t\bar{t}$ production

at NLO in QCD. These values are smaller than the LO denominator predictions partly due to the missing electroweak corrections in the numerator, which amount to an increase by a factor of 1.26, and partly because the total cross section appearing in the denominator is around 25% larger at NLO. Likewise, the NNLO prediction can be computed with NNLO numerator and denominator, and is $A_{FB} = 0.087$, slightly smaller than the value expanded in powers of α, α_s. The corresponding aN^{3}LO prediction is also smaller, $A_{FB} = 0.094$.

B. The polar angle distribution and its asymmetry

The asymmetry (1.2) is equivalent to a FB asymmetry in the polar angle θ between the top quark momentum in the CM frame and the $\hat{z}$ axis, because y_t and $\cos\theta$ have the same sign. Also, in $p\bar{p}$ collisions at the Tevatron the initial state quark and antiquark in $q\bar{q} \to t\bar{t}X$ are supplied by the proton and antiproton, respectively, with a small $\lesssim 0.4\%$ probability for the opposite due to PDF suppression. Then, the initial quark direction almost always coincides with the proton direction, and the asymmetry (1.2) nearly equals the FB asymmetry

$$A_{FB} = \frac{N(\cos\theta > 0) - N(\cos\theta < 0)}{N(\cos\theta > 0) + N(\cos\theta < 0)} \qquad (2.2)$$

in the polar angle between the top and the initial quark directions in the CM frame.

In order to view the asymmetry (2.2) in a more general context, we consider the $2 \to 2$ process $q\bar{q} \to t\bar{t}$, not necessarily at the tree level, using the helicity formalism (Jacob and Wick, 1959). For helicities λ_1, λ_2, λ_3, λ_4 corresponding to the external particles q, $\bar{q}$, t, $\bar{t}$, respectively, angular momentum conservation allows to write the amplitude as

$$A = \sum_J a_{\lambda_1\lambda_2\lambda_3\lambda_4}^J D_{\lambda_i\lambda_f}^{J*}(\phi, \theta, 0), \qquad (2.3)$$

where J labels the total angular momentum and $\lambda_i = \lambda_1 - \lambda_2$, $\lambda_f = \lambda_3 - \lambda_4$; the dependence on the production angles (θ, ϕ) is given by the Wigner functions $D_{m'm}^j(\alpha, \beta, \gamma) \equiv \langle jm'|e^{-i\alpha J_z}e^{-i\beta J_y}e^{-i\gamma J_z}|jm\rangle$ and $a_{\lambda_1\lambda_2\lambda_3\lambda_4}^J$ are constants. The sum runs over all possible values $J = 0, 1, 2, \ldots$ (since plane waves "contain" all possible orbital angular momenta), but in particular cases it may happen that only a few values of J contribute. For example, in the SM at the tree level the process takes place via a spin-1 s-channel gluon, therefore the sum only contains the term $J = 1$.

From the general amplitude (2.3), one obtains with a little algebra the partonic differential cross section,

$$\frac{d\hat{\sigma}}{d\Omega} \propto \sum_{\lambda_1\lambda_2\lambda_3\lambda_4 JJ'l} a_{\lambda_1\lambda_2\lambda_3\lambda_4}^J a_{\lambda_1\lambda_2\lambda_3\lambda_4}^{J'*} \langle J\lambda_i J' - \lambda_i|l0\rangle$$
$$\times \langle J\lambda_f J' - \lambda_f|l0\rangle(-1)^{\lambda_i - \lambda_f} P_l(\cos\theta), \qquad (2.4)$$

with $\langle j_1 m_1 j_2 m_2 | j m \rangle$ Clebsch-Gordan coefficients and P_l a Legendre polynomial of degree l. The interference between top helicity states can be ignored as long as one is only interested in quantities that are independent of the W boson azimuthal angle in the top quark rest frame (see for example Aguilar-Saavedra and Herrero-Hahn, 2013), as is the case for all observables involved in the $2 \to 2$ process, in particular A_{FB}. (Note, however, that the charged lepton rapidity in the laboratory frame is *not* one of such observables.)

One can gain further insight into the asymmetry (2.2) setting $J = J' = 1$, as in the SM at the tree level. Then, the Clebsch-Gordan coefficients in Eq. (2.4) imply that only $l = 0, 1, 2$ contribute, and the corresponding Legendre polynomials are $P_0(x) = 1$, $P_1(x) = x$, $P_2(x) = (3x^2 - 1)/2$. Among them, only P_1 produces a FB asymmetry. Moreover, for $l = 1$ the symmetry properties of Clebsch-Gordan coefficients imply that only $\lambda_i, \lambda_f \neq 0$ contribute to A_{FB}, and

$$
A_{FB} \propto \left[|a^1_{\frac{1}{2}-\frac{1}{2}\frac{1}{2}-\frac{1}{2}}|^2 + |a^1_{-\frac{1}{2}\frac{1}{2}-\frac{1}{2}\frac{1}{2}}|^2 - |a^1_{\frac{1}{2}-\frac{1}{2}-\frac{1}{2}\frac{1}{2}}|^2 \right.
$$
$$
\left. - |a^1_{-\frac{1}{2}\frac{1}{2}\frac{1}{2}-\frac{1}{2}}|^2 \right] . \tag{2.5}
$$

C (or parity P) invariance implies

$$
|a^1_{\frac{1}{2}-\frac{1}{2}\frac{1}{2}-\frac{1}{2}}|^2 = |a^1_{-\frac{1}{2}\frac{1}{2}-\frac{1}{2}\frac{1}{2}}|^2 ,
$$
$$
|a^1_{\frac{1}{2}-\frac{1}{2}-\frac{1}{2}\frac{1}{2}}|^2 = |a^1_{-\frac{1}{2}\frac{1}{2}\frac{1}{2}-\frac{1}{2}}|^2 , \tag{2.6}
$$

so it is clear that the so-called "charge asymmetry" A_{FB} does not entail a violation of the charge conjugation symmetry C. On the other hand, at the tree-level in QCD the modulus squared amplitudes are invariant under the exchange of the t and $\bar{t}$ momenta, keeping the initial quarks fixed,

$$
|a^1_{\frac{1}{2}-\frac{1}{2}\frac{1}{2}-\frac{1}{2}}|^2 = |a^1_{\frac{1}{2}-\frac{1}{2}-\frac{1}{2}\frac{1}{2}}|^2 ,
$$
$$
|a^1_{-\frac{1}{2}\frac{1}{2}-\frac{1}{2}\frac{1}{2}}|^2 = |a^1_{-\frac{1}{2}\frac{1}{2}\frac{1}{2}-\frac{1}{2}}|^2 , \tag{2.7}
$$

implying that the right-hand side of Eq. (2.5) vanishes.

Dropping the $J = 1$ restriction, we see from Eq. (2.4) that in full generality the partonic differential cross section can be expanded in terms of Legendre polynomials,

$$
\frac{d\hat{\sigma}}{d\Omega} = \sum_l a_l P_l(\cos\theta) . \tag{2.8}
$$

The coefficients a_l of this expansion are called "Legendre momenta" and the first ones have been measured by the CDF Collaboration (Aaltonen *et al.*, 2013a), finding an excess in a_1, precisely the coefficient of the lowest-order polynomial generating an asymmetry.

C. Asymmetries at the LHC versus Tevatron

In $p\bar{p}$ collisions at the Tevatron, an asymmetry (2.2) in the angle between the top and initial quark induces

the asymmetry (1.2) between the top and proton directions precisely because the proton and quark directions almost always coincide. At the LHC, the two colliding hadrons are protons, and an asymmetry such as (1.2) vanishes. Nevertheless, since valence quarks have on average a larger momentum fraction than sea antiquarks, a forward top quark (with respect to the quark direction) in the $t\bar{t}$ CM frame has in average a larger $|y|$ in the laboratory frame—with y of either sign—than the backward antiquark. Hence, the asymmetry (1.3) is well suited to probe a partonic asymmetry in the direction between the top and initial quark. Other asymmetries (Hewett *et al.*, 2011; Kuhn and Rodrigo, 2012) are numerically different but based on the same idea.

The SM NLO predictions for the LHC asymmetry, including electroweak contributions and taking the denominator at LO are, at 7 TeV and 8 TeV respectively, $A_C = 0.0115 \pm 0.0006$, $A_C = 0.0102 \pm 0.0005$ (Kuhn and Rodrigo, 2012), and $A_C = 0.0123 \pm 0.0005$, $A_C = 0.0111 \pm 0.0005$ (Bernreuther and Si, 2012). (NNLO predictions are not yet available.) The contributions of different subprocesses are given in Table III, for a CM energy of 8 TeV. The SM prediction for A_C is one order

TABLE III The contributions to the numerator ΔN of the asymmetry (1.3) at NLO for three different scales. The total LO cross sections and the resulting asymmetries are also given. From Bernreuther and Si (2012).

ΔN (pb)		$\mu = m_t/2$	$\mu = m_t$	$\mu = 2m_t$
$O(\alpha_s^3)$	$q\bar{q}$	1.7887	1.2914	0.9567
	qg	0.1162	0.0813	0.0564
$O(\alpha^2)$	$q\bar{q}$	5.13×10^{-2}	4.97×10^{-2}	5.21×10^{-2}
$O(\alpha\alpha_s^2)_{\text{weak}}$	$q\bar{q}$	7.8×10^{-3}	6.3×10^{-3}	5.0×10^{-3}
	qg	2.13×10^{-2}	-1.58×10^{-2}	-4.48×10^{-2}
$O(\alpha\alpha_s^2)_{\text{QED}}$	$q\bar{q}$	0.2020	0.1616	0.1838
	qg	7.2×10^{-3}	5.4×10^{-3}	4.1×10^{-3}
total ΔN		2.1945	1.5799	1.2113
$\sigma_{\text{QCD}}^{\text{LO}}$ (pb)		190.77	142.94	113.21
A_{FB} (%)		1.15	1.11	1.07

of magnitude smaller than for A_{FB} owing to two effects. First, gg fusion is dominant at the LHC, with 80% of the total cross section at these CM energies, and it does not produce any asymmetry but washes out the one produced in $q\bar{q}$ annihilation. Second, the probability that the antiquark has larger momentum fraction than the quark—in which case a forward top has smaller $|y|$ and contributes negatively to A_C—is not negligible, and leads to a further dilution of the generated asymmetry. Note also that at the LHC the qg processes are not suppressed as they are at the Tevatron, but the asymmetry they generate is small.

It is clear that the asymmetries (1.2), (1.3) are different observables, hence a measured value of the latter

consistent with the SM prediction does not preclude an anomaly in the former. In fact, the relation between them is model-dependent (Aguilar-Saavedra and Pérez-Victoria, 2011a). Still, A_{FB} and A_C arise from asymmetries in $q\bar{q}$ annihilation that, for a fixed partonic CM energy $\hat{s}$, are the same at the two colliders. One can write (Aguilar-Saavedra and Juste, 2012)

$$
\begin{aligned}
A_{FB} &= A_u F_u + A_d F_d, \\
A_C &= A_u F_u D_u + A_d F_d D_d,
\end{aligned}
\tag{2.9}
$$

where $A_{u,d}$ are the "intrinsic" asymmetries in the partonic processes $u\bar{u} \rightarrow t\bar{t}X$, $d\bar{d} \rightarrow t\bar{t}X$, respectively, $F_{u,d} = \sigma_{u\bar{u},d\bar{d}}/\sigma$ are the $u\bar{u}$ and $d\bar{d}$ fractions of the cross section, and $D_{u,d}$, dilution factors arising from the already mentioned fact that sometimes the antiquark has larger momentum fraction than the quark. To a good approximation, A_u and A_d are the same at the Tevatron and the LHC, provided one restricts $m_{t\bar{t}}$ to a narrow interval, hence their labelling as "collider-independent". The SM NLO calculations of $A_{u,d}$ including electroweak corrections are presented in Fig. 2 (upper panel), using $m_{t\bar{t}}$ bins of 50 GeV up to 800 GeV. The differences between the Tevatron and LHC values are already smaller than the expected statistical uncertainties, but can be further reduced by applying an upper cut on $p_T^{t\bar{t}}$ (lower panel). As yet, there are not any measurements of $A_{u,d}$ neither at the Tevatron nor at the LHC. They could be measured from the two-dimensional distribution of A_{FB} or A_C as a function of $m_{t\bar{t}}$ and the velocity of the $t\bar{t}$ pair

$$
\beta_z^{t\bar{t}} = \frac{|p_z^t + p_z^{\bar{t}}|}{E_t + E_{\bar{t}}},
\tag{2.10}
$$

using Eqs. (2.9) and exploiting the fact that for fixed $m_{t\bar{t}}$, $A_{u,d}$ are almost independent of $\beta_z^{t\bar{t}}$ while $F_{u,d}$ and $D_{u,d}$ are not. This is a demanding but revealing measurement. Being basically the same quantities at the two colliders, the measurement of $A_{u,d}$ at the LHC is a unique direct test of the Tevatron anomaly. Furthermore, measurements of $A_{u,d}$ at the Tevatron and the LHC could be combined for a more precise determination of the two partonic asymmetries.

In this context, it is worthwhile pointing out that isospin-symmetric corrections to the SM values of $A_{u,d}$ shift A_{FB} and A_C in the same direction. Figure 3 shows the asymmetries A_{FB} and A_C resulting from random variations of $A_{u,d}$ between 1/4 and 4 times their SM NLO values, fixing $F_{u,d}$ and $D_{u,d}$ as in the SM—which is a reasonable approximation given the good agreement of various differential distributions with data. (The random variations are done independently in each bin of $m_{t\bar{t}}$.) An increase in the A_{FB} prediction to fit the Tevatron average[2] also increases A_C leading to a 1σ deviation, which

---

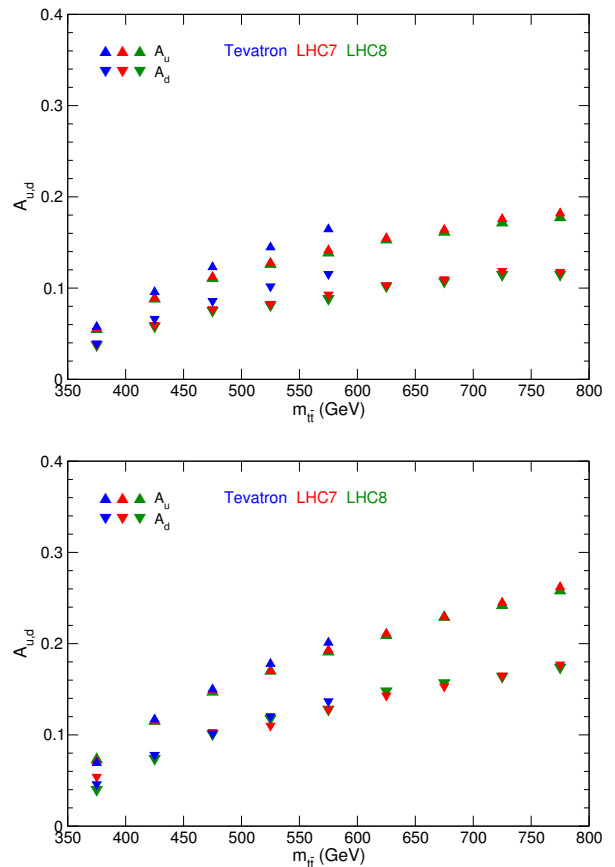[2] In the absence of official combinations, the quoted Tevatron and

FIG. 2 SM predictions for the collider-independent asymmetries A_u, A_d at the Tevatron and the LHC, without $p_T^{t\bar{t}}$ cut (up) and with $p_T^{t\bar{t}} < 30$ GeV (down). From Aguilar-Saavedra et al. (2012a).

reaches almost 2σ if one wants to reproduce the CDF measurement $A_{FB} = 0.164 \pm 0.045$.

Conversely, isospin-breaking corrections to $A_{u,d}$ can generate a positive contribution to A_{FB} with small or vanishing contribution to A_C. This is illustrated by Fig. 4, where $A_{u,d}$ are left completely arbitrary within each $m_{t\bar{t}}$ bin and $F_{u,d}$, $D_{u,d}$ are fixed to their SM values. A positive asymmetry $A_{FB} > 0$ is compatible with a vanishing or negative A_C provided A_u and A_d have a different sign. The implementation of this condition in actual models is discussed at the end of Sec. V.

D. Leptonic asymmetries

In addition to the $t\bar{t}$-based asymmetries, the Tevatron experiments measure asymmetries based on the rapidities

---

LHC averages are weighted averages of the relevant measurements, detailed in Sec. III and IV, respectively.
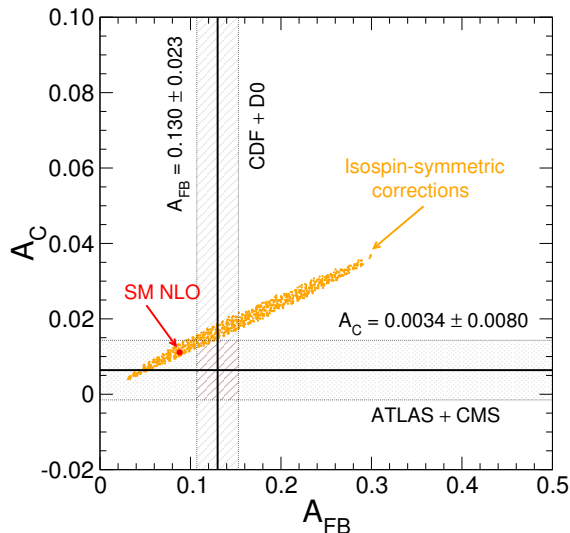
FIG. 3 Relation between A_C and A_{FB} resulting from random isospin-symmetric variations of $A_{u,d}$ around their SM value, as described in the text. Also shown are the simple error-weighted averages of A_{FB} measurements at the Tevatron (see Sect. III.E) and of A_C measurements at the LHC at $\sqrt{s} = 7$ TeV (see Sect. IV.C).
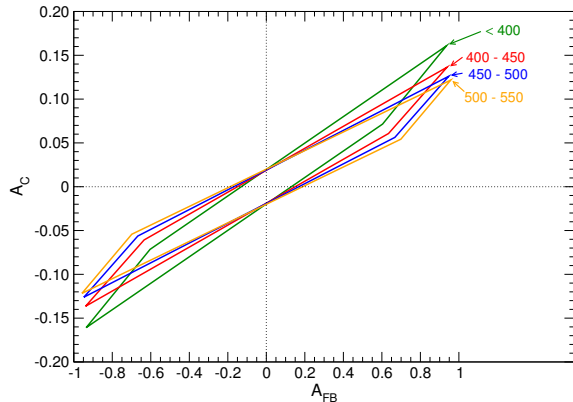

FIG. 4 Allowed asymmetries A_C and A_{FB} in several $m_{t\bar{t}}$ bins (in GeV), which result from arbitrary $A_{u,d}$ within these bins. From Aguilar-Saavedra and Juste (2012).

of the charged leptons from the top quark decay,

$$A_{FB}^{\ell} = \frac{N(q_\ell y_\ell > 0) - N(q_\ell y_\ell < 0)}{N(q_\ell y_\ell > 0) + N(q_\ell y_\ell < 0)},$$
$$A_{FB}^{\ell\ell} = \frac{N(\Delta y_\ell > 0) - N(\Delta y_\ell < 0)}{N(\Delta y_\ell > 0) + N(\Delta y_\ell < 0)}, \quad (2.11)$$

with q_ℓ the lepton charge and $\Delta y_\ell = y_{\ell^+} - y_{\ell^-}$. The former can be measured in the ℓ+jets or dilepton decays of the $t\bar{t}$ pair, whereas the latter requires the two charged leptons and is measured only in the dilepton channel. (The ℓ+jets and dilepton decay modes of the $t\bar{t}$ pair are those in which one or two charged leptons,

respectively, are produced from the decay of the two W bosons.) Within the SM, these asymmetries are generated from the $t\bar{t}$ asymmetry A_{FB}, given the fact that the top (anti-)quarks are produced with zero polarization in the production plane, that is, the plane spanned by the top and initial quark momenta in the $t\bar{t}$ CM frame. The SM predictions at NLO are $A_{FB}^{\ell} = 0.038 \pm 0.003$, $A_{FB}^{\ell\ell} = 0.048 \pm 0.004$ (Bernreuther and Si, 2012), using LO denominators.

In general the leptonic asymmetries and A_{FB} are independent observables in much the same way as A_{FB} and A_C are. This fact is clear when one considers the threshold behavior of $q\bar{q} \to t\bar{t}$ and the possible effect of new physics (Falkowski et al., 2013b). At the threshold, $t\bar{t}$ pairs produced from initial $q_R\bar{q}_R$ states have their spins aligned in the proton direction, independently of θ. The top decay dynamics makes the positive charge lepton tend to follow the top spin direction, so it is preferentially emitted with $y_{\ell^+} > 0$. The negative charge lepton from the top decay tends to be emitted opposite to the top spin, so $y_{\ell^-} < 0$. For initial $q_L\bar{q}_L$ states the behavior is the opposite, and the charged leptons preferentially have $y_{\ell^+} < 0$ and $y_{\ell^-} > 0$. For equal $q_R\bar{q}_R$ and $q_L\bar{q}_L$ cross sections, as when produced by QCD interactions, the two effects cancel and the asymmetries vanish at threshold. But any excess in $q_R\bar{q}_R$—or decrease in $q_L\bar{q}_L$ via interference—caused by new physics will originate positive leptonic asymmetries, independently of A_{FB}. Conversely, a decrease in $q_R\bar{q}_R$ or an excess of $q_L\bar{q}_L$ will generate negative asymmetries.

At the LHC, a leptonic asymmetry

$$A_C^{\ell\ell} = \frac{N(\Delta|y_\ell| > 0) - N(\Delta|y_\ell| < 0)}{N(\Delta|y_\ell| > 0) + N(\Delta|y_\ell| < 0)} \quad (2.12)$$

has also been measured in the dilepton decay mode of the $t\bar{t}$ pair. The SM predictions at NLO are $A_C^{\ell\ell} = 0.0070 \pm 0.0003$ for 7 TeV and $A_C^{\ell\ell} = 0.0064 \pm 0.0003$ for 8 TeV (Bernreuther and Si, 2012).

III. EXPERIMENTAL MEASUREMENTS AT THE TEVATRON

Interest in the $t\bar{t}$ asymmetry was sparked by papers from the CDF and D0 Collaborations in 2008 (Aaltonen, 2008; Abazov et al., 2008) where, in small initial samples from Tevatron Run 2, both experiments observed large Δy asymmetries in $t\bar{t}$ events in the ℓ+jets decay mode. Follow up measurements with roughly 5 fb^{-1} again showed large asymmetries in both experiments, with a significant dependence on $m_{t\bar{t}}$ at CDF (Aaltonen et al., 2011a,b; Abazov et al., 2011a). Subsequent studies examined the differential behavior of the asymmetry in rapidity and $t\bar{t}$ invariant mass, the differential cross-section in the scattering angle, and the asymmetry in the isolated top decay leptons, and also expanded the

asymmetry measurements into the dilepton decay mode. All of these measurements are grounded in the techniques used to measure the $t\bar{t}$ cross section which is the denominator of the asymmetry. The combined Tevatron cross section for $t\bar{t}$ production in $p\bar{p}$ collisions at 1.96 TeV is $\sigma_{t\bar{t}} = 7.60 \pm 0.41$ pb for $m_t = 172.5$ GeV (Aaltonen *et al.*, 2014a).

The Tevatron asymmetry measurements rely on using a well-measured lepton from the decay chain $t \to Wb \to \ell\nu b$ to measure the top quark charge. We review here asymmetry results in both ℓ+jets and dilepton channels using the full Tevatron Run 2 data set, as reported by both the CDF and D0 experiments.

A. Inclusive asymmetry in the ℓ+jets mode

When one and only one top quark decays leptonically, the $t\bar{t}$ final state contains a lepton, missing transverse energy $\not{E}_T$, and four hadronic jets, two of which are initiated by b quarks. These ℓ+jets events contain sufficient information to completely reconstruct the $t\bar{t}$ 4-vectors and the electric charges of the top quarks. The samples are selected requiring a central (here referring to pseudorapidity) isolated electron or muon, with $p_T > 20$ GeV, missing transverse energy $\not{E}_T > 20$ GeV, and at least 3 (D0) or 4 (CDF) jets with $p_T > 20$ GeV. Decay channels through τ leptons are not included, although there is a small leakage of τ events from the $W \to \tau \to e/\mu$ decay chain. The presence of final state b-jets is confirmed using information on reconstructed displaced secondary vertices and tracks with significant impact parameter with respect to the hard-scatter primary vertex. The total efficiency of the selection (including the leptonic branching ratios) is $\sim 3\%$. The non-$t\bar{t}$ backgrounds in this selection are dominated by W+jets events with heavy flavor or incorrectly b-tagged jets, plus small contributions from QCD multijets and electroweak processes. These backgrounds are modeled using Monte Carlo generators and detailed detector simulation, except for the pure QCD multijets component, which is derived from data sidebands.

The most probable 4-vectors for the $t\bar{t}$ production hypothesis are derived for each event. Subtraction of the background processes yields the distribution of Δy for the reconstructed top quarks, which has been distorted by acceptance losses and resolution smearing. These distortions can be estimated from study of the simulated NLO signal model and used to construct a regularized linear transformation that deconvolves (or unfolds) the true production-level distribution from the reconstructed one. The reliability of the unfolding procedure is checked using simulated $t\bar{t}$ samples with a variety of A_{FB} models.

1. CDF

The CDF Collaboration measured the asymmetry with 9.4 fb^{-1} (Aaltonen *et al.*, 2013c). The selection uses the four leading hadronic jets, and also requires a transverse energy sum of all objects $H_T > 200$ GeV, giving 2653 candidate events. The sample composition is found using a detailed accounting of the b-tagging rate in all expected processes; the non-$t\bar{t}$ backgrounds total 530 ± 124 events. In the 4-jet sample, the $t\bar{t}$ 4-vectors are reconstructed using constraints on the W and top masses, varying the jet energies within their expected resolutions, and choosing the jet-parton combination with the lowest χ^2. The Δy distribution is calculated and background shapes, estimated from simulated samples and data side-bands, are subtracted. The asymmetry at the reconstruction level is found to be 0.087 ± 0.026.
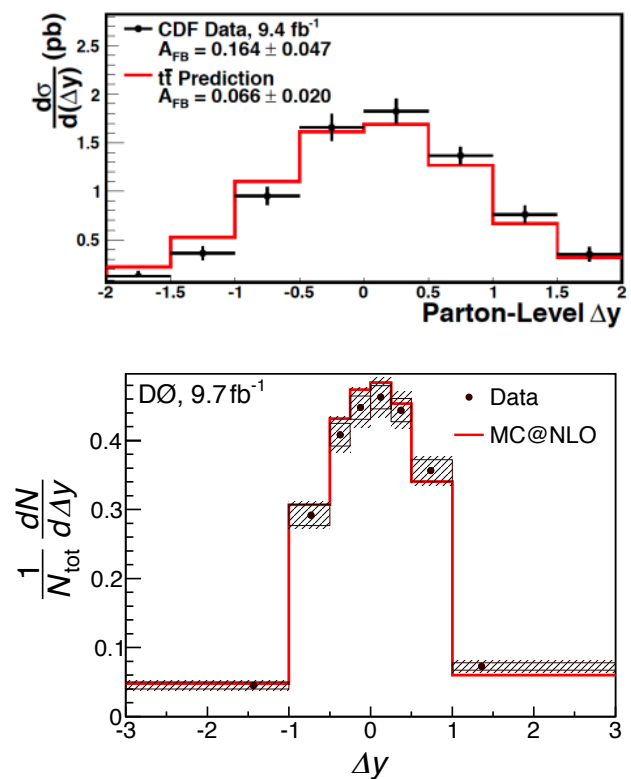
FIG. 5 Production-level Δy distributions. Top: At CDF, where the error bars represent the total statistical and systematic uncertainty in each bin. Bottom: At D0, where the statistical uncertainty is given by the black rectangles and the hashed area represents the total uncertainty including systematic effects. From Aaltonen *et al.* (2013c) and Abazov *et al.* (2014c).

The $t\bar{t}$ signal is modeled using the NLO generator POWHEG (Frixione *et al.*, 2007). Parton showers are added by PYTHIA (Sjostrand *et al.*, 2006), and the result is run through a full detector simulation. The electroweak contribution is included by rescaling the asym-

metric parts of Δy by an additional factor of 1.26 (see Sec. II.A). The one-dimensional Δy distribution is unfolded in eight bins using a response matrix based on POWHEG; the production-level distribution of Δy is given in the top plot in Fig. 5. The inclusive asymmetry is $A_{FB} = 0.164 \pm 0.039\,(\text{stat}) \pm 0.026\,(\text{syst})$. The systematic uncertainty of the measurement is dominated by the background modeling and normalization.

2. D0

The D0 Collaboration has measured the asymmetry in 9.7 fb^{-1} (Abazov $et\ al.$, 2014c). Events are selected in both the exclusive 3-jet and inclusive 4-jet mode with the additional requirement that the leading jet has $p_T \geq 40$ GeV. The b-tagging uses a multivariate analysis (MVA) of the jet fragmentation and track impact parameter information. The $t\bar{t}$ signal is modeled with MC@NLO and showered with HERWIG (Corcella $et\ al.$, 2001). Kinematic reconstruction in the 4-jet sample is weighted over jet energy transfer functions and b-tagging likelihoods. Partial reconstruction in the 3-jet sample uses a MVA with kinematic variables to find the most probable reconstruction of the $t\bar{t}$ system assuming the lost jet is from the hadronically decaying top quark. In both samples the jet-parton combination yielding the highest likelihood value is selected to reconstruct the 4-momenta of the top and antitop quarks. The sample is divided into six channels according to jet and b-tag multiplicity, and the composition of each is found using multivariate discriminants. The total sample is 10947 events with an estimated background of 6202 ± 78. In the 4-jet subsample comparable to the CDF analysis there are 2875 events. The asymmetry in the W+jets background sample is re-weighted according to that observed in the background-dominated 3-jet 0-tag sample. After background subtraction the inclusive asymmetry at the reconstruction level is found to be 0.079 ± 0.027. An unfold in 26/50 bins of true/reconstructed Δy, using the MC@NLO response model gives the production-level distribution shown in the bottom of Fig. 5. The inclusive asymmetry is $A_{FB} = 0.106 \pm 0.030$. The systematic part of the uncertainty is dominated by the background modeling.

Except for very small effects from common assumptions concerning PDF's, the D0 and CDF results are uncorrelated. In this case it is possible to combine the measurements using a simple error-weighted average, yielding $A_{FB} = 0.124 \pm 0.025$.

B. Kinematic dependence of the asymmetry

As the $t\bar{t}$ cross section is a function of the scattering angle, momentum transfer, and $t\bar{t}$ transverse momentum,

TABLE IV Slope α of A_{FB} as a linear function of Δy and $m_{t\bar{t}}$. The predicted slopes have been estimated using the POWHEG generator interfaced to PYTHIA (see Sect. III.A.1 for details). Predictions and measurements have been extracted from Aaltonen $et\ al.$ (2013c) and Abazov $et\ al.$ (2014c).

	$\alpha(\Delta y)$	$\alpha(m_{t\bar{t}})$
predicted	0.097 ± 0.015	$(3.4 \pm 1.2) \times 10^{-4}$
CDF	0.253 ± 0.062	$(15.5 \pm 4.8) \times 10^{-4}$
D0	0.154 ± 0.043	$(3.9 \pm 4.4) \times 10^{-4}$

it is interesting to explore the differential behavior of the asymmetry in these variables.

1. Rapidity difference

In the collider environment, the rapidity difference Δy is the natural proxy for the scattering angle. The rapidity dependent asymmetry

$$A_{FB}(\Delta y) = \frac{N(+\Delta y) - N(-\Delta y)}{N(+\Delta y) + N(-\Delta y)}, \qquad (3.1)$$

follows directly from the information in Fig. 5. The results from both experiments are compared to the NLO prediction in the top panel of Fig. 6. In both cases, the NLO model is well fit with a simple linear form. Since the Δy distribution is continuous at $\Delta y = 0$, the intercept must be consistent with zero. The measurements of both experiments are in good agreement with the linear form, with slopes shown in Table IV. The D0 measurement is 1.3σ above the prediction and the CDF measurement is 1.3σ above the D0 one.

2. $t\bar{t}$ invariant mass

The $\hat{s}$ behavior of the asymmetry is measured in the variation of Δy with the $t\bar{t}$ invariant mass $m_{t\bar{t}}$. A production level measurement requires a two-dimensional unfolding in the space of Δy and $m_{t\bar{t}}$. The CDF Collaboration uses four bins in $m_{t\bar{t}}$ and 2 bins in Δy; the latter choice confines the need for regularization to $m_{t\bar{t}}$ only. The D0 Collaboration uses more granularity, with 26/50 bins in production/reconstruction level Δy, 6 bins in $m_{t\bar{t}}$, and simultaneous regularization of both variables. The results for the two experiments are shown in Fig. 6, bottom, and Table IV. Except at the highest mass, the two results are in modest agreement. The fitted slopes are more discordant, with a difference of 1.8σ.
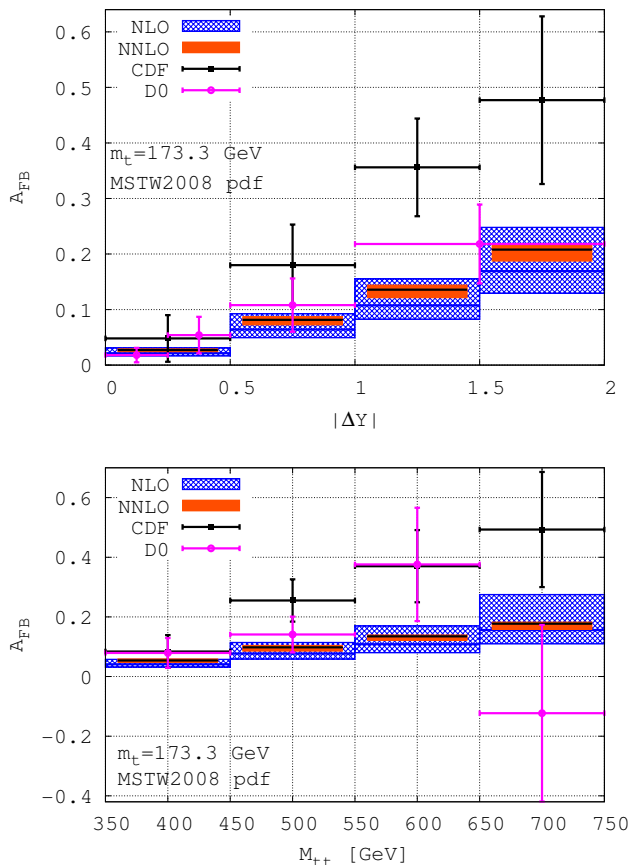
FIG. 6 Production-level dependence of the asymmetry on the rapidity difference (top) and $t\bar{t}$ invariant mass (bottom) for both Tevatron experiments, compared to NLO and NNLO predictions. The horizontal error bars indicate the binning used in each experiment. The CDF measurements (Aaltonen *et al.*, 2013c) are squares and the D0 measurements (Abazov *et al.*, 2014c) are circles. The SM predictions and their scale uncertainties are given by the horizontal lines and associated bands. From Czakon *et al.* (2014).

3. Production angle

The reconstruction of the $t\bar{t}$ four vectors in the $\ell+$ jets mode allows a direct measurement of the differential cross-section in the $t\bar{t}$ scattering angle $d\hat{\sigma}/d\cos\theta$ (in the $t\bar{t}$ rest frame), as discussed in Sec. II.B. The top plot of Fig. 7 shows the differential cross section for two SM predictions and two representative new physics models. The LO QCD prediction shows the characteristic $\sim 1 + \cos^2\theta$ behavior, while the NLO curve shows the addition of a small approximately linear correction. A 1.2 TeV s-channel color octet with axial couplings shows a large linear correction. Alternatively, a 200 GeV flavor changing t-channel Z' shows a strong forward scattering component.

The CDF Collaboration has performed the production

angle measurement characterizing the the cross section as an expansion in Legendre polynomials according to Eq (2.8) (Aaltonen *et al.*, 2013a). The analysis uses the 4-jet sample of Sec. III.A.1, augmented with 3-jet events with an additional soft jet having $p_T > 12$ GeV. A total of 3776 events are used, with estimated background 1026 ± 210. The 4-jet reconstruction gives $\cos\theta$, and backgrounds are subtracted from the distribution. By discretizing in Legendre moments rather than histogram bins, the transfer matrix to the production level is well-conditioned, and the unfold can be done by simple inversion, avoiding regularization. The Legendre coefficients a_l are shown on the bottom of Fig. 7, normalized to the total cross section $a_0 = 1$. In the predictions (i) LO PYTHIA has $a_1 = 0$ and small a_4 from gg initiated t-channel scattering; (ii) NLO QCD has box and and radiative diagrams give corrections to all moments, including the asymmetry producing odd terms; (iii) the s-channel octet model adds a non-zero a_1 to the LO PYTHIA model; (iv) the t-channel model, with leading behavior $1/(1 - \cos\theta)$, has large higher order Legendre terms. The data suggests that the asymmetry arises in the linear term in $\cos\theta$, with coefficient $a_1 = 0.40 \pm 0.09\,(\text{stat}) \pm 0.08\,(\text{syst})$. The statistical precision is limited, but disfavors the large higher order moments characteristic of t-channel models.

4. $t\bar{t}$ transverse momentum

As described in Sec. II.A, the NLO QCD asymmetry should have a strong dependence on the transverse momentum of the $t\bar{t}$ system, $p_T^{t\bar{t}}$. The top plot in Fig. 8 shows the $p_T^{t\bar{t}}$-dependent asymmetry

$$A_{FB}(p_T^{t\bar{t}}) = \frac{N_F(p_T^{t\bar{t}}) - N_B(p_T^{t\bar{t}})}{N_F(p_T^{t\bar{t}}) + N_B(p_T^{t\bar{t}})}. \quad (3.2)$$

for four different SM calculations at the production level. The strong color coherence effect is seen in PYTHIA; it is interesting that the average of this dependence over all $p_T^{t\bar{t}}$ gives the expected LO QCD result $A_{FB} = 0$. The NLO QCD calculation MCFM shows the positive Born-box asymmetry at $p_T^{t\bar{t}} = 0$ and the negative initial/final state radiation (ISR/FSR) interference asymmetry elsewhere. POWHEG has the same NLO matrix elements, with higher order effects approximated by PYTHIA showering, smoothing the MCFM form. The curve called "$t\bar{t}+$Jet" includes the higher order effects at large $p_T^{t\bar{t}}$ explicitly as jets[3], and is in good agreement with the showered POWHEG.

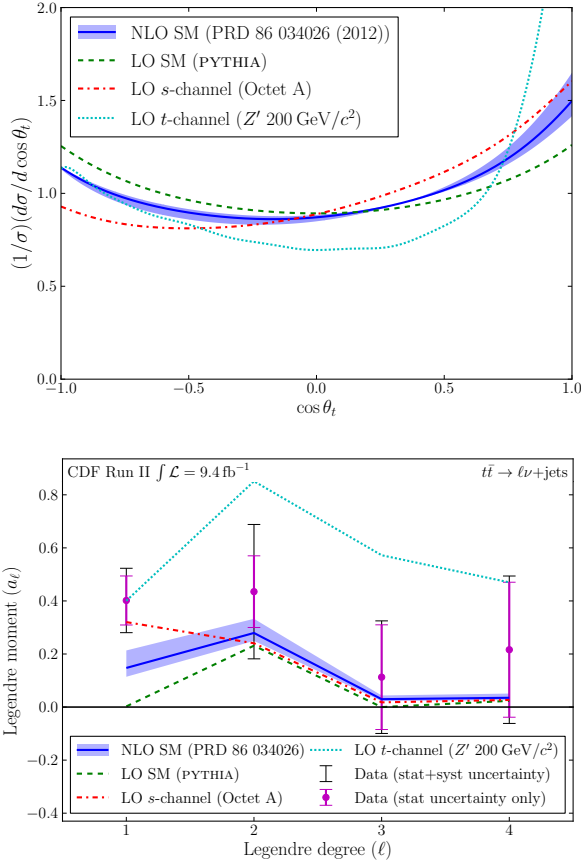[3] K.Melnikov, A. Scharf and M. Schulze, private communication.

FIG. 7 Top: Angular cross-sections for NLO QCD and new physics models. Bottom: Legendre coefficients for data and models. From Aaltonen *et al.* (2013a).
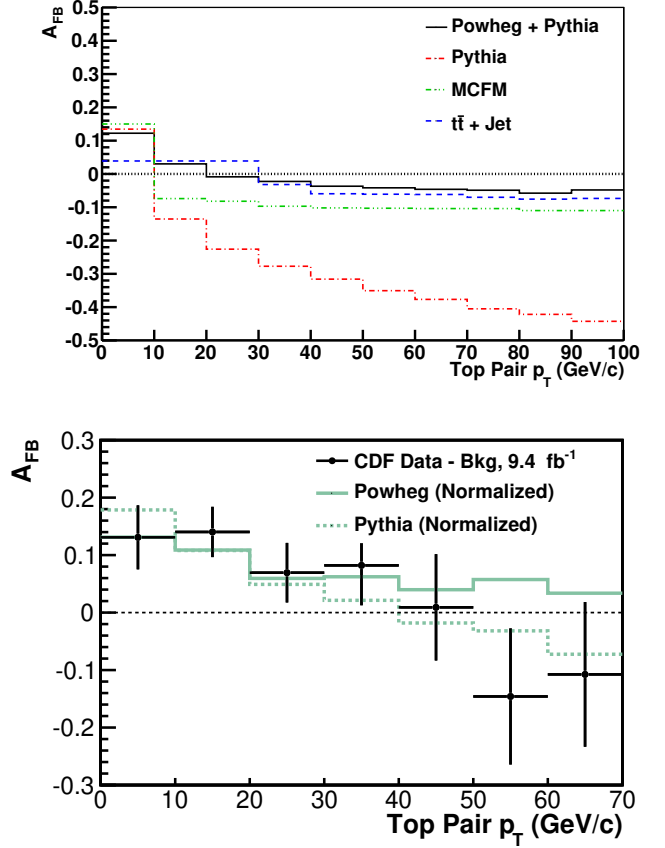

FIG. 8 Top: A_{FB} vs. $p_T^{t\bar{t}}$ for LO and NLO QCD calculations. Bottom: Comparison of data to predictions including an additional $p_T^{t\bar{t}}$ independent asymmetry. From Aaltonen *et al.* (2013c)

.

The CDF Collaboration measured the $p_T^{t\bar{t}}$-dependent asymmetry as part of the study described in Sec. III.A.1. The analysis is performed with the reconstructed, background-subtracted data, avoiding issues with unfolding. The bottom plot in Figure 8 shows $A_{FB}(p_T^{t\bar{t}})$ for the data after background subtraction. The asymmetry in data falls with $p_T^{t\bar{t}}$ as in the top plot, but lies above the predictions there. In order to make a slope comparison they consider a simple normalization ansatz where the excess asymmetry in the data is independent of $p_T^{t\bar{t}}$, as is approximately the case for the NLO QCD effect and also some of the new physics models. Since independent asymmetries add, this produces an additive correction in each $p_T^{t\bar{t}}$ bin equal to the difference of the inclusive A_{FB} in the reconstructed data and the simulated SM. The bottom plot in Fig. 8 shows the comparison of the data to the PYTHIA and POWHEG models normalized in this way. The data are well described by either the POWHEG or PYTHIA modeling in conjunction with a $p_T^{t\bar{t}}$-independent asymmetry according to the inclusive measurement.

C. Inclusive asymmetry in the dilepton mode

When both top quarks decay leptonically, the $t\bar{t}$ final state contains two charged leptons, missing transverse energy $\not{E}_T$ from two overlapping neutrinos, and two hadronic jets initiated by b quarks. The information loss in the overlapping neutrinos prohibits a direct reconstruction of the $t\bar{t}$ kinematics, but the top quark asymmetry can be recovered using probabilistic techniques.

The D0 Collaboration has performed a preliminary measurement in the full Tevatron dataset of 9.7 fb^{-1} (Abazov *et al.*, 2014a). Events are selected requiring two isolated opposite sign electrons or muons having $p_T > 15$ GeV and two or more jets with $E_T > 20$ GeV. Additional selections based H_T, $\not{E}_T$, and the $\not{E}_T$ significance are optimized separately for each of the three modes ee, $e\mu$, and $\mu\mu$. At least one of the two jets is required to be b-tagged by a multivariate discriminant that is also optimized for the flavor of the leptonic mode. The total number of events is 542. Non-$t\bar{t}$ backgrounds to this selection include Z bosons and electroweak di-bosons in

association with jets, and QCD multijets that manage to satisfy the lepton and $\not{E}_T$ requirements. The electroweak backgrounds are modeled with simulated samples, and the QCD multijets background is modeled with data driven techniques. The estimated background contamination is 62 ± 15 events.

The top quark Δy distribution is reconstructed using a novel modification of the matrix-element technique used to measure the top-quark mass at D0 (Abazov *et al.*, 2011b). In each event a likelihood function for Δy is constructed by comparing the final state kinematic configuration to the LO SM matrix element for $t\bar{t}$ production. The number of integrations is reduced by assuming that the initial and final states conserve energy and momentum, that the lepton direction, b-quark direction, and electron energies are perfectly measured, that both $l\nu$ systems have $m_W = 80.4$ GeV, and that both top systems have $m_t = 172.5$ GeV. The muon and jet energy resolution is treated using transfer functions. The final integration over $p_t^{t\bar{t}}$, $\phi^{t\bar{t}}$, the energies of the two leading jets, and the energies of the muons (if applicable), produces a likelihood distribution of Δy for each event. The sum of the event likelihoods estimates the distribution of Δy in the sample. The background models are used to derive the Δy distribution for the non-$t\bar{t}$ components and these are subtracted.

This distribution and its asymmetry includes dilution effects due to the limited detector acceptance, the finite resolution of the detector measurements, and the assumptions in the matrix element integration. The production level asymmetry is recovered from the measured asymmetry using a linear transfer function derived from samples of MC@NLO that have been reweighted for various asymmetries according to the scheme of Hong *et al.* (2014). Tests with simulations of new physics models for the asymmetry show that the technique is unbiased at the level of $\leq 2\%$ as long as the top-quark decays are SM-like. i.e. have no unexpected polarization. The production level asymmetry is found to be $A_{FB} = 0.180 \pm 0.061\,(\text{stat}) \pm 0.032\,(\text{syst})$. The systematic uncertainty is dominated by the hadronization and showering model and the PDF assumptions.

D. Leptonic asymmetries

The leptonic asymmetries defined in Eq. (2.10) are experimentally attractive because the lepton rapidity is very well-measured and free from the complications of combinatorics and jet resolution present in the Δy reconstruction. In the SM, the POWHEG generator and NLO calculations (Bernreuther and Si, 2012) both suggest a ratio $A_{FB}^\ell / A_{FB} \approx 0.5$.

1. Leptonic asymmetries at D0

The D0 Collaboration has measured A_{FB}^ℓ in both decay modes. The measurement in ℓ+jets (Abazov *et al.*, 2014b) uses 9.7 fb^{-1} and the sample selection of Sec. III.A.2. The D0 lepton acceptance extends to $|\eta| = 1.5$ and the analysis and unfold is done with this cut, ignoring leptons of larger rapidity. The significant background from W+jets events is calibrated against a control sample derived from ℓ+3-jet events with no b-tag. Similarly to Abazov *et al.* (2014c), a multivariate technique is used to separate signal and background for events with each sign of qy_l, and for each bin of jet multiplicity $(3, \geq 4)$ and b-tag multiplicity (1,2). The unfold uses the response model of MC@NLO, and the results for each final state category are combined in a weighted average to yield $A_{FB}^\ell = 0.042 \pm 0.030$ (stat+syst), to be compared with the MC@NLO prediction of 0.02 ± 0.001 (statistical error only) for lepton pseudo-rapidity $|\eta| < 1.5$. The ratio $A_{FB}^\ell / A_{FB} = 0.44 \pm 0.27$ is consistent with the POWHEG prediction. This result differs considerably from the 5 fb^{-1} D0 measurement (Abazov *et al.*, 2011a), $A_{FB}^\ell = 0.152 \pm 0.040$, that used only the ℓ+4-jet sample. In the new measurement the large asymmetry in the ℓ+4-jet sample remains, but smaller asymmetries in the ℓ+3-jet samples reduce the overall inclusive value. The dependence of A_{FB}^ℓ on the lepton p_T in new physics models is discussed in Sec. VI.C. The dependence in the data is shown on the top panel in Fig. 9.

The D0 measurement of A_{FB}^ℓ in the dilepton mode uses 9.7 fb^{-1} (Abazov *et al.*, 2013b). Reconstructed electrons and muons must be isolated, have $p_T > 15$ GeV, and opposite signs. Events with like-flavor leptons must have two jets with $E_T > 20$ GeV; $e\mu$ events must have at least one such jet. A multivariate technique is used to require that jets are consistent with originating from b-quarks. Further specialized cuts select on the H_T and $\not{E}_T$ significance for each decay mode. The non-$t\bar{t}$ backgrounds to this selection are modeled using data sidebands, and subtracted from the data. The asymmetries are corrected for the finite lepton acceptance using a scale factor derived from MC@NLO. The asymmetries are found to be $A_{FB}^\ell = 0.044 \pm 0.039$ and $A_{FB}^{\ell\ell} = 0.123 \pm 0.056$. The dilepton A_{FB}^ℓ can be combined with the ℓ+jets result using scale factors obtained from Monte Carlo simulations. The combined asymmetry is $A_{FB}^\ell = 0.047 \pm 0.027$ (Abazov *et al.*, 2014b).

2. Leptonic asymmetries at CDF

The CDF Collaboration has also measured the leptonic asymmetry in both the ℓ+jets and dilepton decay modes. The ℓ+jets measurement (Aaltonen *et al.*, 2013b) uses the same sample as the $\cos\theta$ analysis of Sec. III.B.3, with a total sample of 3864 events and an expected non-$t\bar{t}$
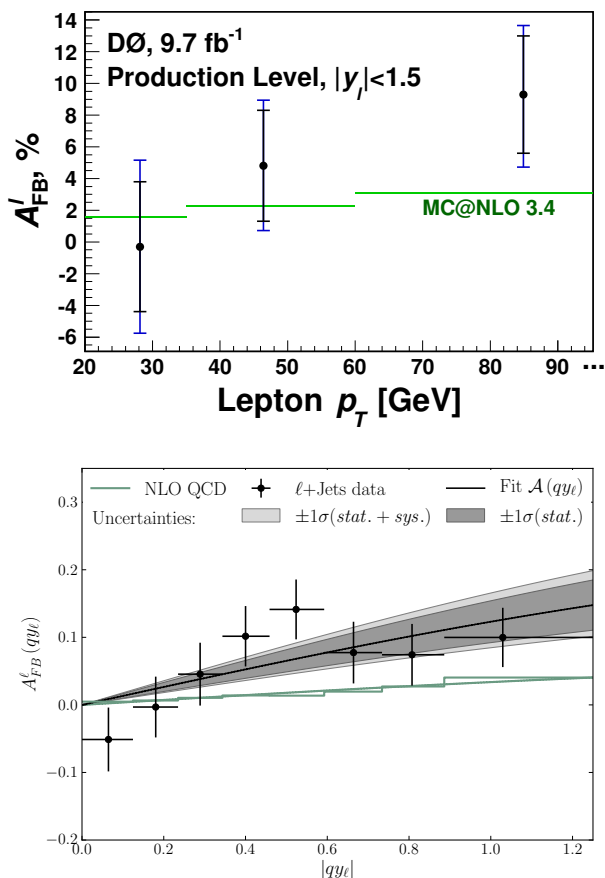
FIG. 9 Top: D0 $A_{\rm FB}^{\ell}$ versus lepton p_T in ℓ+jets, showing statistical/statistical+systematic uncertainties in black/blue. Bottom: $A_{FB}^{l}(qy_l)$ in CDF data with statistical uncertainties with best fit. From Aaltonen *et al.* (2013b) and Abazov *et al.* (2014b).

background of 1026 ± 210. The limited central lepton acceptance of the CDF detector $|\eta| \leq 1.2$ makes an unfolding correction for the full rapidity range impossible. Instead, the measurement relies on the observation that the asymmetric part of the asymmetry

$$A_{FB}^{l}(qy_l) = \frac{N(qy_l) - N(-qy_l)}{N(qy_l) + N(-qy_l)} \qquad (3.3)$$

is described by a simple phenomenological function $F(qy_l) = a \tanh(qy_l/2)$ for all models tested (Hong *et al.*, 2014), while the symmetric part is model independent. $A_{FB}^{l}(qy_l)$ in the measured region can be corrected for backgrounds and acceptance, and used to find the best fit to $F(qy_l)$ in the data. The function $F(qy_l)$ can then be extrapolated to the full rapidity range, and integrated with the model-independent symmetric part (using any generator), allowing a measurement of the production level asymmetry. The $A_{FB}^{l}(qy_l)$ distribution and fit, shown on the bottom in Fig. 9, gives a production level asymmetry of $A_{FB}^{\ell} = 0.094^{+0.032}_{-0.029}$.

The dilepton measurement is done in a sample of 9.1 fb^{-1} (Aaltonen *et al.*, 2014b). The selection requires exactly two opposite sign leptons with $p_T > 20$ GeV and combined invariant mass $m_{\ell\ell} > 10$ GeV/c, $\not{E}_T > 25$ GeV, two or more jets with $E_T > 15$ GeV and $|\eta| < 2.5$, and $H_T > 200$ GeV. A total of 569 events are found. The shape and normalization of the non-$t\bar{t}$ component is estimated with a combination of Monte Carlo and data driven techniques, giving an expected background of 160 ± 21 events. The measurement of A_{FB}^{ℓ} uses both leptons in each event, doubling the statistics. The results are $A_{FB}^{\ell} = 0.072 \pm 0.060$ and $A_{FB}^{\ell\ell} = 0.076 \pm 0.081$. The single lepton result here can be combined with the ℓ+jets channel to give an overall $A_{FB}^{\ell} = 0.090^{+0.028}_{-0.026}$. The ratio $A_{FB}^{\ell}/A_{FB} = 0.55 \pm 0.24$ is consistent with the NLO prediction.

Appealing, again, to the near independence of the CDF and D0 measurements, a simple error weighted average of the two gives a combined Tevatron $A_{FB}^{\ell} = 0.069 \pm 0.019$ compared to the NLO prediction of 0.038 ± 0.003 (Bernreuther and Si, 2012).

E. Tevatron summary

A compendium of the Tevatron measurements is shown in Fig. 10. With the final results from Run 2 at the Tevatron, the significance of the top A_{FB} and A_{FB}^{ℓ} discrepancies are around 1.5σ, with a spread between the two experiments of roughly 1σ. One of the most interesting experimental issues is the evolution of the D0 measurements toward smaller A_{FB}, reducing the tension with the SM suggested by the earlier results. An important part of that evolution was the addition of the 3-jet decay mode, which adds a statistically-independent sample, but also mixes in a different $p_T^{t\bar{t}}$ spectrum, raising the issue of the $p_T^{t\bar{t}}$ modeling for both experiments. The time development of the D0 measurements is discussed in further detail in Abazov *et al.* (2014b,c).

IV. EXPERIMENTAL MEASUREMENTS AT THE LHC

Following the end of operations of the Tevatron collider, measurements at the LHC are being carried out in an attempt to further clarify the experimental picture, which would otherwise remain inconclusive based on the measurements by the CDF and D0 Collaborations using the full dataset, discussed in the previous section. Despite the small $t\bar{t}$ asymmetries expected in pp collisions, the very high statistics $t\bar{t}$ samples available at the LHC can be exploited in the context of selections that are optimized to increase the fraction of $q\bar{q}$ events. This fact, together with the higher kinematic reach at the LHC, makes differential measurements of the charge asymmetry particularly interesting. Indeed, beyond confirming
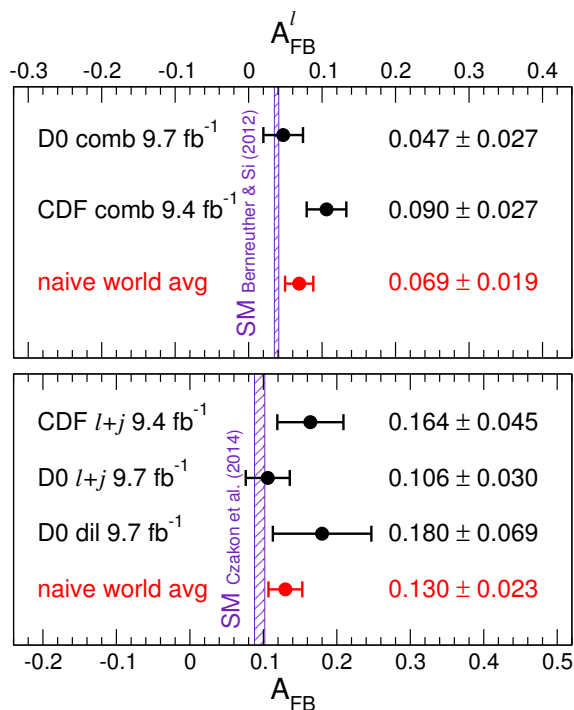
FIG. 10 Summary of A_{FB} and A_{FB}^{ℓ} measurements at the Tevatron

or ruling out the Tevatron anomaly, a new kinematic regime is being explored at the LHC that may unveil signs of new physics the Tevatron could not be sensitive to. Here we review the most recent results from the LHC Run 1 (2011-2012) and give some prospects for run 2.

A. Charge asymmetry measurements

Measurements of the charge asymmetry have been performed by the ATLAS and CMS Collaborations using the full datasets collected at CM energies of 7 TeV and 8 TeV. These measurements have been carried out in the ℓ+jets channel at 7 TeV and 8 TeV, and in the dilepton channel, so far only at 7 TeV.

The measurement of the charge asymmetry involves the reconstruction of the event kinematics under the $t\bar{t}$ hypothesis in order to determine the rapidities of the top quark and antiquark, c.f. Eq. (1.3). This is possible, not only in the ℓ+jets channel, where the presence of a single neutrino still leaves sufficient measurements for kinematic reconstruction, but also in the dilepton channel, where the a-priori under-constrained kinematics from the presence of two neutrinos can be overcome through the application of additional assumptions. The ability to reconstruct the event kinematics is exploited to measure the charge asymmetry differentially, as a function of $m_{t\bar{t}}$, $p_T^{t\bar{t}}$ and the rapidity of the $t\bar{t}$ system, $y_{t\bar{t}}$, in addition to inclusively. The reconstructed distributions used for these

measurements, $\Delta|y|$, as well as the above kinematic variables of the $t\bar{t}$ system, are distorted by effects related to selection efficiencies, detector resolution effects as well as ambiguities in the kinematic reconstruction. Unfolding techniques are used in order to correct these measurements to the parton level and thus be able to compare them with theoretical predictions.

1. Inclusive asymmetry in the ℓ+jets channel

The first measurement of the inclusive charge asymmetry at the LHC was performed by the CMS Collaboration in the ℓ+jets channel using a total integrated luminosity of 1.1 fb^{-1} at 7 TeV, about one fifth of the total dataset eventually cumulated at this CM energy. Since then, improved measurements using the full datasets at 7 TeV and 8 TeV have become available. Here we report only on those most precise measurements.

The ATLAS Collaboration has performed a measurement of the inclusive charge asymmetry in the ℓ+jets channel using the full dataset collected in 2011 at $\sqrt{s} = 7$ TeV, corresponding to an integrated luminosity of 4.7 fb^{-1} (Aad *et al.*, 2014b). Events were collected using single-lepton triggers. The offline selection requires exactly one isolated electron or muon with $p_T > 25$ GeV and $p_T > 20$ GeV, respectively. In order to suppress background from QCD multijets production, requirements are placed on $\not{E}_T$ and the transverse mass reconstructed from the lepton and $\not{E}_T$. In addition, it is required that the event has at least four jets reconstructed with the anti-k_t algorithm (Cacciari *et al.*, 2008) with a radius parameter $R = 0.4$ and satisfying $p_T > 25$ GeV and $|\eta| < 2.5$. In order to suppress background from W+jets production, at least one jet is required to be b-tagged. The typical per-jet b-tagging efficiency and light-jet mistag rate are 70% and 0.7%, respectively. This results in a selected sample of approximately 60000 events, with an estimated $t\bar{t}$ purity of 80%. Simulated $t\bar{t}$ events are modeled using the LO multi-parton matrix-element Monte Carlo generator ALPGEN (Mangano *et al.*, 2003) interfaced with HERWIG for the simulation of showering and fragmentation. After selection, the dominant background is W+jets production, whose normalization is estimated using data, while the shape of the distributions is estimated using the simulation. Smaller backgrounds originate from QCD multijets, single top, Z+jets and diboson production. With the exception of QCD multijets, which is entirely estimated from data, the remaining backgrounds are estimated with the simulation. A likelihood-based kinematic fit is used to reconstruct the 4-momenta of the top and antitop quarks. This likelihood calculation takes as input the measured kinematic quantities of the lepton, $\not{E}_T$ and the leading four jets, and employs transfer functions associating the measured variables to the parton-level ones. The ambigui-

ties resulting from the reconstruction of the leptonically-decaying W boson and the jet-parton assignments are solved by choosing the reconstruction hypothesis leading to the highest likelihood value. Figure 11 (top) displays the reconstructed $\Delta|y|$ distribution. Using simulated $t\bar{t}$
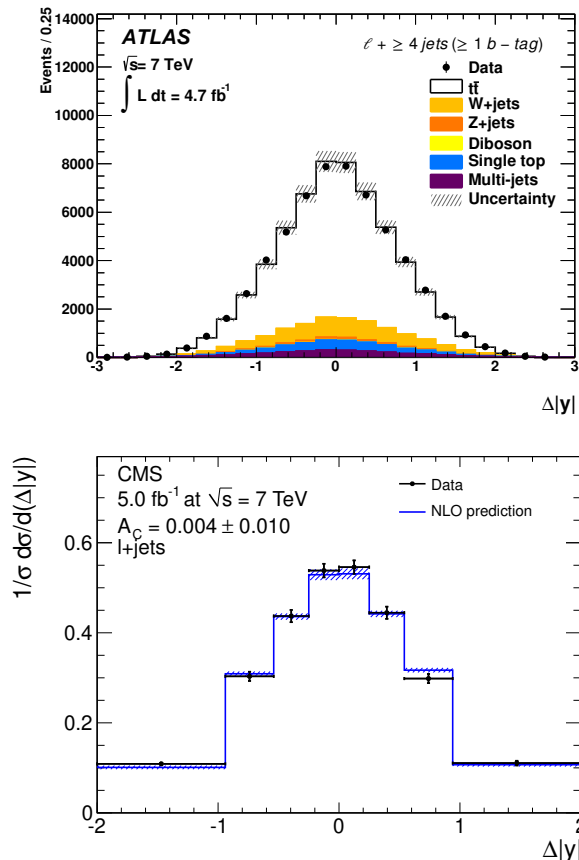

FIG. 11 Top: Reconstructed $\Delta|y|$ distribution after final selection in the ATLAS measurement. Data (dots) is compared to the prediction from the ALPGEN generator (solid line) and its total uncertainty (shaded area). Bottom: Unfolded $\Delta|y|$ distribution after final selection in the CMS measurement. Unfolded data (dots with error bars representing the total uncertainty) are compared to the SM prediction from Kuhn and Rodrigo (2012). The first and last bins include underflow and overflow events, respectively. From Aad *et al.* (2014b) and Chatrchyan *et al.* (2012).

events, the fraction of events with correctly reconstructed $\Delta|y|$ sign is $\approx 75\%$, corresponding to a dilution factor $D = 2 \times 0.75 - 1 = 0.5$. Such dilution results in a reduction by a factor of two of the measured asymmetry relative to the parton-level asymmetry, which is effectively corrected for by the unfolding procedure. After subtracting the background, the measured $\Delta|y|$ distribution is unfolded to the parton level and the charge asymmetry computed, yielding $A_C = 0.006 \pm 0.010\,(\text{stat}) \pm 0.005\,(\text{syst})$. This measurement is in agreement with the SM prediction of $A_C \simeq 0.0115$ (see Sec. II.C).

Similarly, the CMS Collaboration has performed a measurement of the inclusive charge asymmetry in the ℓ+jets channel using the full dataset collected at $\sqrt{s} = 7$ TeV, corresponding to an integrated luminosity of 5 fb^{-1} (Chatrchyan *et al.*, 2012). Events were collected using triggers requiring a single lepton together with at least three jets. The offline selection requires exactly one isolated electron or muon with $p_T > 30$ GeV and $p_T > 20$ GeV, respectively. In contrast to the ATLAS measurement, no minimum requirement on $\not{E}_T$ is made. In addition, it is required that the event has at least four jets reconstructed with the anti-k_t algorithm with a radius parameter $R = 0.5$ and satisfying $p_T > 30$ GeV and $|\eta| < 2.5$. Similar to the ATLAS measurement, a requirement of at least one b-tagged jet is made using an algorithm with a typical b-tagging efficiency of 60% and a light-jet mistag rate of 1%. The corresponding selected data sample has approximately 58000 events, with an estimated $t\bar{t}$ purity of also 80%. In the case of the CMS measurement, simulated $t\bar{t}$ events are modeled using the NLO event generator POWHEG interfaced with PYTHIA for the simulation of showering and fragmentation. The background composition is similar to the one in the ATLAS measurement, and similar strategies are used in the estimation of the background normalization and the modeling of its kinematics. The reconstruction of the 4-momenta of the top and antitop quarks is also based on a likelihood technique, in this case using as inputs the reconstructed invariant masses for the leptonic and hadronic top quarks, the hadronically-decaying W boson, and the b-tagging information of the jets assigned to the final state quarks. Also in this case the reconstruction hypothesis leading to the highest likelihood value is selected. The performance of this reconstruction technique is comparable to that of the ATLAS analysis. After subtracting the background, the measured asymmetry is unfolded to the parton level. Figure 11 (bottom) compares the unfolded $\Delta|y|$ distribution to the theoretical prediction. The resulting measured charge asymmetry is $A_C = 0.004 \pm 0.010\,(\text{stat}) \pm 0.011\,(\text{syst})$, also in agreement with the SM prediction and the ATLAS measurement.

The ATLAS and CMS measurements at $\sqrt{s} = 7$ TeV discussed above have been combined (Aad *et al.*, 2014a). The combination has been performed using the Best Linear Unbiased Estimate (BLUE) method (Lyons *et al.*, 1988; Valassi, 2003), taking into account a detailed categorization of systematic uncertainties and their correlation between both experiments. The combined result is $A_C = 0.005 \pm 0.007\,(\text{stat}) \pm 0.006\,(\text{syst})$, representing a 40% (18%) improvement with respect to the CMS (ATLAS) measurement.

The CMS Collaboration has also performed a measurement of the inclusive charge asymmetry in the ℓ+jets channel using the full dataset collected in 2012 at $\sqrt{s} = 8$ TeV, corresponding to an integrated luminosity of 20 fb^{-1} (Chatrchyan *et al.*, 2013b). This measurement
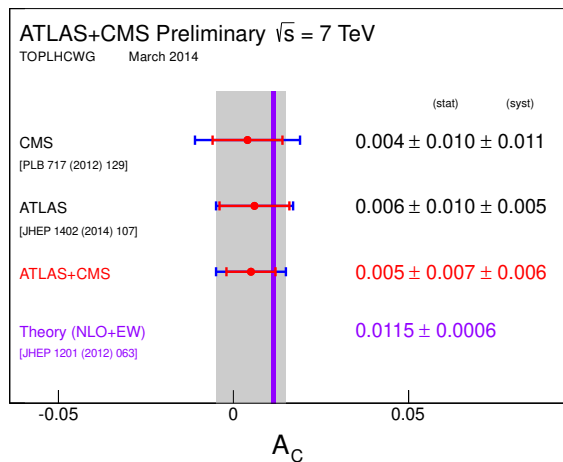
FIG. 12 Summary of the measurements of the inclusive charge asymmetry by the ATLAS and CMS Collaborations in the ℓ+jets channel at 7 TeV, as well as their combination, compared to the theoretical prediction. For each measurement, the outer blue (inner red) error bar indicates the total (statistical) uncertainty. The grey band illustrates the total uncertainty of the combined result. From Aad *et al.* (2014a).

follows closely the strategy for event selection, signal and background modeling, kinematic reconstruction, and unfolding technique used at the previous $\sqrt{s} = 7$ TeV measurement discussed above. The higher $t\bar{t}$ cross section at $\sqrt{s} = 8$ TeV and the 4-fold increase in the integrated luminosity results in a very large sample of approximately 375000 events, with an estimated $t\bar{t}$ purity of 80%. After subtracting the background, the measured asymmetry is unfolded to the parton level. The resulting charge asymmetry is $A_C = 0.005 \pm 0.007 \,(\text{stat}) \pm 0.006 \,(\text{syst})$. It is worth noting that the statistical uncertainty of this measurement does not scale as expected given the increased number of $t\bar{t}$ candidate events compared to the measurement at $\sqrt{s} = 7$ TeV: this is due to the increased number of bins used in the unfolding as well as the smaller improvement resulting from the use of regularization in presence of such large statistics in the data. This measurement has comparable precision to the combination of ATLAS and CMS measurements at $\sqrt{s} = 7$ TeV discussed above and is also in agreement with the SM prediction of $A_C \simeq 0.0102$.

2. Inclusive asymmetry in the dilepton channel

The ATLAS Collaboration has performed a measurement of the inclusive charge asymmetry in the dilepton channel using the full dataset at $\sqrt{s} = 7$ TeV, corresponding to 4.6 fb^{-1} (Aad *et al.*, 2015). Events were collected using single-lepton triggers, and required to have exactly two opposite-sign leptons (ee, $e\mu$, or $\mu\mu$), and at least two jets. The lepton and jet requirements are similar to those used in the measurement in the ℓ+jets channel. In order to suppress background from Z/γ^*+jets production, in the same-flavor dilepton channels the dilepton invariant mass is required to be more than 10 GeV away from the Z boson mass, and $\not{E}_T > 60$ GeV is required. The resulting selected data sample contains approximately 8000 events, with an estimated $t\bar{t}$ purity of 86%. Simulated $t\bar{t}$ events are modeled using the NLO Monte Carlo generator POWHEG interfaced with PYTHIA for the simulation of showering and fragmentation. After selection, the background is dominated by processes with prompt leptons, including Z+jets, single top and diboson production, which are estimated from the simulation. In addition, non-negligible contributions arise from processes with one or two jets misidentified as a lepton, resulting from QCD multijets or W+jets production, which are estimated in situ using data-driven techniques. The reconstruction of the $t\bar{t}$ kinematics is performed using the neutrino weighting technique (Abbott *et al.*, 1998). This technique scans different hypotheses for the values of the pseudorapidities of the two neutrinos in the final state. For each hypothesis, it calculates the full event kinematics assuming the W boson and top quark masses, and then assigns a weight to the resulting solution based on the level of agreement between the calculated and measured missing transverse momentum. Jet energy measurements are accounted for by fluctuating the jet energies within the expected resolutions, and all possible lepton-jet associations are considered. Finally, the solution corresponding to the maximum weight is chosen to represent the event. Figure 13 (top) displays the reconstructed $\Delta|y|$ distribution in the $e\mu$ channel. After subtracting the background, the measured $\Delta|y|$ distributions in the ee, $e\mu$ and $\mu\mu$ channels are unfolded to the parton level and the corresponding charge asymmetries computed. The combination of the measurements in the three channels using the BLUE method yields $A_C = 0.021 \pm 0.025 \,(\text{stat}) \pm 0.017 \,(\text{syst})$.

Similarly, the CMS Collaboration has performed a measurement of the inclusive charge asymmetry in the dilepton channel using the full dataset at $\sqrt{s} = 7$ TeV, corresponding to 5 fb^{-1} (Chatrchyan *et al.*, 2014c). Events were collected using dilepton triggers, and required to have exactly two opposite-sign leptons (ee, $e\mu$, or $\mu\mu$) with $p_T > 20$ GeV and at least two jets. The jet requirements are the same as in the measurement in the ℓ+jets channel. In contrast with the ATLAS measurement, at least one jet is required to be b-tagged. The typical per-jet b-tagging efficiency and light-jet mistag rate are 70% and 1.5%, respectively. In the same-flavor dilepton channels the dilepton invariant mass is required to be above 20 GeV and more than 15 GeV away from the Z boson mass in order to suppress background from Z/γ^*+jets and heavy-quarkonium resonance production. In addition, a requirement of $\not{E}_T > 40$ GeV is made.
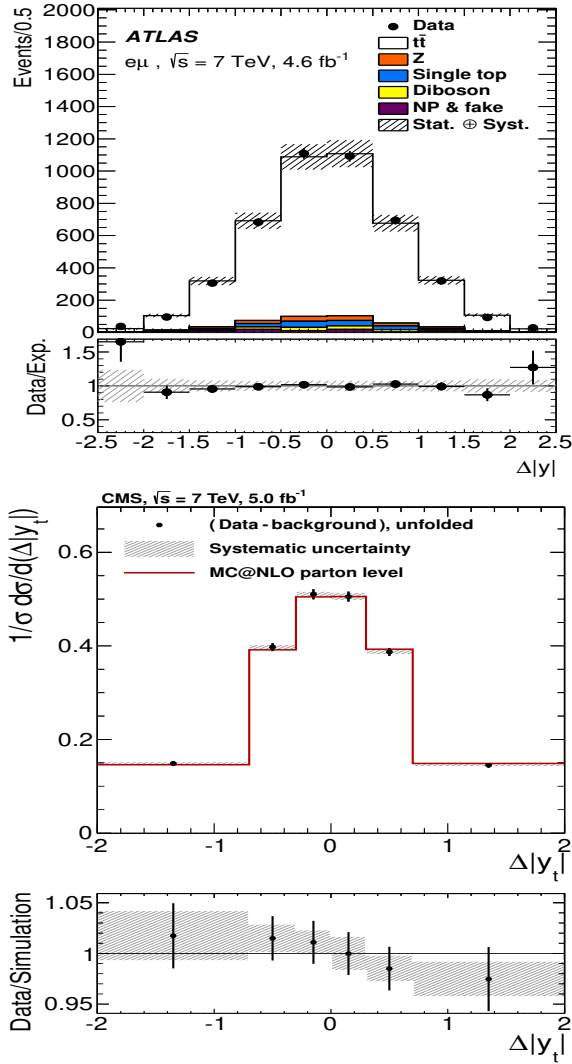
FIG. 13 Top: Reconstructed $\Delta|y|$ distribution in the $e\mu$ channel in the ATLAS measurement. Data (dots) is compared to the prediction from the POWHEG generator (solid line) and its total uncertainty (shaded area). Bottom: Unfolded $\Delta|y|$ distribution after final selection in the CMS measurement. Unfolded data (dots with error bars representing the stat uncertainty and hatched bands representing the systematic uncertainty) are compared to the MC@NLO prediction. The bottom panel displays the ratio between the data and the MC@NLO prediction. The first and last bins include underflow and overflow events, respectively. From Aad *et al.* (2015) and Chatrchyan *et al.* (2014c).

The resulting selected data sample contains approximately 10000 events, with an estimated $t\bar{t}$ purity of 92%. The increased purity, compared to the ATLAS measurement, results from the b-tagging requirement. Simulated $t\bar{t}$ events are modeled using MC@NLO interfaced with HERWIG. After selection, the background is dominated by single top production, followed by Drell-Yan and $t\bar{t}$ non-dileptonic backgrounds. The reconstruction

of the $t\bar{t}$ kinematics is performed using a weighting technique, referred to as Analytical Matrix Weighting Technique (Chatrchyan *et al.*, 2011a), similar in spirit to the one used in the ATLAS measurement. Each event can have up to 8 possible solutions for the $t\bar{t}$ system, each of which is assigned a weight based on the probability of observing the given configuration. The solution with the highest weight is selected to reconstruct the $t\bar{t}$ kinematics. About 14% of events have no solution, which is taken as an additional selection requirement. After subtracting the background, the measured asymmetry is unfolded to the parton level. Figure 13 (bottom) compares the unfolded $\Delta|y|$ distribution to the theoretical prediction. The resulting measured charge asymmetry is $A_C = -0.010 \pm 0.017\,(\text{stat}) \pm 0.008\,(\text{syst})$.

3. Kinematic dependence of the asymmetry

Given the small expected inclusive charge asymmetry at the LHC, comparable to the experimental uncertainties, it is of particular importance to measure the charge asymmetry differentially, as a function of variables that are suitable to enhance it in particular kinematic regions, especially those where new physics effects may be more apparent. The ATLAS and CMS Collaborations have measured the charge asymmetry as a function of $p_T^{t\bar{t}}$, $y_{t\bar{t}}$ and $m_{t\bar{t}}$, each of which is particularly sensitive to a certain aspect. The ATLAS Collaboration has measured the charge asymmetry as a function of the above kinematic variables in the ℓ+jets channel using the full dataset at 7 TeV. The CMS Collaboration has performed similar measurement in the ℓ+jets channel, at both 7 TeV and 8 TeV. These measurements are based on the analyses described in Sec. IV.A.1.

As discussed in Sec. II, the transverse momentum of the $t\bar{t}$ system provides sensitivity to the different diagrams contributing to the charge asymmetry with different sign. The low $p_T^{t\bar{t}}$ region is dominated by the Born and box diagrams, whose interference results in a positive contribution to the charge asymmetry, while the high $p_T^{t\bar{t}}$ region should be dominated by events with an extra jet in the final state, often originating from initial or final-state radiation diagrams, whose interference results in a negative contribution to the charge asymmetry. Figure 14 shows the unfolded A_C measurements as a function of $p_T^{t\bar{t}}$ from the ATLAS and CMS Collaborations. Good agreement is found with the SM prediction within the experimental uncertainties.

The rapidity of the $t\bar{t}$ system in the laboratory frame, $|y_{t\bar{t}}|$, is sensitive to the ratio of contributions from the $q\bar{q}$ and gg initial states to $t\bar{t}$ production, and thus provides a means to enhance the charge asymmetry by increasing the $q\bar{q}$ fraction (Kuhn and Rodrigo, 2012). Indeed, $t\bar{t}$ events produced through gg fusion will tend to populate the central rapidity region, while $q\bar{q}$-mediated produc-
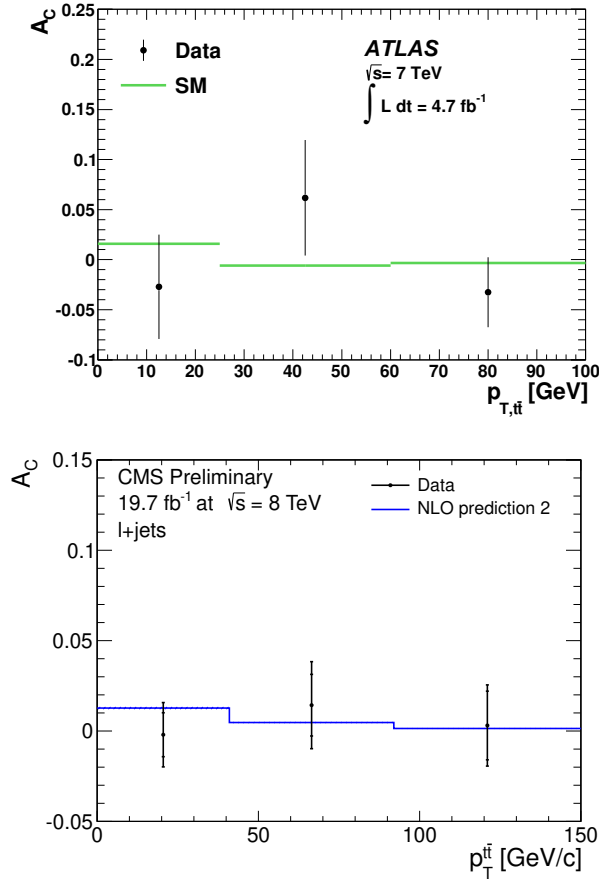
FIG. 14 A_C as a function of $p_T^{t\bar{t}}$ from the ATLAS measurement (top) and the CMS measurement (bottom). Unfolded data (dots with error bars representing the total uncertainty) are compared to the SM prediction from Bernreuther and Si (2012). From Aad *et al.* (2014b) and Chatrchyan *et al.* (2013b).

FIG. 15 A_C as a function of $y_{t\bar{t}}$ from (top) the ATLAS measurement and (bottom) the CMS measurement. Unfolded data (dots with error bars representing the total uncertainty) are compared to the SM predictions from Kuhn and Rodrigo (2012) (NLO prediction 1) and Bernreuther and Si (2012) (NLO prediction 2, also referred to as SM in the top figure). Also shown are the predictions for an axigluon exchanged in the s-channel for two assumed mass values (Aguilar-Saavedra and Pérez-Victoria, 2011d), as well as for an effective axial-vector coupling of the gluon (EAG) (Gabrielli *et al.*, 2012). From Aad *et al.* (2014b) and Chatrchyan *et al.* (2013b).

tion will typically result in $t\bar{t}$ events boosted along the beam direction and thus having larger values of $|y_{t\bar{t}}|$. A requirement on minimum $|y_{t\bar{t}}|$ is equivalent to a requirement on the z-component of the $t\bar{t}$-system velocity, $\beta_z^{t\bar{t}}$, since $y_{t\bar{t}} = 1/2 \log[(1 + \beta_z^{t\bar{t}})/(1 - \beta_z^{t\bar{t}})]$ (Aguilar-Saavedra *et al.*, 2012b). The ATLAS Collaboration has measured the inclusive charge asymmetry after the requirement of $\beta_z^{t\bar{t}} > 0.6$, obtaining $A_C = 0.011 \pm 0.017\,(\text{stat}) \pm 0.007\,(\text{syst})$, in good agreement with the SM prediction of $A_C = 0.020^{+0.006}_{-0.007}$ (Bernreuther and Si, 2012). Figure 15 shows the unfolded A_C measurements as a function of $y_{t\bar{t}}$ from the ATLAS and CMS Collaborations. Again, good agreement is found with the SM prediction within the experimental uncertainties.

Finally, the dependence of the charge asymmetry on the invariant mass of the $t\bar{t}$ system, $m_{t\bar{t}}$, is particularly interesting because of its sensitivity to new heavy particles mediating $t\bar{t}$ production, whose amplitudes would interfere with the SM ones, leading to additional con-
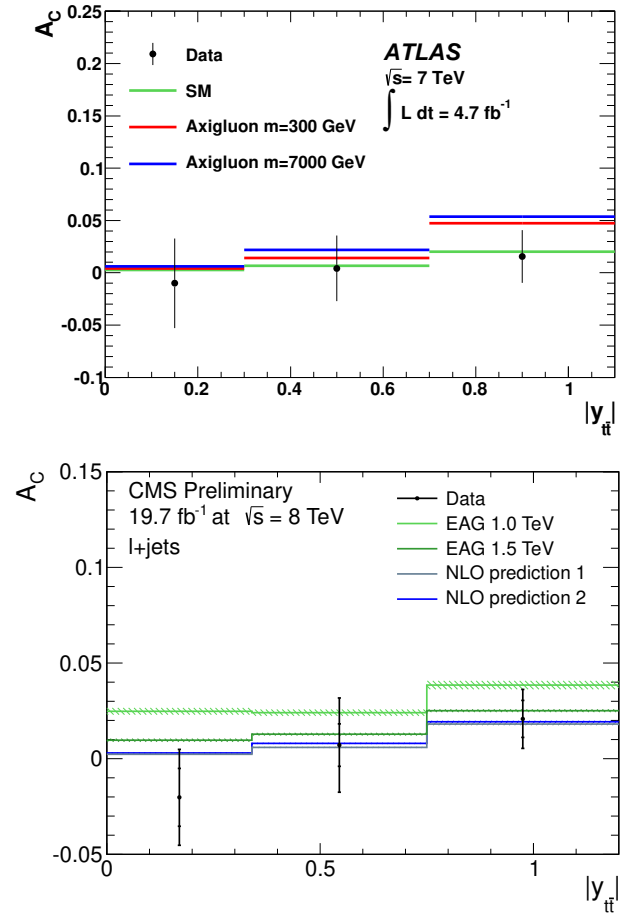
tributions (positive or negative) to the charge asymmetry. The ATLAS Collaboration has measured the inclusive charge asymmetry after the requirement of $m_{t\bar{t}} > 600$ GeV, obtaining $A_C = 0.018 \pm 0.021\,(\text{stat}) \pm 0.005\,(\text{syst})$, in good agreement with the SM prediction of $A_C = 0.0175^{+0.0005}_{-0.0004}$ (Bernreuther and Si, 2012). More interesting is the differential measurement of the charge asymmetry as a function of $m_{t\bar{t}}$, shown in Figure 16 for both the ATLAS and CMS Collaborations. In addition, the ATLAS Collaboration has measured this distribution after the requirement of $\beta_z^{t\bar{t}} > 0.6$, shown in Fig. 17 in an attempt to further increase the $q\bar{q}$ fraction, and thus the sensitivity to new physics contributions. Such measurement, currently limited by statistical uncertainties, will

become more interesting with the full dataset at 8 TeV. All differential measurements as a function of $m_{t\bar{t}}$ are found to be in good agreement with the SM predictions.
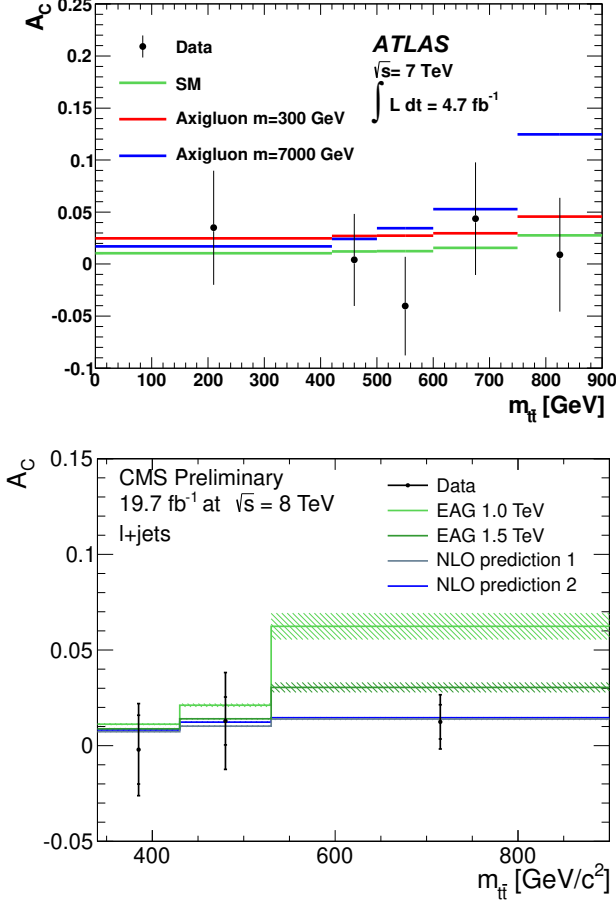

FIG. 16 A_C as a function of $m_{t\bar{t}}$ from (top) the ATLAS measurement and (bottom) the CMS measurement. Unfolded data (dots with error bars representing the total uncertainty) are compared to the SM predictions from Kuhn and Rodrigo (2012) (NLO prediction 1) and Bernreuther and Si (2012) (NLO prediction 2, also referred to as SM in the top figure). Also shown are the predictions for an axigluon exchanged in the s-channel for two assumed mass values (Aguilar-Saavedra and Pérez-Victoria, 2011d), as well as for an effective axial-vector coupling of the gluon (EAG) (Gabrielli et al., 2012). From Aad et al. (2014b) and Chatrchyan et al. (2013b).

While preliminary combinations of ATLAS and CMS measurements of the inclusive asymmetry are starting to become available, so far only in the ℓ+jets channel at 7 TeV (see Sec. IV.A.1), combinations of the differential measurements have not yet performed, owing to different choices in binning for these kinematic variables adopted by the Collaborations. It would be important to harmonize these choices in the near future, in order to be able to maximally exploit the LHC measurements through their quantitative comparison and eventual combination.
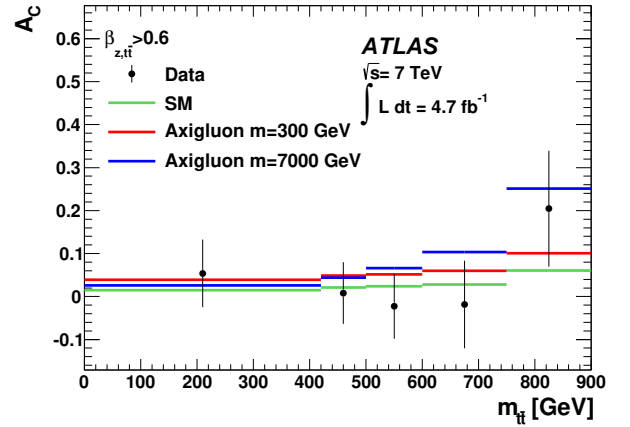

FIG. 17 A_C as a function of $m_{t\bar{t}}$ after the requirement $\beta_z^{t\bar{t}} > 0.6$ from the ATLAS measurement. Unfolded data (dots with error bars representing the total uncertainty) are compared to the SM prediction from Bernreuther and Si (2012). Also shown are the predictions for an axigluon exchanged in the s-channel for two assumed mass values (Aguilar-Saavedra and Pérez-Victoria, 2011d). From Aad et al. (2014b).

B. Leptonic asymmetry measurements

Measurements of the leptonic asymmetry at the LHC have so far only been performed in the dilepton channel. In this case, the observable used is $A_C^{\ell\ell}$, based on the difference of the absolute values if the pseudorapidities of the positive and negative leptons (see Eq. 2.12). Although this asymmetry is diluted by the top quark decay, it has the advantage that it can be measured without reconstructing the $t\bar{t}$ kinematics, and especially the fact that it has a very small experimental dilution owing to the precise lepton reconstruction at the LHC experiments. Existing measurements by the ATLAS and CMS Collaborations are based on the analyses described in Sec. IV.A.2.

Both ATLAS and CMS have measured the inclusive $A_C^{\ell\ell}$ at 7 TeV obtaining $A_C^{\ell\ell} = 0.024 \pm 0.015\,(\text{stat}) \pm 0.009\,(\text{syst})$ and $A_C^{\ell\ell} = 0.009 \pm 0.010\,(\text{stat}) \pm 0.006\,(\text{syst})$, respectively, in good agreement with the SM prediction of $A_C^{\ell\ell} = 0.0070 \pm 0.0003$. In addition, the CMS experiment has measured $A_C^{\ell\ell}$ differentially as a function of $p_T^{t\bar{t}}$, $y_{t\bar{t}}$ and $m_{t\bar{t}}$, taking advantage of the kinematic reconstruction performed and discussed in Sec. IV.A.2. Figure. 18 shows the unfolded $A_C^{\ell\ell}$ as a function of $y_{t\bar{t}}$ and $m_{t\bar{t}}$, compared to the parton-level predictions from the MC@NLO generator.

C. LHC summary

A summary of the inclusive A_C and $A_C^{\ell\ell}$ measurements by the ATLAS and CMS Collaborations is shown in Fig. 19. Also shown are simple error-weighted averages
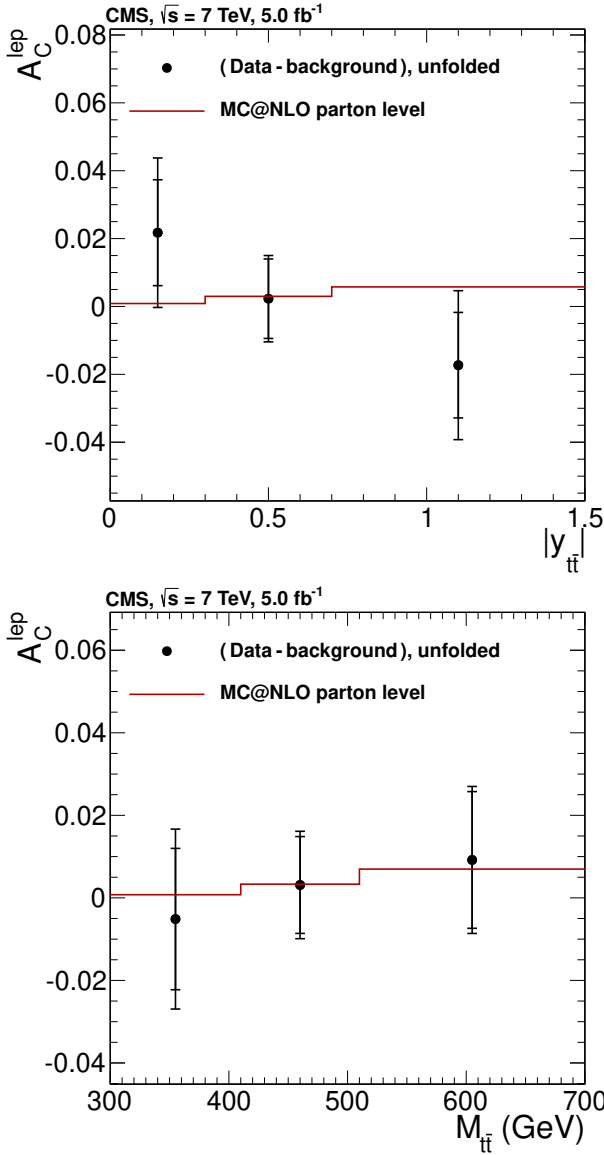
FIG. 18 Top: $A_C^{\ell\ell}$ as a function of $y_{t\bar{t}}$. Bottom: $A_C^{\ell\ell}$ as a function of $m_{t\bar{t}}$. In these figures $A_C^{\ell\ell}$ are denoted by A_C^{lep}. Both measurements are from the CMS Collaboration. Unfolded data (dots with error bars representing the total uncertainty) are compared to the parton-level predictions from MC@NLO. From Chatrchyan et al. (2014c).
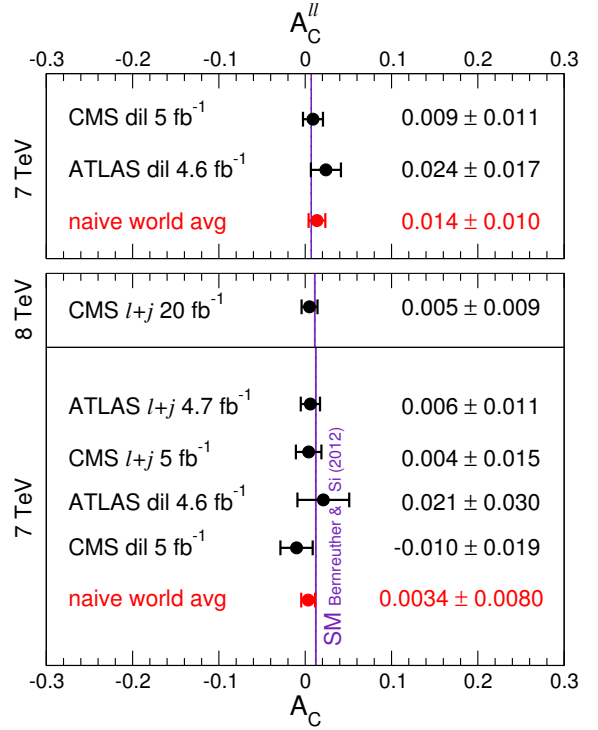

FIG. 19 Summary of inclusive A_C and $A_C^{\ell\ell}$ measurements by the ATLAS and CMS Collaborations, compared to the respective SM predictions. The uncertainties on the experimental measurements include both statistical and systematic contributions. Also shown are simple error-weighted averages of ATLAS and CMS measurements at 7 TeV.

D. Future LHC prospects

Because of the increased importance of $gg \to t\bar{t}$ with rising CM energy, the predicted SM asymmetry for the second LHC run is roughly one half of the asymmetry for $7-8$ TeV, i.e. $A_C = 0.0067 \pm 0.0004$ at 14 TeV (Bernreuther and Si, 2012). The measurement will be difficult and demanding, and, likely, rather unconclusive. If one assumes that the systematic uncertainties will be of the same magnitude as in current measurements (this may be too optimistic due to the increased pile-up), the uncertainty will still be of the same order as the asymmetry itself, with the disadvantage with respect to $7, 8$ TeV that potential deviations from the SM are further smeared by gg fusion. On the other hand, one can exploit the high $t\bar{t}$ statistics to make measurements at high $\beta_z^{t\bar{t}}$, $m_{t\bar{t}}$ or $|y_t|$, where the SM prediction is larger. In this respect, an interesting proposal is to exploit the large coverage of the LHCb detector to make measurements in the very forward region $2 \leq |y_t| \leq 5$ (Kagan et al., 2011).

The large luminosity and cross sections at the second LHC run will also allow for measurements in the production of $t\bar{t}$ pairs in association with a photon (Aguilar-Saavedra et al., 2014) or a W boson (Maltoni et al., 2014).

for the 7 TeV measurements, neglecting correlations in systematic uncertainties between both experiments. All measurements so far are found to be consistent with the SM predictions. The complete set of inclusive measurements using the full 8 TeV dataset, as well as differential measurements combining multiple channels within and across experiments would be quite important for more precise tests.

A charge asymmetry can be also defined in these processes as in (1.3),

$$A_C^{t\bar{t}\gamma, t\bar{t}W} = \frac{N(\Delta|y| > 0) - N(\Delta|y| < 0)}{N(\Delta|y| > 0) + N(\Delta|y| < 0)}. \quad (4.1)$$

In $t\bar{t}\gamma$, the presence of the photon enhances the $q\bar{q}$ fraction with respect to $t\bar{t}$ production, since a photon cannot be emitted from initial gluons (and radiative top decay $t \to Wb\gamma$ can be suppressed with suitable kinematical cuts). Additionally, the extra photon changes the relative importance of $u\bar{u}$ and $d\bar{d}$ contributions, since it couples differently to up and down quarks. We show in Fig. 20 the $q\bar{q}$ fraction $F_u + F_d$ and the ratio F_d/F_u for $t\bar{t}(\gamma)$ production at the LHC with 8 and 14 TeV, as well as for $t\bar{t}$ at the Tevatron. The presence of the extra photon is much more effective to "approach" the Tevatron point than kinematical cuts on $\beta_z^{t\bar{t}}$ or $m_{t\bar{t}}$.
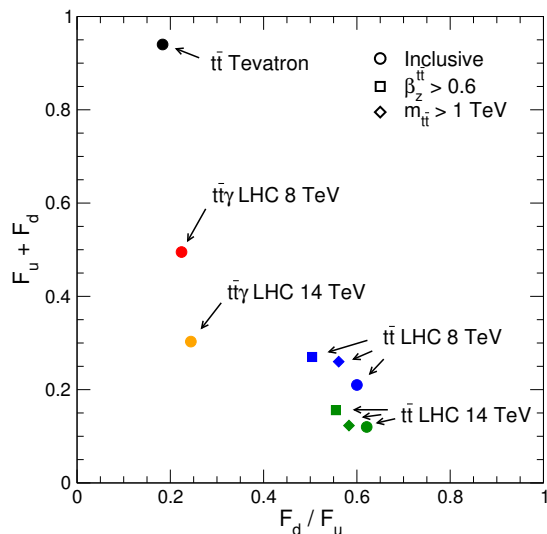

FIG. 20 $F_d/F_u = \sigma(d\bar{d})/\sigma(u\bar{u})$ and $q\bar{q}$ fraction $F_u + F_d$ for $t\bar{t}$ and $t\bar{t}\gamma$ production in the SM. For comparison, we also plot these quantities in $t\bar{t}$ production after imposing high-$m_{t\bar{t}}$ or high-$\beta_z^{t\bar{t}}$ requirements. From Aguilar-Saavedra et al. (2014).

Within the SM the asymmetry in $t\bar{t}\gamma$, $A_C^{t\bar{t}\gamma} = -0.038$ at 14 TeV, appears already at the tree level, due to the interference of photon emission in the initial state and from a top quark. New physics can also contribute to this asymmetry. Intriguingly, if there exists some conspiracy between new physics contributions in $u\bar{u}$ and $d\bar{d}$ initial states to render a SM-like A_C in $t\bar{t}$ production at the LHC (see Sec. II.C), a measurement of the asymmetry in $t\bar{t}\gamma$ could uncover it, since the balance between these contributions is different for this process. This is shown in Fig. 21, using as new physics benchmark a new color octet with mass $M = 250$ GeV and arbitrary couplings to the up, down and top quark that give a good fit to all $t\bar{t}$ data. It is observed that, even when the asymmetry

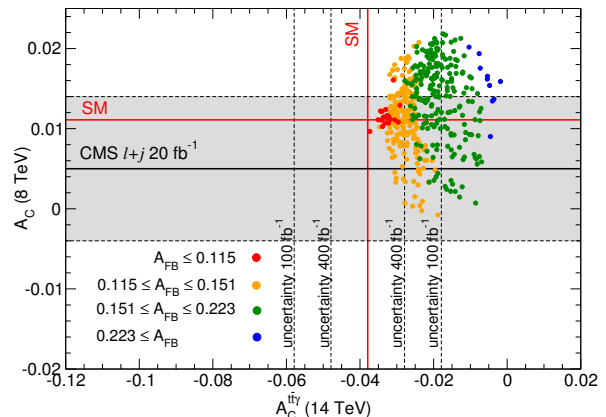in $t\bar{t}$ is close to the SM prediction, there can be sizeable deviations in $t\bar{t}\gamma$.

FIG. 21 Charge asymmetry $A_C^{t\bar{t}\gamma}$ in $t\bar{t}\gamma$ at 14 TeV versus A_C at 8 TeV for points in the parameter space of a new color octet. The horizontal band is the current 8 TeV measurement in Chatrchyan et al. (2013b) and its uncertainty. The vertical dashed lines represent the expected statistical uncertainty for 100 fb^{-1} and 400 fb^{-1}. The SM predictions are also included. From Aguilar-Saavedra et al. (2014).

An independent handle is provided by $t\bar{t}W^{\pm}$ production. At LO, $t\bar{t}W^+$ ($t\bar{t}W^-$) can only be produced from $u\bar{d}, c\bar{s}$ ($\bar{u}d, \bar{c}s$) states, and symmetric gg fusion only contributes at NNLO. Hence the asymmetry generated is also larger than in the SM, $A_C^{t\bar{t}W} = 0.022^{+0.0043}_{-0.0033}$ at NLO for 14 TeV (Maltoni et al., 2014).[4] New physics can also contribute to this asymmetry, and the deviations with respect to the SM prediction may be more significant than in $t\bar{t}$ production. This is demonstrated in Fig. 22, using as new physics benchmark a color octet with mass $M = 200$ GeV (labelled as I, II) and $M = 2$ TeV (III, IV). The coupling is chosen as left-handed (I, III) or axial (II, IV). (For a purely right-handed coupling to the light quarks the contribution of the octet to the amplitude vanishes and its presence would be unnoticed in $t\bar{t}W^{\pm}$.) The upper panel corresponds to the asymmetry in $t\bar{t}$, and the lower panel to the asymmetry in $t\bar{t}W^{\pm}$.

V. NEW PHYSICS INTERPRETATIONS

An appealing possibility is that the deviations between (some of) the experimental results and the SM predictions for A_{FB} are a signal of new physics in $t\bar{t}$ production. This would agree well with the general expectation that the top quark may be particularly sensitive to

---

[4] In this reference, the asymmetry is built using the t, $\bar{t}$ pseudo-rapidities rather than the rapidities; the difference with respect to the asymmetry defined from rapidities is small. Also, NLO denominators are used.
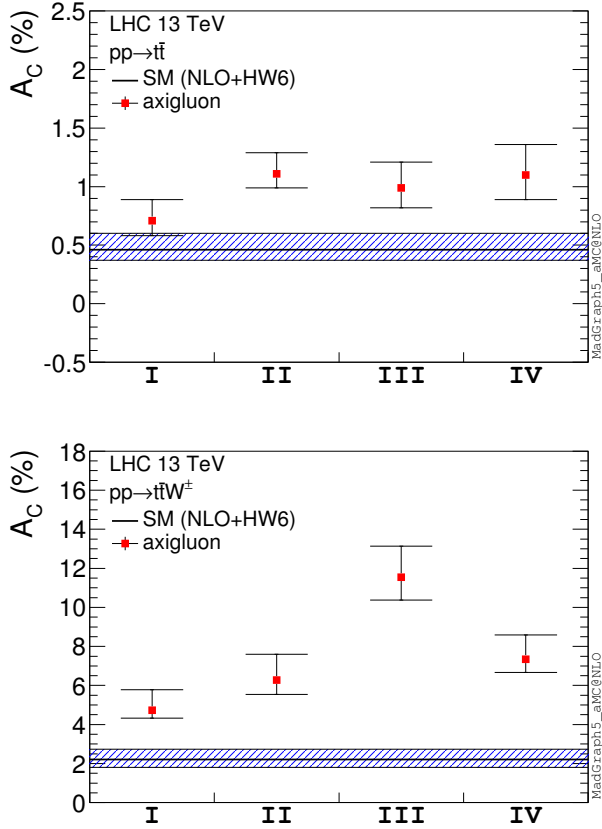
FIG. 22 Top: Charge asymmetry in $t\bar{t}$ production at 13 TeV for the SM (horizontal band) and four benchmark points of a color octet, labelled as "axigluon". Bottom: The same, but in $t\bar{t}W^{\pm}$ production. From Maltoni *et al.* (2014).

new physics in the electroweak breaking sector, due to its large Yukawa coupling.[5] In the last few years, different extensions of the SM have been proposed to explain the excess of the measured A_{FB}. To match the experimental central values, the new-physics contribution must be comparable to the SM one. Then, some effects in other observables, either in $t\bar{t}$ production or elsewhere, can be generically expected. We discuss them in sections VI and VII, respectively. These effects often translate into strong constraints on viable explanations.

The most obvious constraint is already used in this section as a first filter to select the possible new physics that

---

[5] This is actually the case in many popular explicit models. For instance, in composite-Higgs models, the large Yukawa coupling of the top quark arises from the fact that it is mostly composite. Therefore, it couples strongly to the resonances of the composite sector. These resonances could thus mediate top-quark pair production and contribute to the charge asymmetries. More generally, all natural scenarios of electroweak symmetry breaking introduce new particles associated to the top-quark to partially cancel its large radiative contributions to the Higgs mass. These particles often give rise to new effects in the top-quark sector.

could explain the discrepancies. It comes from the agreement of the SM prediction of the total cross section at Tevatron, $\sigma_{\mathrm{SM}} = 7.5 \pm 0.5$ pb (Aliev *et al.*, 2011), and the measured value, $\sigma_{\exp} = 7.60 \pm 0.41$ pb (Aaltonen *et al.*, 2014a). Writing the cross section in the presence of new physics as $\sigma = \sigma_{\mathrm{SM}} + \delta\sigma_{\mathrm{int}} + \delta\sigma_{\mathrm{quad}}$, this agreement implies that the interference between SM and new-physics amplitudes, $\delta\sigma_{\mathrm{int}}$, and the modulus square of the new-physics amplitude, $\delta\sigma_{\mathrm{quad}}$, must satisfy the condition

$$\delta\sigma_{\mathrm{int}} + \delta\sigma_{\mathrm{quad}} \simeq 0. \qquad (5.1)$$

This equation requires $\sigma_{\mathrm{int}} \lesssim 0$, since $\delta\sigma_{\mathrm{quad}}$ is positive semidefinite. To obtain a tighter bound, let us decompose $\delta\sigma = \delta\sigma^F + \delta\sigma^B$, where $\delta\sigma^F$ and $\delta\sigma^B$ represent the contributions of the forward and backward hemispheres, respectively, to the corresponding terms in the cross section. Eq. (5.1) allows us to approximate the new-physics contribution to the FB asymmetry, $\Delta A_{FB} = A_{FB} - A_{FB}^{\mathrm{SM}}$, as

$$\Delta A_{FB} \simeq \frac{\delta\sigma_{\mathrm{int}}^F - \delta\sigma_{\mathrm{int}}^B + \delta\sigma_{\mathrm{quad}}^F - \delta\sigma_{\mathrm{quad}}^B}{\sigma_{\mathrm{SM}}}. \qquad (5.2)$$

Because the term $\delta\sigma_{\mathrm{quad}}^B$ is positive semidefinite, the model-independent condition (5.1) implies, in particular, $\delta\sigma_{\mathrm{int}}^B \lesssim -\frac{1}{2}\Delta A_{FB}\sigma_{\mathrm{SM}}$. A sizable positive A_{FB}^{new} thus requires a sizable and negative $\delta\sigma_{\mathrm{int}}^B$ (Grinstein *et al.*, 2011a). So, we learn that new physics interfering with the SM amplitudes—with the tree-level ones for a significant effect—is preferred. Conversely, incoherent new physics (see Isidori and Kamenik, 2011 for an example) cannot generate a large asymmetry.

The restrictions on new physics stemming from Eq. (5.1) are much stronger than the plain requirement of interference, which in practice is quite mild. We can distinguish two scenarios:

- *Linear new physics.* If $\delta\sigma_{\mathrm{int}} \simeq 0$, the quadratic terms $\delta\sigma_{\mathrm{quad}}^{F,B}$ must be suppressed, so sizable corrections to the asymmetry come from the interference terms only. The suppression of quadratic terms is natural when the scale of new physics is large or its couplings to the SM fields small.

- *Quadratic new physics.* If $\delta\sigma_{\mathrm{int}}$ is sizable (and necessarily negative), ΔA_{FB} can be produced by interference and/or quadratic contributions, with the same or opposite sign. In this scenario, the cancellation (5.1) is non-trivial. This has important consequences: First, the parameters of the theory have to be tuned, generically, as they appear with different powers in both terms. Second, to give rise to sizable quadratic contributions, the new physics must either be present at low scales (below 1 TeV) or couple strongly to the SM. Third, this cancellation, imposed at the Tevatron relevant energies, needs not hold at higher energies. As discussed in

Sec. VI, this typically leads to an excess in the LHC $t\bar{t}$ cross section at high values of $m_{t\bar{t}}$.

As customary, we neglect in the following the interference of new physics with NLO QCD amplitudes. The error in the asymmetry in this approximation can be estimated to be smaller than or comparable to A_{FB}^{SM}, in the linear and quadratic scenarios, respectively.

A. Heavy new physics

If the new degrees of freedom are heavy in comparison with Tevatron and LHC energies, their effect can be parametrized model-independently by an effective Lagrangian that involves only the SM fields. In view of the recent experimental results in Higgs physics (Aad *et al.*, 2014c; Chatrchyan *et al.*, 2014a), we include the Higgs doublet explicitly as a SM field, and assume that electroweak symmetry is broken by a vacuum expectation value of this field, just as in the SM. In the electroweak symmetric phase, the effective Lagrangian must be invariant under $SU(3)_C \times SU(2)_L \times U(1)_Y$ gauge transformations. It can expanded as

$$\mathcal{L}_{\text{eff}} = \mathcal{L}_{\text{SM}} + \sum_{n=1}^{\infty} \frac{1}{\Lambda^n} \sum_{i=1}^{r_n} \left[C_i^{(n)} \mathcal{O}_i^{(n)} + \text{h.c.} \right], \quad (5.3)$$

where $\mathcal{L}_{\text{SM}}$ is the SM Lagrangian, Λ is the characteristic scale of new physics, $C_i^{(n)}$ are dimensionless coefficients and $\mathcal{O}_i^{(n)}$ are local gauge-invariant operators of dimension $4+n$. The expansion (5.3) is appropriate for decoupling new physics, which can be either weakly or strongly interacting. This is related to the renormalizability of $\mathcal{L}_{\text{SM}}$. The first terms are expected to be give a good approximation for processes with typical energy $E \ll \Lambda$. In the case of $t\bar{t}$ production, we have $E \lesssim m_{t\bar{t}}$.

The $t\bar{t}$ cross section and asymmetry calculated with $\mathcal{L}_{\text{eff}}$ inherit this perturbative structure. The first corrections to the SM predictions appear at order $1/\Lambda^2$, from the interference of the SM amplitude with an amplitude that has one insertion of a dimension-6 operator. These are the only effects that need to be taken into account in the linear scenario. For the quadratic scenario, on the other hand, we also need to consider $1/\Lambda^4$ corrections. They can arise in three different manners: (i) from the interference of the SM amplitude with an amplitude with two insertions of dimension-6 operators; (ii) from the modulus square of an amplitude with one insertion of a dimension-6 operator; (iii) from the interference of the SM amplitude with an amplitude with one insertion of a dimension-8 operator.

The contributions of the third kind depend on many free parameters and have always been neglected in the literature. Several arguments have been given to justify this approximation (Aguilar-Saavedra and Pérez-Victoria, 2011c; Delaunay *et al.*, 2011). Let us consider

a fixed scale Λ, much larger than the $t\bar{t}$ invariant masses that the Tevatron and the LHC can produce. If the series is to converge rapidly, it is plausible that the coefficients $C_i^{(4)}$ are not larger than the coefficients $C_i^{(2)}$, to ensure that $C_i^{(4)} m_{t\bar{t}}^2 / \Lambda^2 \ll C_i^{(2)}$. Because it turns out that some coefficients $C_j^{(2)}$ relatively larger than 1 are needed in the quadratic scenario, this implies that the coefficients $C_i^{(4)}$ are smaller than $[C_j^{(2)}]^2$. Then, the contributions from dimension-8 operators will be suppressed with respect to the other $1/\Lambda^4$ contributions. This behavior has been confirmed in explicit weakly-coupled models and it is also expected, from naive dimensional analysis, in strongly-coupled theories. On the other hand, the interfering dimension-8 operators will have a structure similar to the one of interfering dimension-6 operators (typically, with additional covariant derivatives), so to a large extent their effects on inclusive observables can be absorbed into corrections to the coefficients of the dimension-6 operators. All this suggests that considering only the corrections from dimension-6 operators does not entail a significant loss of generality, even in a quadratic scenario. A direct consequence of this approximation is that all the observables will depend only on ratios $C_i^{(2)}/\Lambda^2$. Let us add, nevertheless, a word of caution: the hierarchy of coefficients we have assumed above may be spoiled by the elimination of redundant dimension-6 operators, as the necessary field redefinitions can induce dimension-8 operators with $C_i^{(4)} \sim [C_i^{(2)}]^2$. For this reason, we consider in the following a complete basis of dimension-6 operators, including the ones that vanish by the dimension-4 equations of motion. Of course, when working to order $1/\Lambda^2$ the redundant operators can be safely eliminated.

We focus on the operators contributing to $q\bar{q} \to t\bar{t}$ partonic processes, $q = u, d$, which are the most relevant at the Tevatron. We can distinguish operators with one quark current, which modify the trilinear vertices of the SM amplitudes, and operators with two fermionic currents, which produce contact four-fermion interactions. Oblique corrections do not generate an asymmetry, and are furthermore very restricted by gauge symmetry and electroweak precision tests.

Let us first discuss operators with one quark current, which can modify the vertices in the SM diagrams with exchange of a gauge boson. Amplitudes with *s*-channel exchange of a γ or Z boson with anomalous couplings will give contributions suppressed by α^2/Λ^2, since they do not interfere with the SM gluon amplitude, due to the different color structure. On the other hand, flavor-changing dtW and utZ anomalous couplings, which would give rise to *t*-channel amplitudes and $\alpha\alpha_s/\Lambda^2$ interfering contributions, must be very small, due to flavor-physics constraints. We can thus focus on quark-quark-gluon vertices in diagrams with an exchanged gluon. There are

eight non-flavor-changing operators of this type:

$$\mathcal{O}_{uG\phi} = \bar{q}_L \lambda^a \sigma^{\mu\nu} u_R \tilde{\phi} G^a_{\mu\nu}, \qquad \mathcal{O}_{tG\phi} = \bar{Q}_L \lambda^a \sigma^{\mu\nu} t_R \tilde{\phi} G^a_{\mu\nu},$$
$$\mathcal{O}_{dG\phi} = \bar{q}_L \lambda^a \sigma^{\mu\nu} d_R \phi G^a_{\mu\nu} \qquad (5.4)$$

and

$$\mathcal{O}_{qG} = \bar{q}_L \lambda^a D^\nu q_L G^a_{\mu\nu}, \qquad \mathcal{O}_{QG} = \bar{Q}_L \lambda^a D^\nu Q_L G^a_{\mu\nu},$$
$$\mathcal{O}_{uG} = \bar{u}_R \lambda^a \gamma^\mu D^\nu u_R G^a_{\mu\nu}, \quad \mathcal{O}_{tG} = \bar{t}_R \lambda^a \gamma^\mu D^\nu t_R G^a_{\mu\nu},$$
$$\mathcal{O}_{dG} = \bar{d}_R \lambda^a \gamma^\mu D^\nu d_R G^a_{\mu\nu}. \qquad (5.5)$$

Here, λ^a are Gell-Mann matrices, D_μ is the covariant derivative, q_L and Q_L represent, respectively, first and third-generation left-handed quark doublets, and u_R, d_R, t_R are the right-handed up, down and top quarks, respectively. These operators arise only at the loop level, so their coefficients will be suppressed by $1/16\pi$ if the fundamental theory is weakly coupled. The Hermitian (anti-Hermitian) parts of the chirality-flipping operators in (5.4) give chromomagnetic (chromoelectric) dipole moments to the involved quarks. None of them generates a FB asymmetry, but the Hermitian parts contribute to the cross section at the interfering level (Atwood *et al.*, 1995; Haberl *et al.*, 1996). More relevant for us are the operators in (5.5). Their axial combinations generate derivative axial-vector couplings of the gluon to the quarks. As shown in Gabrielli and Raidal (2011), the gluon-exchange diagram with two of these axial couplings interferes with the SM amplitude, producing a FB asymmetry. This is a $1/\Lambda^4$ contribution of the first kind. Quite large coefficients or a low scale are needed to obtain a sizable effect. On the other hand, these couplings give only $1/\Lambda^4$ quadratic contributions to the cross section. Therefore, an explanation of the Tevatron anomaly with these axial operators is as disfavored as in incoherent scenarios. This problem might always be mitigated by negative contributions to $\delta\sigma_{\text{int}}$ from other operators, in particular, the vector combinations of the operators in (5.5).

Let us next consider the impact of four-quark operators on top pair production. A complete basis has been given in Aguilar-Saavedra (2011). In contrast to the two-quark operators considered above, they can be generated at tree level. Seven of these operators can produce non-negligible interfering $1/\Lambda^2$ contributions to $t\bar{t}$ observables (Degrande *et al.*, 2011) :

$$\mathcal{O}_{Qq}^{(1)} = \tfrac{1}{2} \left(\bar{Q}_L \gamma^\mu \lambda^a Q_L \right) \left(\bar{q}_L \gamma_\mu \lambda^a q_L \right),$$
$$\mathcal{O}_{Qq}^{(3)} = \tfrac{1}{2} \left(\bar{Q}_L \gamma^\mu \lambda^a \tau^I Q_L \right) \left(\bar{q}_L \gamma_\mu \lambda^a \tau^I q_L \right),$$
$$\mathcal{O}_{tu} = \tfrac{1}{2} \left(\bar{t}_R \gamma^\mu \lambda^a t_R \right) \left(\bar{u}_R \gamma_\mu \lambda^a u_R \right),$$
$$\mathcal{O}_{td} = \tfrac{1}{2} \left(\bar{t}_R \gamma^\mu \lambda^a t_R \right) \left(\bar{d}_R \gamma_\mu \lambda^a d_R \right),$$
$$\mathcal{O}_{Qu} = \tfrac{1}{2} \left(\bar{Q}_L \gamma^\mu \lambda^a Q_L \right) \left(\bar{u}_R \gamma_\mu \lambda^a u_R \right),$$
$$\mathcal{O}_{Qd} = \tfrac{1}{2} \left(\bar{Q}_L \gamma^\mu \lambda^a Q_L \right) \left(\bar{d}_R \gamma_\mu \lambda^a d_R \right),$$
$$\mathcal{O}_{qt} = \tfrac{1}{2} \left(\bar{q}_L \gamma^\mu \lambda^a q_L \right) \left(\bar{t}_R \gamma_\mu \lambda^a t_R \right), \qquad (5.6)$$

with τ^I the Pauli matrices. We have not written operators that are very constrained by flavor physics, nor an operator that only interferes with the QCD amplitude after a down-quark mass insertion. The $1/\Lambda^2$ corrections to the $u\bar{u} \to t\bar{t}$ and $d\bar{d} \to t\bar{t}$ cross sections only depend, respectively, on the "vector-vector" combinations of coefficients

$$C_{Vv}^u = C_{qt} + C_{tu} + C_{Qu} + C_{Qq}^{(1)} + C_{Qq}^{(3)},$$
$$C_{Vv}^d = C_{qt} + C_{td} + C_{Qd} + C_{Qq}^{(1)} - C_{Qq}^{(3)}, \qquad (5.7)$$

whereas the $1/\Lambda^2$ corrections to the charge asymmetries in these processes depend on the "axial-axial" combinations

$$C_{Aa}^u = -C_{qt} + C_{tu} - C_{Qu} + C_{Qq}^{(1)} + C_{Qq}^{(3)},$$
$$C_{Aa}^d = -C_{qt} + C_{td} - C_{Qd} + C_{Qq}^{(1)} - C_{Qq}^{(3)}, \qquad (5.8)$$

which contribute, respectively, to the collider-independent asymmetries A_u and A_d. In the absence of other corrections, the linear scenario is realized, for $u\bar{u}$ and $d\bar{d}$ initial states separately, when $C_{Vv}^u = C_{Vv}^d = 0$. If this condition is met, $O(1/\Lambda^4)$ corrections must be subleading and the correction to the inclusive FB asymmetry is

$$\Delta A_{FB}^{\text{linear}} = [0.093 \, C_{Aa}^u + 0.014 \, C_{Aa}^d] \times \left(\frac{1 \text{ TeV}}{\Lambda} \right)^2, \quad (5.9)$$

We see that at the Tevatron the asymmetry (and also the cross section) is significantly more sensitive to the operators involving the u quark, due to the larger $u\bar{u}$ fraction F_u. The coefficients have to be relatively large to reproduce a large asymmetry, e.g. to match the central value of the CDF measurement of A_{FB}. For instance if $C_{Aa}^d = 0$, we need $C_{Aa}^u > 0.8$ when $\Lambda > 1 \text{ TeV}$ and $C_{Aa}^u > 3$ when $\Lambda > 2 \text{ TeV}$.

If the cross section is modified at order $1/\Lambda^2$, the quadratic $1/\Lambda^4$ terms are important and other four-quark operators must be taken into account, in addition to the ones in (5.6). In this quadratic scenario, C_{Vv}^u (or C_{Vv}^d) must be sizable and negative, to compensate for the quadratic terms. General analyses with all the dimension-6 operators to $O(1/\Lambda^4)$ have been performed in Aguilar-Saavedra and Pérez-Victoria (2011c) and Delaunay *et al.* (2011). They show that the Tevatron cross section and FB asymmetry can be well fitted in large regions of the space of operator coefficients, not necessarily obeying the condition $C_{Vv}^u = C_{Vv}^d = 0$.

A general feature of dimension-6 operators, and therefore of heavy new physics, is that they affect the $t\bar{t}$ observables more significantly at high $m_{t\bar{t}}$. This agrees, at least qualitatively, with the mass dependence of the FB asymmetry observed by the CDF collaboration. On the other hand, the cross section is also distorted at large invariant masses, and the deviations could be observable

at the LHC. This leads to strong constraints, discussed in Sec. VI. The energy sensitivity is much more dramatic for the $1/\Lambda^4$ corrections.

The same operators and combinations of coefficients are relevant for the charge asymmetry at the LHC. Already at the $1/\Lambda^2$ level, it is clear that heavy new physics allows in principle for different sizes and signs of A_C, consistent with $A_{FB} > 0$. Indeed, the coefficients C_{Aa}^u and C_{Aa}^d, which are independent in this formalism, can be adjusted to reproduce the required values of A_u and A_d in Eqs. (2.9). As we will see below, these two coefficients are actually generated by independent couplings in explicit models that realize the linear scenario.

B. Light extra particles

Large contributions to the FB asymmetry can be most naturally produced by tree-level exchanges of new particles. Lorentz invariance and the renormalizability of the corresponding SM extensions—which avoids extra higher-scale suppressions—limit their spin to be either 0 or 1.[6] These new particles can be exchanged in the s, t or u channels, depending on their precise interactions with quarks. The corresponding forms of the propagator have a significant impact on the rapidity and invariant-mass distributions of the asymmetries and cross section:

- s channel: The propagator itself does not modify the angular distributions, so any charge asymmetry must be produced by chiral couplings. To avoid a visible peak in the differential cross section, these particles must be either heavier than the available energies at the LHC, lighter than the $t\bar{t}$ threshold or very broad. In the first case, the cross sections and asymmetries increase faster than in the infinite-mass limit, especially when $m_{t\bar{t}}$ gets close to the mass of the new particle. In the second case, the dependence with $m_{t\bar{t}}$ is rather mild. In the third case, their behavior will depend on the precise mass and width of these particles. In all cases, the conservation of angular momentum, as imposed in Eq. (2.4), implies that the expansion in Legendre polynomials (2.8) of the non-standard contributions to the differential cross section has only a few terms: for scalars only the Legendre momenta a_0 and a_1 can be modified—the latter only if there is interference with the gluon-exchange amplitude, whereas vectors can contribute to a_0, a_1 and a_2 at most.

- t channel: The propagator favors forward top quarks, so it alone can generate a positive FB asym-

metry. The asymmetries are increased at high rapidities and invariant mass. In this case, since $\cos\theta$ appears in the denominator, higher-order Legendre momenta will accompany the lower-order ones. This angular dependence is disfavored by the corresponding CDF results shown in Fig. 7.

- u channel: The propagator prefers to send the top quarks backwards. Hence, it favors a negative asymmetry. To obtain a positive FB asymmetry, the numerator of the amplitude has to counteract this effect. However, as the invariant mass increases, the influence of the propagator becomes more significant, and eventually the asymmetries become negative. Another problem of u-channel exchanges is that they also contribute to higher Legendre momenta.

These different behaviors become milder as the mass of the exchanged particle increases, relative to the Mandelstam variable in the denominator of the propagator. In the heavy-particle limit, the propagator approaches a constant and the effect is described, in all three cases, by a four-fermion operator. The coefficients of these operators are given by ratios $g_1 g_2/M^2$, with $g_{1,2}$ trilinear couplings and M the mass of the new boson. They have been calculated explicitly, for arbitrary scalars and vector bosons, in Aguilar-Saavedra and Pérez-Victoria (2011c).

The possible quantum numbers and interactions of the new particles are strongly restricted by the requirement of $SU(3)_C \times SU(2)_L \times U(1)_Y$ invariance of the SM extension, in the electroweak symmetric phase. In particular, the extra fields must furnish complete representations of this symmetry. There are ten possible irreducible representations of new vector bosons and eight irreducible representations of scalars contributing to $q\bar{q} \to t\bar{t}$. They are collected in Table V, together with the relevant interaction Lagrangian. We also indicate the symmetry properties, if any, of the coupling matrices g_{ij}.

Allowing for general couplings, the relevant components of the Z', $\mathcal{W}$, G, H, ϕ and Φ multiplets can be exchanged in either the s or the t channels in $q\bar{q} \to t\bar{t}$ processes, whereas those of W' and G' can be exchanged in the t channel only, and those of the other ten multiplets, in the u channel only. Obviously, t- and u-channel exchanges require flavor-changing couplings. All these fields can produce interfering contributions $\delta\sigma_{\rm int}^{F,B}$.

Any new physics contributing at the tree level to $t\bar{t}$ production can be characterized by these multiplets and their interactions. In practice, to perform explicit analyses it is necessary to choose particular directions in this multi-dimensional space. Although scenarios with several multiplets can be interesting, most of the models that have been proposed to explain the anomaly in the FB asymmetry are extensions of the SM with just one of these multiplets. Among these simple models, the following ones have been studied in greater detail:

---

[6] Spin 2 particles have been considered in Grinstein *et al.* (2012). Their derivative couplings increase their effects with energy and lead to strong LHC constraints.

TABLE V Vector bosons and scalar representations mediating $q\bar{q} \to t\bar{t}$. The notation is standard, with left-handed doublets q_{Li}, right-handed singlets u_{Ri}, d_{Ri}, $\tilde{\phi} = \epsilon\phi$ and $\psi^c = C\bar{\psi}^T$, where $\epsilon = i\tau^2$ and C is the charge conjugation matrix. The indices a, b, c represent color, with ε_{abc} the totally antisymmetric tensor, and the indices i, j denote the family number in the interaction basis.

Label	Rep.	Interaction Lagrangian	Sym.
Z'_μ	$(1,1)_0$	$-\left(g_{ij}^q \bar{q}_{Li}\gamma^\mu q_{Lj} + g_{ij}^u \bar{u}_{Ri}\gamma^\mu u_{Rj} + g_{ij}^d \bar{d}_{Ri}\gamma^\mu d_{Rj}\right) Z'_\mu$	$g = g^\dagger$
$\mathcal{W}_\mu$	$(1,3)_0$	$-g_{ij}\bar{q}_{Li}\gamma^\mu \tau^I q_{Lj}\, \mathcal{W}_\mu^I$	$g = g^\dagger$
W'_μ	$(1,1)_1$	$-g_{ij}\bar{d}_{Ri}\gamma^\mu u_{Rj}\, W_\mu'^{\dagger} + \text{h.c.}$	$-$
G_μ	$(8,1)_0$	$-\left(g_{ij}^q \bar{q}_{Li}\gamma^\mu \frac{\lambda^a}{2} q_{Lj} + g_{ij}^u \bar{u}_{Ri}\gamma^\mu \frac{\lambda^a}{2} u_{Rj} + g_{ij}^d \bar{d}_{Ri}\gamma^\mu \frac{\lambda^a}{2} d_{Rj}\right) G_\mu^a$	$g = g^\dagger$
H_μ	$(8,3)_0$	$-g_{ij}\bar{q}_{Li}\gamma^\mu \tau^I \frac{\lambda^a}{2} q_{Lj}\, H_\mu^{aI}$	$g = g^\dagger$
G'_μ	$(8,1)_1$	$-g_{ij}\bar{d}_{Ri}\gamma^\mu \frac{\lambda^a}{2} u_{Rj}\, G_\mu'^{\,a\dagger} + \text{h.c.}$	$-$
Q_μ	$(3,2)_{\frac{1}{6}}$	$-g_{ij}\varepsilon_{abc}\bar{d}_{Rib}\gamma^\mu \epsilon q_{Ljc}^c\, Q_\mu^{a\dagger} + \text{h.c.}$	$-$
Q'_μ	$(3,2)_{-\frac{5}{6}}$	$-g_{ij}\varepsilon_{abc}\bar{u}_{Rib}\gamma^\mu \epsilon q_{Ljc}^c\, Q_\mu'^{\,a\dagger} + \text{h.c.}$	$-$
Y_μ	$(\bar{6},2)_{\frac{1}{6}}$	$-g_{ij}\frac{1}{2}\left[\bar{d}_{Ria}\gamma^\mu \epsilon q_{Ljb}^c + \bar{d}_{Rib}\gamma^\mu \epsilon q_{Lja}^c\right] Y_\mu^{ab\dagger} + \text{h.c.}$	$-$
Y'_μ	$(\bar{6},2)_{-\frac{5}{6}}$	$-g_{ij}\frac{1}{2}\left[\bar{u}_{Ria}\gamma^\mu \epsilon q_{Ljb}^c + \bar{u}_{Rib}\gamma^\mu \epsilon q_{Lja}^c\right] Y_\mu'^{\,ab\dagger} + \text{h.c.}$	$-$
ϕ	$(1,2)_{\frac{1}{2}}$	$-g_{ij}^u \bar{q}_{Li} u_{Rj}\, \tilde{\phi} - g_{ij}^d \bar{q}_{Li} d_{Rj}\, \phi + \text{h.c.}$	$-$
Φ	$(8,2)_{\frac{1}{2}}$	$-g_{ij}^u \bar{q}_{Li}\frac{\lambda^a}{2} u_{Rj}\, \tilde{\Phi}^a - g_{ij}^d \bar{q}_{Li}\frac{\lambda^a}{2} d_{Rj}\, \Phi^a + \text{h.c.}$	$-$
ω'	$(3,1)_{-\frac{1}{3}}$	$-g_{ij}\varepsilon_{abc}\bar{d}_{Rib} u_{Rjc}^c\, \omega'^{a\dagger} + \text{h.c.}$	$-$
Ω'	$(\bar{6},1)_{-\frac{1}{3}}$	$-g_{ij}\frac{1}{2}\left[\bar{d}_{Ria} u_{Rjb}^c + \bar{d}_{Rib} u_{Rja}^c\right] \Omega'^{ab\dagger} + \text{h.c.}$	$-$
ω	$(3,1)_{-\frac{4}{3}}$	$-g_{ij}\varepsilon_{abc}\bar{u}_{Rib} u_{Rjc}^c\, \omega^{a\dagger} + \text{h.c.}$	$g = -g^T$
Ω	$(\bar{6},1)_{-\frac{4}{3}}$	$-g_{ij}\frac{1}{2}\left[\bar{u}_{Ria} u_{Rjb}^c + \bar{u}_{Rib} u_{Rja}^c\right] \Omega^{ab\dagger} + \text{h.c.}$	$g = g^T$
σ	$(3,3)_{-\frac{1}{3}}$	$-g_{ij}\varepsilon_{abc}\bar{q}_{Lib}\tau^I \epsilon q_{Ljc}^c\, \sigma^{a\dagger} + \text{h.c.}$	$g = -g^T$
Σ	$(\bar{6},3)_{-\frac{1}{3}}$	$-g_{ij}\frac{1}{2}\left[\bar{q}_{Lia}\tau^I \epsilon q_{Ljb}^c + \bar{q}_{Lib}\tau^I \epsilon q_{Lja}^c\right] \Sigma^{Iab\dagger} + \text{h.c.}$	$g = g^T$

Color-octet vector G (Ferrario and Rodrigo, 2008).[7] Exchanged in the s channel via flavor-diagonal couplings, it gives an amplitude that interferes with the SM gluon-exchange diagram. The corresponding contribution to the charge asymmetries in $q\bar{q} \to t\bar{t}$ is proportional to the product of axial couplings $g_A^{u,d} g_A^t$, where $g_A^{u,d} = g_{11}^{u,d} - g_{11}^q$ and $g_A^t = g_{33}^t - g_{33}^q$. When $m_{t\bar{t}} < M_G$ ($m_{t\bar{t}} > M_G$), g_A^q and g_A^t must have opposite (same) sign for a positive contribution. In the heavy-mass limit, it is described by a set of operators with $C_{Aa}^q/\Lambda^2 = -g_A^q g_A^t / 4M_G^2$. This multiplet is particularly promising for several reasons. The main one is that $\delta\sigma_{\text{int}} = 0$ (linear new physics) when the vector couplings to either the light quarks or the top vanish, i.e. either $g_V^u = g_{11}^q + g_{11}^u = 0$ and $g_V^d = g_{11}^q + g_{11}^d = 0$, or $g_V^t = g_{33}^q + g_{33}^u = 0$ (when all vector couplings vanish, the octet is an axigluon). The octet G is actually the only multiplet that can produce, on its own, positive charge asymmetries without interfering contributions to the cross section. Another welcomed feature of an octet

vector boson in the s channel is that it reproduces well the observed values of the Legendre momenta, since it only contributes with $J = 1$ to the amplitude. The main issue is, as in any s-channel model, to hide the resonant peak in the cross section, produced by the quadratic terms. The solutions have already been mentioned, and are further discussed in the next section. On the other hand, di-jet and four-top-quark data constrain the possible values of the couplings of the octet to the light quarks and the top, respectively. These bounds are discussed in Sec. VII. This multiplet appears naturally in extensions of the SM with a $SU(3) \times SU(3) \to SU(3)_C$ symmetry-breaking pattern (Frampton and Glashow, 1987). In particular, it can emerge as the lightest Kaluza-Klein excitation of the gluons in extra-dimensional theories with gauge fields in the bulk (Djouadi *et al.*, 2010).

Neutral Z' boson (Jung *et al.*, 2010). This SM singlet is particularly interesting when exchanged in the t channel via flavor-changing tu couplings. A negative asymmetry is produced at the interfering level, so significant quadratic contributions are required to obtain a positive correction to the FB asymmetry, and also to cancel $\delta\sigma_{\text{int}}$. As we will see below in this section and in the following ones, this popular model is strongly disfavored by dif-

---

[7] The specific couplings and mass range studied in this paper led to the prediction of a negative FB asymmetry, but arbitrary signs can be obtained in general, as explained below.

ferent Tevatron and LHC observables. From the model-building point of view, these vectors could be the gauge bosons of an extra local flavor symmetry (Jung *et al.*, 2011).

Charged W' boson (Cheung *et al.*, 2009). This isosinglet couples to right-handed quarks and contributes in the t channel to the partonic process $d\bar{d} \to t\bar{t}$. Larger couplings are needed to compensate the lower $d\bar{d}$ luminosity. This field also produces negative ΔA_{FB} at the interfering level and, similarly to the Z', is disfavored by available data. Right-handed W' bosons appear in left-right extensions of the SM gauge group.

Scalar isodoublet ϕ (Nelson *et al.*, 2011). This Higgs-like doublet works best when exchanged in the t channel. It gives positive asymmetry at the interfering level. For small masses, the required couplings to achieve a sizable ΔA_{FB} and a cancellation of $\delta\sigma_{int} + \delta\sigma_{quad}$ are relatively small. The particular flavor-changing couplings in such a two-doublet model can be justified with flavor symmetries.

Color-triplet scalar ω (Shu *et al.*, 2010). This isosinglet of charge $4/3$ can only be exchanged in the u channel, with flavor-violating right-handed tu interactions. Once again, its interference contribution to the asymmetry is negative, so large couplings and a significant cancellation are required. Moreover, masses $M_\omega > 220$ GeV are necessary to soften the effect of the u channel propagator. These fields are included in the scalar sector of many Grand Unified models (Dorsner *et al.*, 2010).

Color-sextet scalar Ω (Shu *et al.*, 2010). Another isosinglet of charge $4/3$, it also contributes in the u channel via flavor-violating right-handed tu couplings and, again, intermediate masses are preferred. However, in this case the interference contribution to ΔA_{FB} is positive.[8] These fields also appear in models of Grand Unification.

We show in Fig. 23 the predictions of these models for the inclusive and high-mass values of the FB asymmetry (Aguilar-Saavedra and Pérez-Victoria, 2011e). The colored regions showing these predictions are obtained by a parameter-space scan, subject to some loose constraints from the total $t\bar{t}$ cross section at the Tevatron and the high-mass tail at the LHC. We only consider positive contributions of the new particles to the asymmetry. For the color octet, we use a very heavy axigluon, represented by the corresponding four-fermion operators. We see that most of these simple models can reproduce simultaneously the CDF excess in the inclusive and high-mass FB asymmetries. The exception is the Z' boson, which overpredicts them, especially at high $m_{t\bar{t}}$. The reason is that large couplings are necessary in this case

————————

[8] A wrong sign in Shu *et al.* (2010) was corrected in Arhrib *et al.* (2010).

to ensure the cancellation of interference and quadratic terms, in the region with a positive asymmetry. A conclusion one can draw from these plots is that the mass dependence observed by the CDF collaboration can be explained naturally by new physics, without the need of contrived models. Let us, nevertheless, point out that a different mass dependence results from light octets G. In particular, for octets with mass under the $t\bar{t}$ threshold the invariant-mass distributions of the FB and charge asymmetries are flatter, so they agree better with the findings of the D0 collaboration (Aguilar-Saavedra and Pérez-Victoria, 2011d). On the other hand, the precise dependence on the polar angle measured by the CDF collaboration is best reproduced among these simple models by the color octet G, since the t and u exchanges generate higher-order Legendre momenta.

In Sec. II.C we have argued that A_{FB} and A_C are independent in general. However, actual models give correlated predictions for both. Let us then consider the predictions of the new particles for the charge asymmetry A_C at the LHC. As implied by Eq. (2.9), the relative contributions of a given model to A_{FB} and A_C depend on their relative contributions to u and d initiated processes. In Fig. 24 we plot the predicted values of A_{FB} and A_C for a parameter scan in the same simple models considered above, except the Z', which as explained above cannot reproduce the Tevatron data. These models follow a similar slope, except in the case of the W' boson. This particle leads to twice the slope of the others because the $d\bar{d} \to t\bar{t}$ process has higher relative importance at the LHC than at the Tevatron. As a result, the W' boson is disfavored, since the agreement of its prediction, within one sigma, with the average of the measured A_{FB} leads to a two sigma disagreement in A_C. The other models in this set cannot reproduce the central values of the A_{FB} and A_C measurements either, but they are consistent with them at the one sigma level. More extreme behaviors, including different signs for A_{FB} and A_C, are also possible. For instance, in the explicit octet model proposed in Drobnak *et al.* (2012b) this is achieved with light-quark axial couplings g_A^u and g_A^d of opposite sign and with $|g_A^d| > |g_A^u|$. In particular, it is possible to accomodate the central values of the Tevatron and LHC asymmetries (see also Álvarez and Leskow, 2012; Drobnak *et al.*, 2012a; and Ko *et al.*, 2013). This requires a cancellation of new physics effects in A_C, which could be uncovered by the measurement of a charge asymmetry in $t\bar{t}\gamma$ production at the LHC (see Sec. IV.D).

Finally, let us note that, in order to discriminate between different models, the analysis of the $m_{t\bar{t}}$ dependence of A_C (see Sec. IV.A.3) could be useful (Aguilar-Saavedra and Pérez-Victoria, 2011a). We display the predictions for three models in Fig. 25. For illustration we include the point corresponding to the ATLAS measurement $A_C = 0.018 \pm 0.022$ for $m_{t\bar{t}} > 600$ GeV (Aad *et al.*,
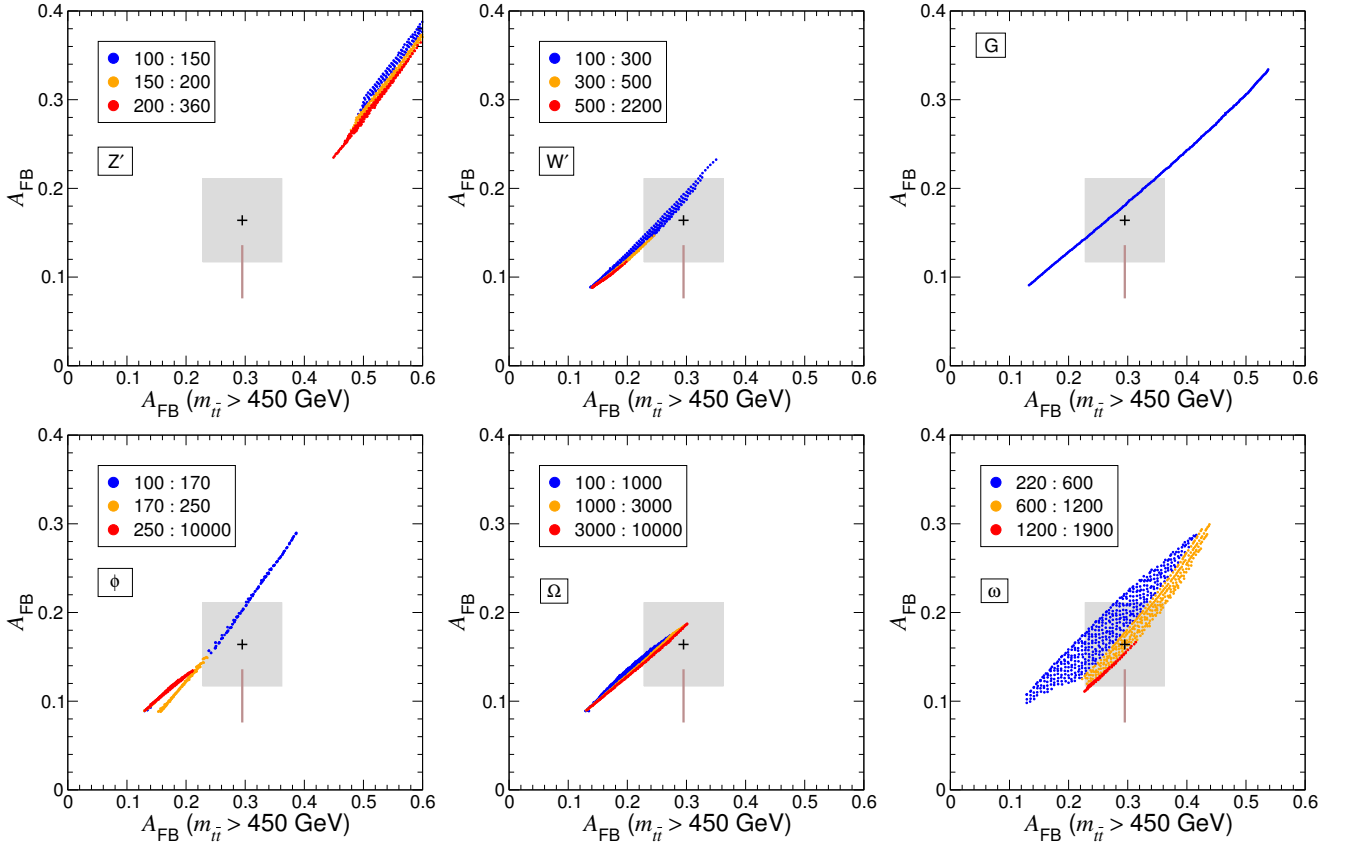
FIG. 23 Inclusive versus high-mass asymmetries at the Tevatron, for several new physics models. The numbers in the legends indicate the mass range for the new particle, in GeV. The crosses correspond to the CDF measurements, with the shaded boxes indicating the 1σ uncertainty. The vertical lines corresponds to the D0 measurement of the inclusive FB asymmetry, with the corresponding 1σ uncertainty (the position in the horizontal axis is arbitrary). From Aguilar-Saavedra and Pérez-Victoria (2011e), updated.

2014b). The discrimination power will be much higher with 8 TeV data, when the available statistics allows to measure A_C at higher $t\bar{t}$ invariant mass.

VI. CORRELATED EFFECTS IN $t\bar{t}$ PRODUCTION

A. Enhancement of the high-$m_{t\bar{t}}$ tail

The distortion of the $m_{t\bar{t}}$ differential distribution with respect to the SM prediction is a rather general consequence of hypothetical new physics contributions to $t\bar{t}$ production (Aguilar-Saavedra and Pérez-Victoria, 2011c; Delaunay et al., 2011), especially in the quadratic new physics scenario. Then, since the bulk of the $t\bar{t}$ cross section results from moderate $m_{t\bar{t}}$ not far from the threshold, the agreement of the predicted Tevatron cross section with the experimental measurements—which is a basic requirement for realistic models—has the almost unavoidable consequence that deviations appear in the high-$m_{t\bar{t}}$ tail. These deviations are illustrated in Fig. 26, for the Tevatron (top panel) and the LHC

with 7 TeV (bottom panel), for linear heavy new physics parametrized by a non-zero C_{Aa}^u in Eq. (5.8) that fits the former CDF measurements from Aaltonen et al. (2011a), $A_{FB} = 0.158 \pm 0.075$ (dashed line and green area) and $A_{FB} = 0.475 \pm 0.114$ for $m_{t\bar{t}} > 450$ GeV (solid line and red area). For quadratic new physics scenarios the tail enhancements are larger than the corresponding ones in Fig. 26, which are "minimal" for heavy new physics.

For light mediators the tail enhancements are much less pronounced (Aguilar-Saavedra and Pérez-Victoria, 2011d,e). Moreover, at the Tevatron the potential deviations in the high-$m_{t\bar{t}}$ tail may remain hidden if the new physics contributions concentrate in the forward region, in which the detection efficiency is small due to the detector coverage (Gresham et al., 2011a). This is the case for example when light Z' or W' particles are exchanged in the t channel. Also, the statistical uncertainties in the high-$m_{t\bar{t}}$ tail are large at the Tevatron. But at the LHC the detectors have a larger rapidity coverage and the analyzed datasets have much higher statistics, allowing for precise measurements of the $m_{t\bar{t}}$ spectrum over
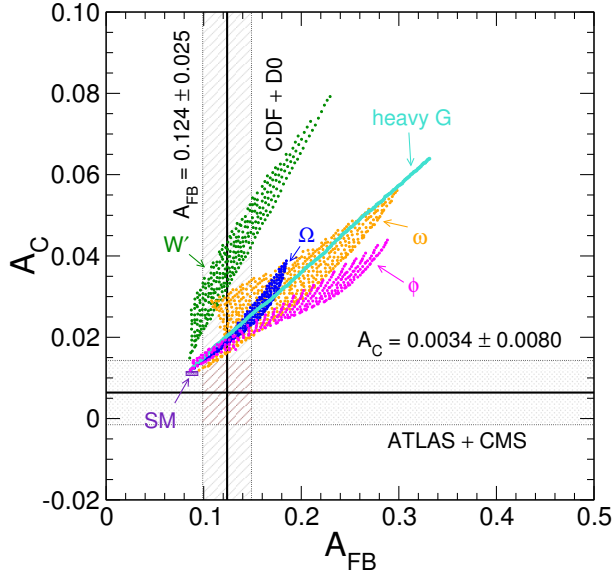
FIG. 24 Comparison of predictions for the inclusive asymmetries A_{FB} and A_C for several simple models, together with the experimental measurements. From Aguilar-Saavedra and Pérez-Victoria (2011a), updated.
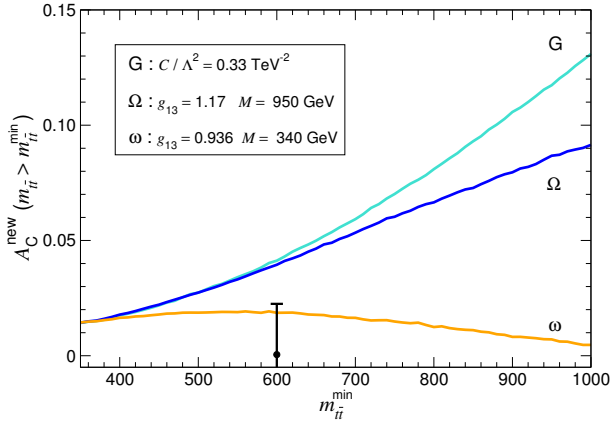

FIG. 25 Dependence of the charge asymmetry on an $m_{t\bar{t}}$ lower cut in three simple models, for a point with $\Delta A_{FB} \simeq 0.13$, $A_C^{\text{new}} \simeq 0.016$. The ATLAS measurement for $m_{t\bar{t}} > 600$ GeV is also included. From Aguilar-Saavedra and Pérez-Victoria (2011a), adapted.

FIG. 26 Enhancement of the high-$m_{t\bar{t}}$ tail at the Tevatron (top) and the LHC (bottom) for heavy new physics. The lower dot-dashed line is the SM LO prediction. The dashed and solid lines correspond to two non-zero C_{Aa}^u values chosen to have inclusive $A_{FB} = 0.158$ and $A_{FB} = 0.475$ for $m_{t\bar{t}} > 450$ GeV, respectively. The bands represent the variation around these values (see text for details). From Blum et al. (2011a).

a wide range. In general they exhibit a good agreement with the SM prediction, as illustrated in Fig. 27. (Electroweak Sudakov corrections slightly reduce the high-$m_{t\bar{t}}$ tail with respect to the fixed-order Monte Carlo predictions, see Manohar and Trott, 2012.) This imposes severe constraints on quadratic new physics models that accommodate an excess A_{FB}. Although a precise statement requires a dedicated analysis taking into account the possibly different $t\bar{t}$ acceptance in the presence of new contributions, the tail enhancements in the Z' and W' models are so pronounced that they are eventually
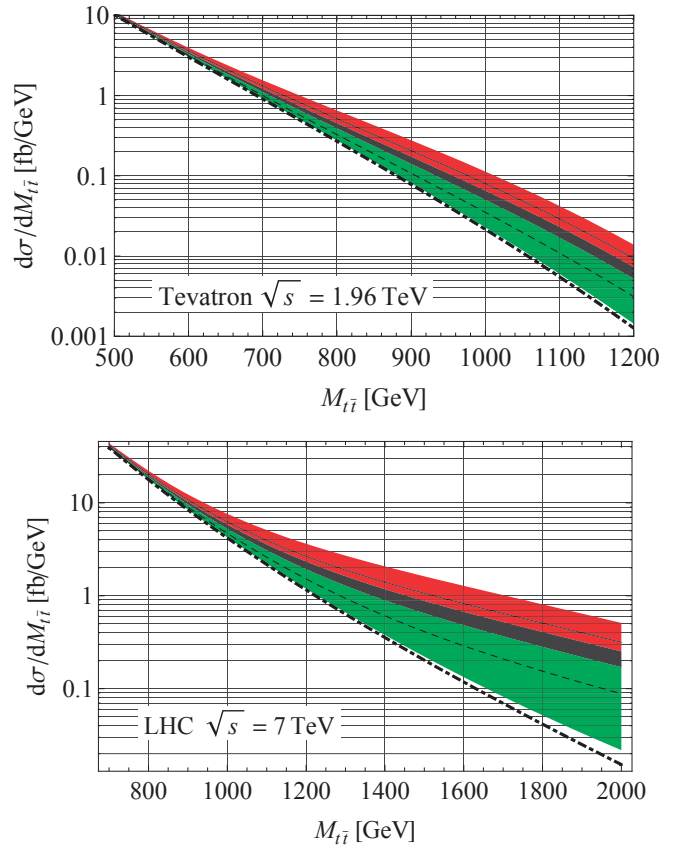
excluded as candidates to yield an A_{FB} excess. On the other hand, for u-channel color sextets and triplets, as well as for a scalar isodoublet, an asymmetry excess is compatible with the observed differential $m_{t\bar{t}}$ spectrum.

In the linear new physics models where $\delta\sigma_{\text{int}}$ vanishes (also when considered differentially as a function of $m_{t\bar{t}}$) and $\delta\sigma_{\text{quad}}$ is small—for example, a color octet G exchanged in the s channel—the $m_{t\bar{t}}$ distribution is preserved except at the resonance, where a potentially large enhancement results from $\delta\sigma_{\text{quad}}$. As it has been previously mentioned, this enhancement can be hidden if the octet is wide or if it is lighter than the $t\bar{t}$ threshold. In the former case, new particles may be required to yield extra G decay modes that account for its large width, for example new quarks (Barcelo et al., 2012a,b) or colored scalars (Marques Tavares and Schmaltz, 2011). Figure 28 shows the $m_{t\bar{t}}$ distribution for the SM and when an extra octet G with mass $M = 850$ GeV, is included, without and with extra decay modes that yield a large
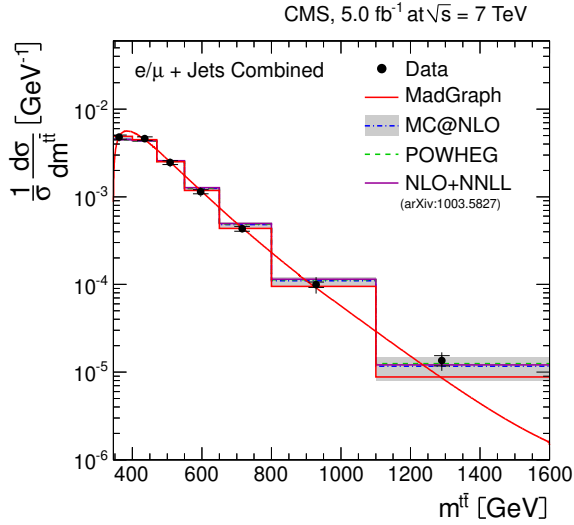
FIG. 27 Normalized $t\bar{t}$ invariant mass distribution at the LHC with 7 TeV, measured in the semileptonic decay channel, and SM predictions from several Monte Carlo generators. From Chatrchyan *et al.* (2013a).

width $\Gamma/M = 0.7$. In case that G is lighter than the $t\bar{t}$ threshold (Aguilar-Saavedra and Pérez-Victoria, 2011d) the $m_{t\bar{t}}$ spectrum is preserved independently of Γ. Nevertheless, a large width may be required in order to comply with other collider constraints (see Sec. VII). If G is very heavy, the tail enhancement corresponds to the one shown in Fig. 26.
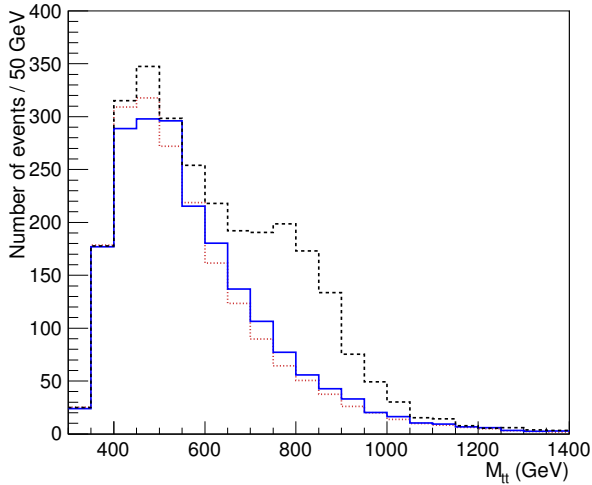

FIG. 28 Normalized $t\bar{t}$ invariant mass distribution at the LHC with 7 TeV, for the SM (dotted line), the SM plus a narrow G (dashed line) and the SM plus a wide G (solid line). The predictions are normalized to an integrated luminosity of 1 fb^{-1}. From Barcelo *et al.* (2012b).

B. Top quark polarization and $t\bar{t}$ spin correlations

New $t\bar{t}$ production mechanisms in general modify the top quark and antiquark polarizations, as well as their spin correlation, especially if the coupling of the top quark to the new states exchanged is chiral (Krohn *et al.*, 2011). The color triplet and sextet scalars ω, Ω have a right-handed coupling to the top quark as a consequence of gauge symmetry, as described in Sec. V. On the other hand, the coupling of the top quark to a color octet G and scalar doublet ϕ can have any chirality.

In order to discuss angular distributions in the decay of the $t\bar{t}$ pair, let us fix a reference system (x, y, z) in the top quark rest frame and another one (x', y', z') in the top antiquark rest frame, and consider the decay products $X = \ell^+, \nu, u, \bar{d}, \dots$, $X' = \ell^-, \bar{\nu}, \bar{u}, d, \dots$ from the top quark and antiquark, respectively. Then, the double-differential polar angle distribution (see for example Bernreuther *et al.*, 2001) is

$$\frac{1}{\sigma}\frac{d^2\sigma}{d\cos\theta_X \, d\cos\theta_{X'}} = \frac{1}{4}[1 + P_z\alpha_X \cos\theta_X + P_{z'}\alpha_{X'} \cos\theta_{X'} + C\alpha_X\alpha_{X'}\cos\theta_X\cos\theta_{X'}] , (6.1)$$

with θ_X, $\theta_{X'}$ being the polar angles of the X, X' 3-momenta in their respective reference systems. The coefficients P_z, $P_{z'}$ are the polarizations of the top quark and antiquark in the $\hat{z}$ and $\hat{z}'$ axes, respectively. The coefficient C measures the spin correlation between the top quark and antiquark, namely

$$C = \frac{N(\uparrow\uparrow) + N(\downarrow\downarrow) - N(\uparrow\downarrow) - N(\downarrow\uparrow)}{N(\uparrow\uparrow) + N(\downarrow\downarrow) + N(\uparrow\downarrow) + N(\downarrow\uparrow)} , \quad (6.2)$$

where the up and down arrows indicate spins in the $\pm\hat{z}$, $\pm\hat{z}'$ directions for the top quark and antiquark, respectively. The quantities $\alpha_{X,X'}$ are the so-called *spin analyzing powers* of the decay products (Jezabek, 1994), and have opposite sign for particles and antiparticles. For the charged leptons $\alpha_{\ell^+} = -\alpha_{\ell^-} = 1$ in the SM at the tree level, with small QCD corrections (Bernreuther *et al.*, 2004). Because $|\alpha_X| \leq 1$ in general, the charged lepton distributions have the maximum possible dependence on the top polarization and spin correlation.

For $t\bar{t}$ pairs produced via QCD interactions the polarizations P_z, $P_{z'}$ vanish for $\hat{z}$, $\hat{z}'$ in the production plane, and a small polarization orthogonal to that plane arises at the loop level. The spin correlations are non-zero in general. At the Tevatron, there are no measurements of the top polarization[9] but the CDF and D0 Collaborations have measured the spin correlations using the

---

[9] In Abazov *et al.* (2013a) the $\cos\theta_\ell$ distributions are investigated but results are not presented at the production level.

TABLE VI Summary of the most precise polarization and spin correlation measurements at the Tevatron and at the LHC with 7 TeV, compared to the corresponding SM predictions.

Collider	basis	measurement	SM prediction
Tevatron	beamline	$C = 0.58 \pm 0.20$	$0.791^{+0.013}_{-0.014}$
LHC7	helicity	$P = -0.014 \pm 0.029$	0
LHC7	helicity	$C = 0.17 \pm 0.09$	0.310 ± 0.006

beamline basis, that is, with $\hat{z}$ and $\hat{z}'$ in the proton direction (Abazov *et al.*, 2012; Abe *et al.*, 2010, 2011). At the LHC, the top polarization has been measured in the helicity basis (Aad *et al.*, 2013b; Chatrchyan *et al.*, 2014b), that is, selecting $\hat{z}$ in the direction of the top momentum in the $t\bar{t}$ CM frame $\vec{p}_t$ and $\hat{z}' = -\hat{z}$. (The measurements assume assuming CP conservation so that $P_z = -P_{z'} \equiv P$.) The spin correlation in this basis has also been measured by the ATLAS and CMS Collaborations (Aad *et al.*, 2013c; Chatrchyan *et al.*, 2014b). The naive averages of these measurements can be found in Table VI together with the SM predictions (Bernreuther and Si, 2010, 2013).

The measurement of C in the beamline basis at the Tevatron does impose some constraints on the parameter space of the models explaining the Tevatron anomalies (Fajfer *et al.*, 2012). But more restrictive are the precise measurements obtained at the LHC. The measurement of P_z excludes at the 2σ level the color triplet as a viable candidate to explain the anomalies, and also disfavors the color sextet, as it can be seen in the upper panel of Fig. 29, where the curves represent the allowed values of the new physics contribution ΔA_{FB} and P_z for each model, resulting from a fit. Note that for an axigluon one has $P_z = 0$, as depicted in Fig. 29, but this is no longer the case if either the coupling to the light quarks or to the top quark is not purely axial. The measurement of C in the bottom panel is in some tension with the predictions of all the four models as well as with the SM prediction, at the 1.5σ level. (A lower spin correlation can be accommodated with general color octets, see Aguilar-Saavedra (2014a).) With 8 TeV data the measurements of P and C are not expected to be much more precise than the current 7 TeV ones in Table VI, whose uncertainties are nearly dominated by systematics. Instead, to take advantage of the higher statistics at 8 TeV the most interesting possibility would be to measure the polarization and spin correlation at high $m_{t\bar{t}}$ and/or high $\beta_z^{t\bar{t}}$ where the effect of new physics may be larger.

In addition to the "longitudinal" helicity axis $\hat{z}$, there are two other independent directions in which the top polarization can be investigated. We can specify them by choosing $\hat{y}$ perpendicular to the production plane, and $\hat{x}$
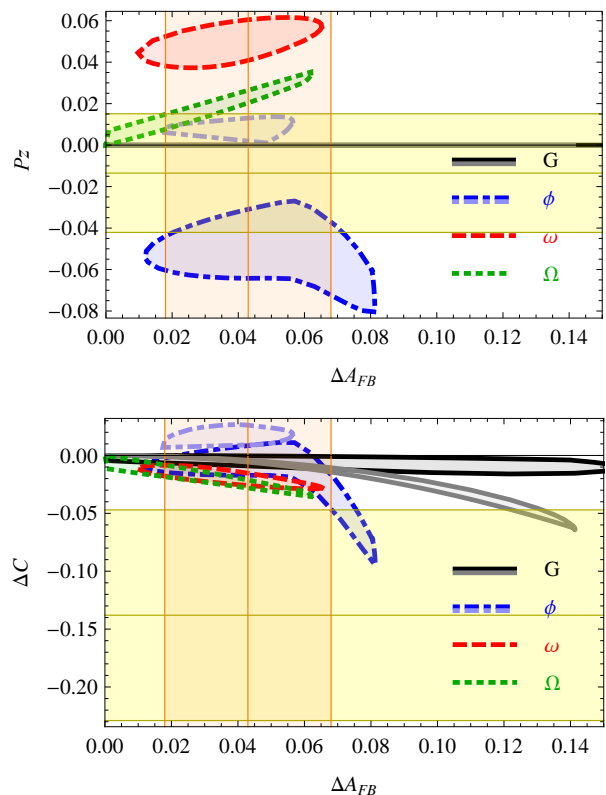

FIG. 29 Top quark 'longitudinal' polarization P_z (upper panel) and new physics contributions to C at the LHC (lower panel) versus new physics contributions to A_{FB}, for four models: (i) light (black) and heavy (gray) axigluon G; (ii) light (dark blue) and heavy (light blue) scalar doublet ϕ; (iii) color triplet ω; and (iv) color sextet Ω. The shaded bands correspond to the central value and 1σ uncertainty for the corresponding measurement. From Fajfer *et al.* (2012).

orthogonal to the $\hat{z}$ and $\hat{y}$,

$$\hat{z} = \frac{\vec{p}_t}{|\vec{p}_t|}, \quad \hat{y} = \frac{\vec{p}_t \times \vec{p}_p}{|\vec{p}_t \times \vec{p}_p|}, \quad \hat{x} = \hat{y} \times \hat{z}, \qquad (6.3)$$

with $\vec{p}_p$ the proton momentum in the top quark rest frame. (At the LHC, one can use the motion of the $t\bar{t}$ pair in the laboratory frame to select a preferred direction among the two protons, see Baumgart and Tweedie, 2013.) The $\hat{x}$ and $\hat{y}$ directions are usually denoted as "transverse" and "normal", respectively. The transverse polarization can be non-zero, for example in s-channel color octet models (Aguilar-Saavedra, 2014b; Baumgart and Tweedie, 2011). A polarization in the normal direction requires a complex phase in the amplitude, which may be provided by the propagator of the octet if it is produced on-shell (Baumgart and Tweedie, 2013). Neither the transverse nor the normal polarizations have been measured at the Tevatron nor the LHC.

C. Interplay of asymmetries and top polarization

The several new physics models proposed to explain the A_{FB} anomaly give different predictions for the leptonic asymmetries, as it was soon noticed (Krohn *et al.*, 2011). New particles that couple to t_R produce larger leptonic asymmetries than those coupling to t_L. This is illustrated in Fig. 30, which depicts the relation between new physics contributions to the asymmetries ΔA_{FB} and ΔA_{FB}^ℓ, for a color octet with mass $M = 250$ GeV exchanged in the s-channel. The relation between the asymmetries is given for three chiralities of the $\bar{q}qG$ coupling (axial, right-handed and left-handed) chosen such that $g_A^u = g_A^d > 0$, and a continuous variation of the chirality of the $\bar{t}tG$ coupling along the curves, including vector, axial, left-handed and right-handed couplings. The sign of ΔA_{FB}^ℓ in each case is explained by the threshold behavior (see Sec. II.D). The two asymmetries are *de facto* uncorrelated, and their combined measurement can give information of the chirality of the couplings of the new particle to the top quark.
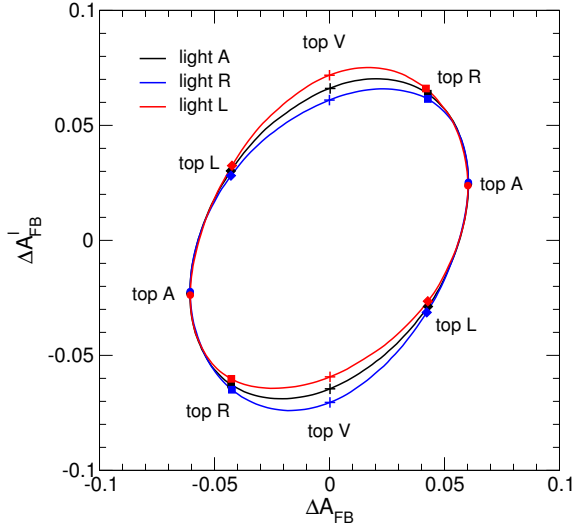

FIG. 30 Relation between ΔA_{FB} and ΔA_{FB}^ℓ, for three choices of light quark couplings and continuous variation of the chirality of top quark couplings to a color octet G. The abbreviations refer to axial (A), vector (V), left-handed (L) and right-handed (R). From Aguilar-Saavedra (2014b).

The longitudinal polarization P_z (in the helicity basis) is also uncorrelated from the asymmetries, and in general it can be positive, negative, or nearly zero. This can also be illustrated with the color octet model, where P_z depends not only on the coupling to the top quark but also on the light quark couplings. Figure 31 shows the polarization at the Tevatron as a function of the continuous parameter

$$\phi_h = \arg(g_A^t + i g_V^t) \in [0, 2\pi], \qquad (6.4)$$

for three choices of light quark couplings, all with $g_A^{u,d} > 0$. (We do not consider vector couplings to u, d since in this case the interference with the SM amplitudes does not generate any asymmetry A_{FB}.) One can see that $P_z = 0$ if the top quark coupling is either vectorial or axial. On the other hand, $P_x = 0$ only when the top quark coupling is axial. In particular, one can see that for an axigluon $P_x = P_z = 0$; P_y is also small unless it is produced on its mass shell.
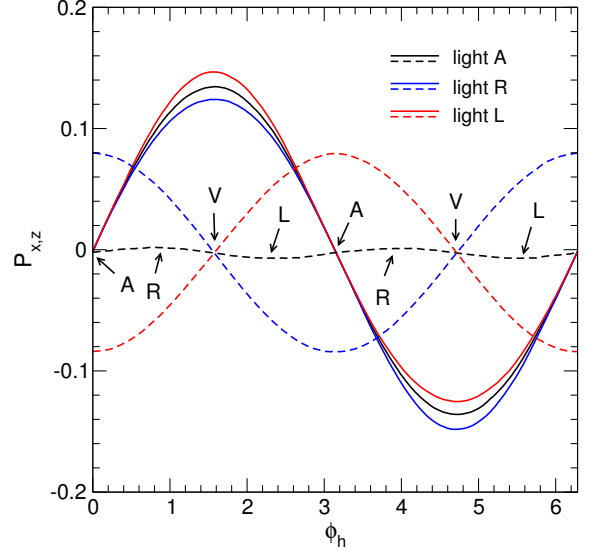

FIG. 31 Longitudinal (dashed lines) and transverse polarization (solid lines), for three choices of light quark couplings and continuous variation of the chirality of top couplings (see Eq. (6.4)). The abbreviations refer to axial (A), vector (V), left-handed (L) and right-handed (R). From Aguilar-Saavedra (2014b).

Once it is established that A_{FB} and A_{FB}^ℓ (and also A_C) are in general independent, one can attempt to fit these asymmetries—as well as other $t\bar{t}$ observables—in the context of any new physics model that explain the Tevatron anomalies. A light color octet is the best suited candidate for this since, as we have mentioned throughout Sec. V and Sec. VI, it can reproduce the Tevatron and LHC asymmetries while keeping good agreement with the remaining $t\bar{t}$ data. A fit including the Tevatron and LHC cross sections, asymmetries and polarization observables has been performed in Aguilar-Saavedra (2014a). The global agreement of the SM is $\chi^2/\text{d.o.f.} = 15.8/10$ for 10 measurements (1.3σ). While the overall consistency with data is good within the SM, the agreement can be improved to $\chi^2/\text{d.o.f.} = 8.1/8$ ($\chi^2/\text{d.o.f.} = 6.4/6$) for an octet with a reference mass $M = 250$ GeV, $\Gamma/M = 0.2$, and right-handed (general) couplings to quarks. Color octets with pure axial or left-handed couplings to quarks do not improve the fit with respect to the SM, and are thus disfavored on a purely statistical basis.

Finally, one can go a step further diagnosing poten-

tial new physics and study the relation between A_{FB} and A_{FB}^{ℓ} differentially, for example as a function of the charged-lepton transverse momentum p_T^{ℓ} (Falkowski *et al.*, 2013a). Different SM extensions predict not only different ratios A_{FB}^{ℓ}/A_{FB} but also quite a different dependence on p_T^{ℓ}. This is shown in Fig. 32, for p_T^{ℓ} (in GeV) in the intervals $[0, 20[, [20, 40[, [40, 60[, [60, 100[, [100, 150[, [150, \infty[$. The direction of the curves is such that for the L and R benchmarks A_{FB} grows with p_T^{ℓ}, and for the SM and A benchmark A_{FB}^{ℓ} increases. This information could be used to distinguish these models from SM-based explanations of the asymmetry due to some mismodeling effect that could enhance the observed asymmetry with respect to the prediction. For example, a color octet with right-handed couplings that gives a good fit of all inclusive measurements could be distinguished from a SM-like effect. In analogy with the Tevatron, at the LHC the p_T^{ℓ} dependence of leptonic asymmetries versus A_C can be used to investigate the presence of new physics (Carmona *et al.*, 2014).
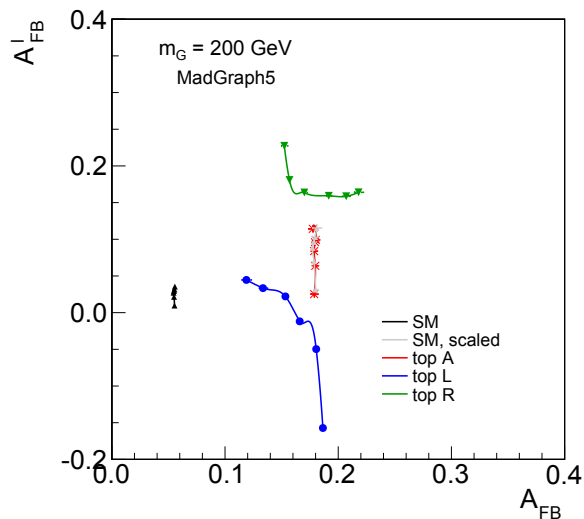

FIG. 32 Differential relation between A_{FB} and A_{FB}^{ℓ} (including SM and new physics contributions, if any) as a function of the lepton transverse momentum, for the SM, a 'scaled SM' in which the SM predictions of A_{FB} and A_{FB}^{ℓ} are scaled by a common factor in order to have $A_{FB} = 0.18$, and for a color octet with three choices of couplings to the top quark. From Falkowski *et al.* (2013a).

VII. OTHER CONSTRAINTS AND EFFECTS

New-physics interpretations of the excess in A_{FB} often have other implications beyond their impact on $t\bar{t}$ observables. They are less universal, with different kinds of effects predicted for different classes of models. In all cases, the absence of those signals of new physics puts strong constraints on the corresponding model parameter spaces. In this section we review the most important non-$t\bar{t}$ effects associated with models with extra particles that contribute at tree-level to the charge asymmetries.

A. Flavor physics

Most models of new physics motivated by the anomaly in the FB asymmetry require a non-trivial flavor structure. Indeed, t- and u-channel exchanges involve intergenerational couplings of the new particles to the first and third families, while s-channel heavy octets must have couplings with different sign, and thus non-universal, to generate a positive ΔA_{FB}. Conciliating these features with the stringent bounds on flavor-changing neutral currents (FCNC) is not straightforward. In particular, the possible couplings to quarks are constrained.

Usually, FCNC can be avoided by aligning the couplings of the new particles with specific directions in flavor space. However, a complete alignment in both the up and the down sectors is not possible when the quark doublets Q_L and q_L are involved. In this case, bounds can be extracted from a combination of measurements in $B - \bar{B}$ mixing and B decays, $D - \bar{D}$ mixing and $K - \bar{K}$ mixing (Bai *et al.*, 2011; Blum *et al.*, 2009, 2011b; Duraisamy *et al.*, 2011; Zhu, 2011). These bounds require small or near-degenerate couplings to Q_L and q_L, or sufficiently large masses. For this reason, in many of the proposed models the extra particles are chosen to have chiral right-handed couplings to the top quark.

In the case of s-channel exchanges, which only involve diagonal couplings, all flavor problems would be avoided from the start if the couplings were family universal, and thus diagonal in any flavor basis. The only interesting s-channel multiplet for the FB asymmetry is the color octet. If heavy, it requires that the axial couplings to light and top quarks, g_A^q and g_A^t, have opposite signs, which precludes universality. Once more, light octets with $M \lesssim 450$ GeV present an advantage here: because they need g_A^q and g_A^t of the same sign, all the axial and vector couplings can be chosen, in principle, to be equal for the three families (Marques Tavares and Schmaltz, 2011). In this case, the couplings to Q_L do not produce FCNC, so an axigluon without vector couplings is not constrained by flavor physics. An obstacle to such a universal octet is that the usual dijet bounds require, for a sizable asymmetry, non-universal couplings with $|g_A^t| \gg |g_A^q|$ (see below). However, these bounds are relaxed when the octet has an enhanced width, which is anyway needed for agreement with other observables, see Sec. VI.A and Sec. VII.D.

The required large flavor-changing tu (or td) couplings of new particles exchanged in the t or u channels, on the other hand, do not allow for universality. Some degree

of alignment is then needed to comply with existing non-top FCNC limits. Specifically, the off-diagonal couplings mixing the first and second and the second and third families must be suppressed in the mass-eigenstate basis. While this particular pattern can be arranged in flavor models, it is unnatural and requires some tuning (Jung *et al.*, 2011; Shelton and Zurek, 2011). This situation is improved in specific cases. Most notably, the color triplet ω has, in any basis, antisymmetric coupling matrices in flavor space (Ligeti *et al.*, 2011). This property forbids tree-level FCNC. The most dangerous loop contributions are also absent for this field, and other flavor bounds can be avoided if the tc and cu couplings are small in the gauge basis (Dorsner *et al.*, 2010; Giudice *et al.*, 2011).

An interesting and natural way to avoid flavor problems and justify the unusual patterns of couplings needed in these models was proposed in Grinstein *et al.* (2011a). If the interactions of the new particles respect the SM quark flavor group $G_F = U(3)_{u_R} \times U(3)_{d_R} \times U(3)_{q_L}$, or its subgroup $H_F = U(2)_{u_R} \times U(2)_{d_R} \times U(2)_{q_L} \times U(1)_3$ (with the quarks in the first two families in doublets of the corresponding $SU(2)$ factors), then the only breaking of these global symmetries comes from the SM Yukawa couplings. (More generally, a small breaking of H_F from the new-physics sector can be allowed.) In this minimal-flavor-violation scenario, FCNC are under control, since they are absent before flavor breaking. Moreover, the large intergenerational couplings required in t, u-channel models are not only flavor-symmetric, but also a consequence of non-trivial flavor representations. Analogously, different signs of g_A^q and g_A^t for a color-octet are automatic if the field is also an octet under the flavor symmetry (t channel exchange is also important in this case). An additional virtue of these flavor-symmetric models is that limits from same-sign top pair production are avoided, as discussed in Sec. VII.B. All the relevant flavor representations of G_F and H_F have been classified and analyzed in detail in Grinstein *et al.* (2011b).

B. Same-sign top quark pair production

The production of same-sign top quark pairs would be a striking signal of physics beyond the SM. At hadron colliders, charge conservation implies that tt pairs can only be produced from initial up or charm quarks. Therefore the LHC, being a pp machine, is especially well suited to studying this signal.

The possible scalar and vector bosons that can produce tt pairs at the tree level are a subset of the multiplets in Table V: the neutral components of Z', $\mathcal{W}$, G, H, ϕ and Φ, exchanged in the t channel, and the charge $4/3$ components of Q', Y', Ω and Σ, exchanged in the s channel (Aguilar-Saavedra and Pérez-Victoria, 2011b). The negative results so far at the LHC (see for example Aad *et al.*, 2012d) put strong constraints on particular combi-

nations of the couplings of these fields, which we collect in Table. VII.

TABLE VII Limits at 95% confidence level, from Aad *et al.* (2012d), on the couplings of arbitrary heavy vector bosons and scalars that mediate the production of same-sign top-quark pairs. The fields and couplings are defined in Table V. For the fields Z' and G, we have defined $|g_{13}| = (|g_{13}^q|^2 + |g_{13}^u|^2)^{1/2}$.

Field	Limit
Z'_μ	$|g_{13}|/M < 0.57$ TeV^{-1}
W'_μ	$|g_{13}|/M < 0.57$ TeV^{-1}
G_μ	$|g_{13}|/M < 0.99$ TeV^{-1}
H_μ	$|g_{13}|/M < 0.99$ TeV^{-1}
Q'_μ	$|g_{11}g_{33}|/M^2 < 0.34$ TeV^{-2}
Y'_μ	$|g_{11}g_{33}|/M^2 < 0.63$ TeV^{-2}
ϕ	$|g_{13}^u g_{31}^u|/M^2 < 0.92$ TeV^{-2}
Φ	$|g_{13}^u g_{31}^u|/M^2 < 1.8$ TeV^{-2}
Ω	$|g_{11}g_{33}|/M^2 < 0.33$ TeV^{-2}
Σ	$|g_{11}g_{33}|/M^2 < 0.16$ TeV^{-2}

For arbitrary allowed couplings, these 10 multiplets can contribute to both $t\bar{t}$ and tt production. However, in general there is no direct relation between the observables in both processes, since they involve different combinations of couplings. In fact, a direct relation exists if and only if the following conditions are met: (i) the extra multiplet contributes to both $t\bar{t}$ and tt in the t channel only and (ii) the extra multiplet is self-conjugate under CP, which is only possible for real representations of the gauge group. The reason is that in this case the new-physics amplitudes in tt and $t\bar{t}$ processes are related by a CP transformation of one of the vertices. Therefore, the stringent tt bounds put in deep trouble the explanations of the FB anomaly with t exchanges of Z' (Berger *et al.*, 2011) and also of G, $\mathcal{W}$ and H (Aguilar-Saavedra and Pérez-Victoria, 2011b). In particular, they are sufficient to exclude the simplest Z' models, as shown in Fig. 33. A neat solution to save these models is to embed these fields in a non-trivial representation of a flavor symmetry, as discussed in the previous section. Then, the conservation of "top number" prevents $uu/cc \to tt$ processes (Jung *et al.*, 2011). Equivalently, the extended symmetry ensures a cancellation of the contribution to these processes of the different irreducible components that form these reducible representations of the gauge group. Note that, even for real flavor representations, the extended fields are no longer self-conjugate when the flavor indices are fixed.

Finally, although no strong conclusions can be derived for the complex fields ϕ and Φ, some regions of their parameter space relevant to the FB asymmetry in $t\bar{t}$ are
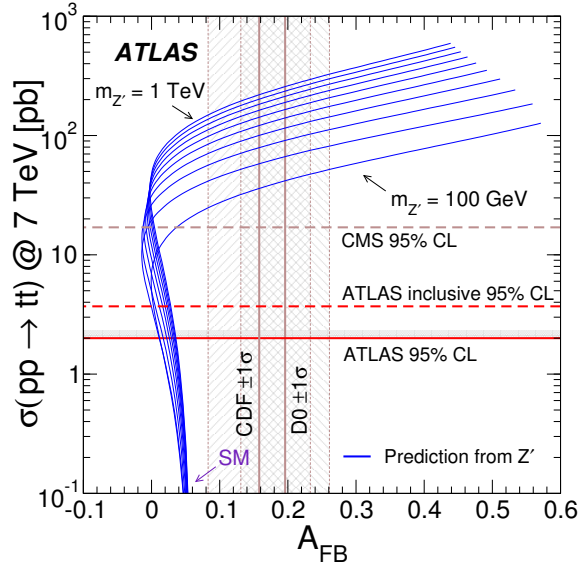
FIG. 33 Predictions for A_{FB} at the Tevatron and the $pp \rightarrow tt$ cross section at the LHC for a real Z' boson with right-handed couplings. Each curve corresponds to a different mass. The horizontal lines indicate the 95% C.L. upper limits on the cross section from measurements by the ATLAS and CMS Collaborations (Aad *et al.*, 2012a,d; Chatrchyan *et al.*, 2011b), while the vertical bands correspond to measurements of A_{FB}, with half the final luminosity, by the CDF and D0 Collaborations (Aaltonen *et al.*, 2011a; Abazov *et al.*, 2011a). From Aad *et al.* (2012d).

forbidden by the absence of tt signals (Aguilar-Saavedra and Pérez-Victoria, 2011b).

C. Top quark-jet resonances

In models with t- or u-channel exchange of a new boson R, the same flavor-violating vertices that are necessary for $t\bar{t}$ production will give rise to the production of R through the process $qg \rightarrow R\tilde{t}$, with $\tilde{t} = t$ or $\bar{t}$. We assume in the following that the field R is not self-conjugate, to avoid the same-sign limits we have just discussed. If $M_R > m_t$, this particle can subsequently decay into $\tilde{t}q$, giving rise to $t\bar{t}$ plus jet events with a top-jet (tj) or anti-top-jet ($\bar{t}$) resonance (Gresham *et al.*, 2011b). At the LHC, where the initial partons are predominantly quarks, rather than anti-quarks, the resonance will be most often found in $\bar{t}j$ when R is a t-channel mediator, and in tj when it is a u-channel mediator. This is dictated by the couplings of the corresponding particles, and can be understood as a consequence of baryon-number conservation.

These signals have been searched for by experiments at the Tevatron and the LHC. In particular, the ATLAS Collaboration has performed a search of W' and ω in the ℓ+jets channel with the 2011 dataset (Aad *et al.*,
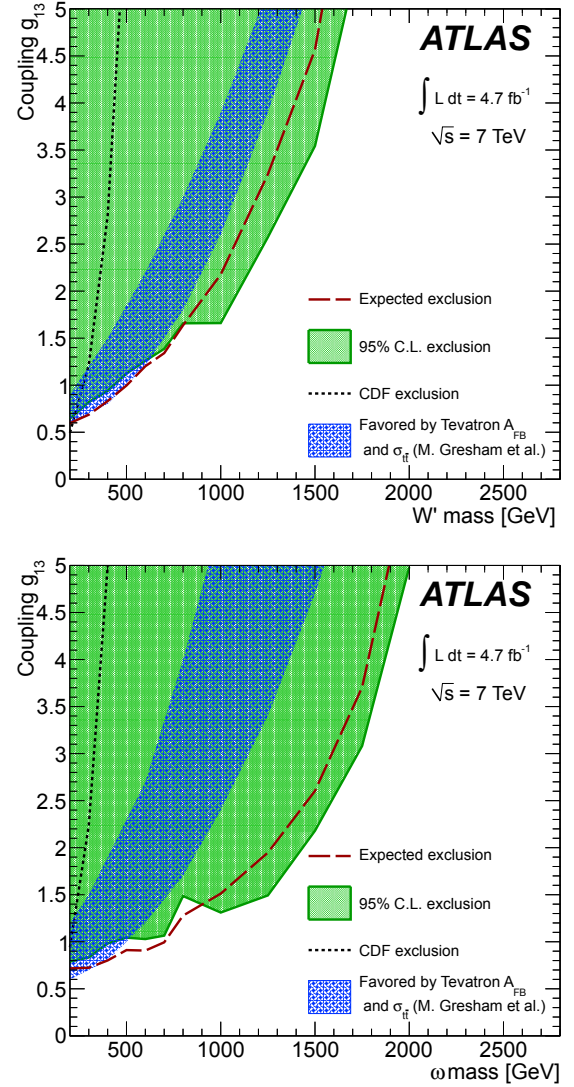

FIG. 34 Expected and observed 95% C.L. upper limits on W' (upper plot) and ω (lower plot) in terms of their mass and the coupling. The dark blue areas are the regions favored by the $t\bar{t}$ cross section and FB asymmetry measured by the CDF and D0 Collaborations with half the final luminosity (Aaltonen *et al.*, 2011a; Abazov *et al.*, 2011a). From Aad *et al.* (2012c)

2012c). The results are summarized in Fig. 34. Similar bounds apply to any particle exchanged in the t or u channels. We see that most of the regions of parameters that could account for the large values of the FB asymmetry measured in 2011 (Aaltonen *et al.*, 2011a; Abazov *et al.*, 2011a) are basically excluded, even without taking into account strong bounds from the $m_{t\bar{t}}$ tail, which can independently rule out a W' explanation. This analysis is, however, not sensitive to the regions with M_R below the top quark mass.

D. Dijet and dijet-pair resonances

All particles that mediate $t\bar{t}$ production in the s channel have $q\bar{q}$ couplings $g^q_{V,A}$, and will therefore contribute to dijet production. Searches for new phenomena in dijet final states have been performed by the UA1 and UA2 Collaborations (Albajar *et al.*, 1988; Alitti *et al.*, 1993) and also at the Tevatron (Aaltonen *et al.*, 2009; Abazov *et al.*, 2004) and the LHC (Aad *et al.*, 2012b, 2013a; Chatrchyan *et al.*, 2013d) experiments. These searches are complementary, as they cover different mass ranges. Most of them search for bumps in the dijet invariant mass distribution originating from new narrow resonances, but some analyze also angular distributions, which are useful to put bounds on broad or heavy particles, parametrized by contact interactions (Chatrchyan *et al.*, 2013c). A convenient mass-coupling interpretation of the narrow-resonance limits from the different experiments has been given, for singlets Z' and octets G, in Dobrescu and Yu (2013).

Dijet bounds require a relatively weak coupling of the new particles to the light quarks, with $|g^q_A| \lesssim 0.3$ for narrow octets lighter than 2 TeV. For a given ΔA_{FB}, these limits translate into lower bounds for the axial couplings to the top quark. For instance, the limit $|g^q_A| \lesssim 0.15$ for a narrow octet with $M_G = 1$ TeV (Aad *et al.*, 2012b; Dobrescu and Yu, 2013) implies that $|g^t_A| \gtrsim 6$ is required to reproduce the world average $A_{FB} = 0.13$. For lighter octets, smaller $|g^t_A|$ are allowed. At any rate, this direct interpretation of the dijet limits is actually rather conservative. Indeed, one should take into account that large values of the couplings g^t_A will increase the width of the resonance and lower its branching fraction into dijets. Open channels into other particles would further weaken these bounds.

Let us next discuss the constraints obtained from four-jet final states. The pair production of color-octets from initial-state gluons is determined by $SU(3)_C$ gauge symmetry and the unitarity of the theory (Gross *et al.*, 2013). Pair production is proportional to α_s and enhanced by color and spin factors, so it is large at the LHC for light octets. When each octet decays into two jets, an event with a pair of resonant dijets is produced. The ATLAS and CMS Collaborations have studied these signatures and have basically excluded narrow octets with masses between 100 and 740 GeV (Aad *et al.*, 2011, 2013e; Chatrchyan *et al.*, 2013e), assuming 100% branching ratio into dijets. This excludes the light-G explanation of the FB asymmetry,[10] unless the octets are broad or have a significant branching ratio into multijets via additional

intermediate resonances (Gross *et al.*, 2013).

E. Four-top quark production

Since, due to dijet bounds, large couplings g^t_A are required for an explanation of the asymmetry measurements, pair-produced octets will decay dominantly into two $t\bar{t}$ pairs, if kinematically allowed.[11] Such four-top quark final states have a very small background in the SM. They are difficult to reconstruct, but a simple search of this signal can be performed studying the production of same-sign dileptons (Aad *et al.*, 2013d) and trileptons. In this way, it is possible to exclude octets G with masses between 350 and 650 GeV (Aguilar-Saavedra and Santiago, 2012) unless, once again, the width is enhanced by the decay to non-SM particles.

VIII. OUTLOOK

The large FB asymmetries observed in a succession of measurements at the Tevatron have triggered a detailed exploration, from both the experimental and the theoretical sides, of observables related to $t\bar{t}$ production at hadron colliders. Independently of the nature of the discrepancies—which are significantly milder after the latest analyses—this effort has lead to a better understanding of the properties of the top quark and of the effects of possible new physics connected to the top-quark sector. The resulting expertise will certainly be valuable in future searches at the LHC.

The fact that the Tevatron measurements with the full dataset are closer to the SM predictions than previous measurements, with half the luminosity, strongly suggests that the former discrepancies were due to simple statistical fluctuations in the data. However, at this point the question is not completely settled. Even if the two collaborations give average results in the ℓ+jets channel that are statistically compatible, it is intriguing that the CDF and D0 measurements of both asymmetries, A_{FB} and A^ℓ_{FB}, are actually quite similar in the 4-jet sample. It is only the inclusion of the 3-jet sample, which yields lower values of these asymmetries, that lowers the D0 averages and make them more consistent with the SM predictions. This sample is not considered in the CDF analyses. While the differences between the results from 3-jet and 4-jet samples may be purely statistical, the possibility of some mismodeling effect, either in the 4-jet or the 3-jet samples, must be investigated in more detail. On the other hand, the recent measurement of A_{FB} in the dilepton channel by the D0 Collaboration yields a

---

[10] Octets G generating a sizable FB asymmetry and with mass smaller than 100 GeV are excluded by electroweak precision tests, due to their loop contribution to the $\bar{q}qZ$ vertex (Gresham *et al.*, 2013).

---

[11] Four top final states also originate from diagrams with a non-resonant octet. This is especially relevant below the $t\bar{t}$ threshold.

large asymmetry (even larger than the CDF value in the ℓ+jets channel but also with a larger uncertainty). A measurement by the CDF Collaboration in the dilepton channel with the full dataset might shed some light on this issue.

Because the Tevatron asymmetries cannot be directly measured at the LHC, the confirmation or rebuttal of a possible anomaly is quite difficult. One important step would be to measure the dependence of the asymmetries on the $t\bar{t}$ velocity $\beta_z^{t\bar{t}}$ to obtain the 'collider-independent' asymmetries A_u, A_d, discussed in Sec. II.C. This measurement is quite demanding from the experimental side, since it requires a 3-dimensional unfolding in $m_{t\bar{t}}$, β and $|\Delta y|$. But it offers a unique possibility of testing at the LHC the same quantities that are in the origin of the Tevatron A_{FB}.

The possibility of unexpectedly large higher-order QCD corrections that might significantly increase the value of the predicted FB asymmetry at the Tevatron seems now excluded by the recent NNLO calculation of A_{FB}. Indeed, the NNLO corrections turn out to be small, as expected, shifting the central value from $A_{FB} = 0.088$ to $A_{FB} = 0.095$. Moreover, the NNLO predictions, even when considered differentially, lie well inside the uncertainty bands of the previous NLO results, see Fig. 6. A proper combination of the CDF and D0 differential results is crucial to asess the agreement of theory with data, taking into account experimental bin-to-bin correlations and theory uncertainties.

Finally, the explanation of the asymmetry excess with new physics faces two serious problems. The first one is that almost all successful models are rather *ad hoc,* since they are not clearly motivated by other compelling theoretical or experimental reasons, and usually non-generic choices of parameters are required to avoid the most obvious constraints. The second problem is that, even with such parameters, most new physics models still predict a series of observable signals that have not been found. In particular, the measurements of either A_C, $t\bar{t}$ differential distributions or top polarization disfavor most of the models. Searches for tj resonances, on the other hand, exclude large regions of the parameter space of models with t-channel exchanges. Among the simple explanations in terms of just one multiplet, the model that can better account for all the $t\bar{t}$ data, including the Tevatron and LHC asymmetries, is, arguably, an s-channel color-octet vector boson. It should be noted, nevertheless, that this model requires some non-trivial ingredients to comply with all the measurements. Another model that survives the different tests is a light scalar isodoublet exchanged in the t channel.

The next LHC run with $13-14$ TeV and high luminosity will bring the possibility of new, independent measurements in addition to the current ones. One example is the charge asymmetry in $t\bar{t}\gamma$ production, which has the potential of showing deviations with respect to the SM

predictions even for A_C in perfect agreement with the SM. Otherwise, it will further constrain the parameter space of the different models, rendering them less viable. Another example is the asymmetry in $t\bar{t}W^\pm$. Whatever the final outcome is, it is likely that some of the questions posed by the Tevatron asymmetries will be answered in the next years. And of course, some unexpected surprises might be waiting along the road.

REFERENCES

Aad, G., *et al.* (ATLAS Collaboration) (2011), Eur.Phys.J. **C71**, 1828, arXiv:1110.2693 [hep-ex].
Aad, G., *et al.* (ATLAS Collaboration) (2012a), Phys.Rev. **D85**, 032004, arXiv:1201.1091 [hep-ex].
Aad, G., *et al.* (ATLAS Collaboration) (2012b), Phys.Lett. **B708**, 37, arXiv:1108.6311 [hep-ex].
Aad, G., *et al.* (ATLAS Collaboration) (2012c), Phys.Rev. **D86**, 091103, arXiv:1209.6593 [hep-ex].
Aad, G., *et al.* (ATLAS Collaboration) (2012d), JHEP **1204**, 069, arXiv:1202.5520 [hep-ex].
Aad, G., *et al.* (ATLAS Collaboration) (2013a), JHEP **1301**, 029, arXiv:1210.1718 [hep-ex].
Aad, G., *et al.* (ATLAS Collaboration) (2013b), Phys.Rev.Lett. **111**, 232002, arXiv:1307.6511 [hep-ex].
Aad, G., *et al.* (ATLAS Collaboration) (2013c), ATLAS-CONF-2013-101.
Aad, G., *et al.* (ATLAS Collaboration) (2013d), ATLAS-CONF-2013-051.
Aad, G., *et al.* (ATLAS Collaboration) (2013e), Eur.Phys.J. **C73**, 2263, arXiv:1210.4826 [hep-ex].
Aad, G., *et al.* (ATLAS and CMS Collaborations) (2014a), ATLAS-CONF-2014-012, CMS-PAS-TOP-14-006.
Aad, G., *et al.* (ATLAS Collaboration) (2014b), JHEP **1402**, 107, arXiv:1311.6724 [hep-ex].
Aad, G., *et al.* (ATLAS Collaboration) (2014c), ATLAS-CONF-2014-009.
Aad, G., *et al.* (ATLAS Collaboration) (2015), arXiv:1501.07383 [hep-ex].
Aaltonen, T. A., *et al.* (CDF Collaboration) (2009), Phys.Rev. **D79**, 112002, arXiv:0812.4036 [hep-ex].
Aaltonen, T. A., *et al.* (CDF Collaboration) (2011a), Phys.Rev. **D83**, 112003, arXiv:1101.0034 [hep-ex].
Aaltonen, T. A., *et al.* (CDF Collaboration) (2011b), http://www-cdf.fnal.gov/physics/new/top/2011/DilAfb/cdfpubnote.pdf.
Aaltonen, T. A., *et al.* (CDF Collaboration) (2013a), Phys.Rev.Lett. **111** (18), 182002, arXiv:1306.2357 [hep-ex].

Aaltonen, T. A., *et al.* (CDF Collaboration) (2013b), Phys.Rev. **D88**, 072003, arXiv:1308.1120 [hep-ex].

Aaltonen, T. A., *et al.* (CDF Collaboration) (2013c), Phys.Rev. **D87**, 092002, arXiv:1211.1003 [hep-ex].

Aaltonen, T. A., *et al.* (CDF Collaboration, D0 Collaboration) (2014a), Phys.Rev. **D89**, 072001, arXiv:1309.7570 [hep-ex].

Aaltonen, T. A., *et al.* (CDF Collaboration) (2014b), Phys.Rev.Lett. **113**, 042001, arXiv:1404.3698 [hep-ex].

Aaltonen, T. A. o. (CDF Collaboration) (2008), Phys.Rev.Lett. **101**, 202001, arXiv:0806.2472 [hep-ex].

Abachi, S., *et al.* (D0 Collaboration) (1995), Phys.Rev.Lett. **74**, 2632, arXiv:hep-ex/9503003 [hep-ex].

Abazov, V. M., *et al.* (D0 Collaboration) (2004), Phys.Rev. **D69**, 111101, arXiv:hep-ex/0308033 [hep-ex].

Abazov, V. M., *et al.* (D0 Collaboration) (2008), Phys.Rev.Lett. **100**, 142002, arXiv:0712.0851 [hep-ex].

Abazov, V. M., *et al.* (D0 Collaboration) (2011a), Phys.Rev. **D84**, 112005, arXiv:1107.4995 [hep-ex].

Abazov, V. M., *et al.* (D0 Collaboration) (2011b), Phys.Rev.Lett. **107**, 082004, arXiv:1105.0320 [hep-ex].

Abazov, V. M., *et al.* (D0 Collaboration) (2012), Phys.Rev.Lett. **108**, 032004, arXiv:1110.4194 [hep-ex].

Abazov, V. M., *et al.* (D0 Collaboration) (2013a), Phys.Rev. **D87**, 011103, arXiv:1207.0364 [hep-ex].

Abazov, V. M., *et al.* (D0 Collaboration) (2013b), Phys.Rev. **D88**, 112002, arXiv:1308.6690 [hep-ex].

Abazov, V. M., *et al.* (D0 Collaboration) (2014a), http://www-d0.fnal.gov/Run2Physics/WWW/results/ prelim/TOP/T104/T104.pdf, D0 note 6445-CONF.

Abazov, V. M., *et al.* (D0 Collaboration) (2014b), Phys.Rev. **D90**, 072001, arXiv:1403.1294 [hep-ex].

Abazov, V. M., *et al.* (D0 Collaboration) (2014c), Phys.Rev. **D90** (7), 072011, arXiv:1405.0421 [hep-ex].

Abbott, B., *et al.* (D0 Collaboration) (1998), Phys.Rev.Lett. **80**, 2063, arXiv:hep-ex/9706014 [hep-ex].

Abe, F., *et al.* (CDF Collaboration) (1995), Phys.Rev.Lett. **74**, 2626, arXiv:hep-ex/9503002 [hep-ex].

Abe, F., *et al.* (CDF Collaboration) (2010), CDF note 10211.

Abe, F., *et al.* (CDF Collaboration) (2011), CDF note 10719.

Aguilar-Saavedra, J. A. (2011), Nucl.Phys. **B843**, 638, arXiv:1008.3562 [hep-ph].

Aguilar-Saavedra, J. A. (2014a), JHEP **1408**, 172, arXiv:1405.5826 [hep-ph].

Aguilar-Saavedra, J. A. (2014b), Phys.Lett. **B736**, 132, arXiv:1405.1412 [hep-ph].

Aguilar-Saavedra, J. A., E. Álvarez, A. Juste, and F. Rubbo (2014), JHEP **1404**, 188, arXiv:1402.3598 [hep-ph].

Aguilar-Saavedra, J. A., W. Bernreuther, and Z.-G. Si (2012a), Phys.Rev. **D86**, 115020, arXiv:1209.6352 [hep-ph].

Aguilar-Saavedra, J. A., and R. V. Herrero-Hahn (2013), Phys.Lett. **B718**, 983, arXiv:1208.6006 [hep-ph].

Aguilar-Saavedra, J. A., and A. Juste (2012), Phys.Rev.Lett. **109**, 211804, arXiv:1205.1898 [hep-ph].

Aguilar-Saavedra, J. A., A. Juste, and F. Rubbo (2012b), Phys.Lett. **B707**, 92, arXiv:1109.3710 [hep-ph].

Aguilar-Saavedra, J. A., and M. Pérez-Victoria (2011a), Phys.Rev. **D84**, 115013, arXiv:1105.4606 [hep-ph].

Aguilar-Saavedra, J. A., and M. Pérez-Victoria (2011b), Phys.Lett. **B701**, 93, arXiv:1104.1385 [hep-ph].

Aguilar-Saavedra, J. A., and M. Pérez-Victoria (2011c), JHEP **1105**, 034, arXiv:1103.2765 [hep-ph].

Aguilar-Saavedra, J. A., and M. Pérez-Victoria (2011d), Phys.Lett. **B705**, 228, arXiv:1107.2120 [hep-ph].

Aguilar-Saavedra, J. A., and M. Pérez-Victoria (2011e), JHEP **1109**, 097, arXiv:1107.0841 [hep-ph].

Aguilar-Saavedra, J. A., and J. Santiago (2012), Phys.Rev. **D85**, 034021, arXiv:1112.3778 [hep-ph].

Ahrens, V., A. Ferroglia, M. Neubert, B. D. Pecjak, and L. L. Yang (2011), Phys.Rev. **D84**, 074004, arXiv:1106.6051 [hep-ph].

Albajar, C., *et al.* (UA1 Collaboration) (1988), Phys.Lett. **B209**, 127.

Aliev, M., H. Lacker, U. Langenfeld, S. Moch, P. Uwer, *et al.* (2011), Comput.Phys.Commun. **182**, 1034, arXiv:1007.1327 [hep-ph].

Alitti, J., *et al.* (UA2 Collaboration) (1993), Nucl.Phys. **B400**, 3.

Almeida, L. G., G. F. Sterman, and W. Vogelsang (2008), Phys.Rev. **D78**, 014008, arXiv:0805.1885 [hep-ph].

Álvarez, E., and E. C. Leskow (2012), Phys.Rev. **D86**, 114034, arXiv:1209.4354 [hep-ph].

Arhrib, A., R. Benbrik, and C.-H. Chen (2010), Phys.Rev. **D82**, 034034, arXiv:0911.4875 [hep-ph].

Atwood, D., A. Kagan, and T. Rizzo (1995), Phys.Rev. **D52**, 6264, arXiv:hep-ph/9407408 [hep-ph].

Bai, Y., J. L. Hewett, J. Kaplan, and T. G. Rizzo (2011), JHEP **1103**, 003, arXiv:1101.5203 [hep-ph].

Barcelo, R., A. Carmona, M. Chala, M. Masip, and J. Santiago (2012a), Nucl.Phys. **B857**, 172, arXiv:1110.5914 [hep-ph].

Barcelo, R., A. Carmona, M. Masip, and J. Santiago (2012b), Phys.Lett. **B707**, 88, arXiv:1106.4054 [hep-ph].

Baumgart, M., and B. Tweedie (2011), JHEP **1109**, 049, arXiv:1104.2043 [hep-ph].

Baumgart, M., and B. Tweedie (2013), JHEP **1308**, 072, arXiv:1303.1200 [hep-ph].

Berger, E. L., Q.-H. Cao, C.-R. Chen, C. S. Li, and H. Zhang (2011), Phys.Rev.Lett. **106**, 201801, arXiv:1101.5625 [hep-ph].

Bernreuther, W., A. Brandenburg, Z.-G. Si, and P. Uwer (2001), Phys.Rev.Lett. **87**, 242002, arXiv:hep-ph/0107086 [hep-ph].

Bernreuther, W., A. Brandenburg, Z.-G. Si, and P. Uwer (2004), Nucl.Phys. **B690**, 81, arXiv:hep-ph/0403035 [hep-ph].

Bernreuther, W., and Z.-G. Si (2010), Nucl.Phys. **B837**, 90, arXiv:1003.3926 [hep-ph].

Bernreuther, W., and Z.-G. Si (2012), Phys.Rev. **D86**, 034026, arXiv:1205.6580 [hep-ph].

Bernreuther, W., and Z.-G. Si (2013), Phys.Lett. **B725** (1-3), 115, arXiv:1305.2066 [hep-ph].

Blum, K., C. Delaunay, O. Gedalia, Y. Hochberg, S. J. Lee, *et al.* (2011a), Phys.Lett. **B702**, 364, arXiv:1102.3133 [hep-ph].

Blum, K., Y. Grossman, Y. Nir, and G. Perez (2009), Phys.Rev.Lett. **102**, 211802, arXiv:0903.2118 [hep-ph].

Blum, K., Y. Hochberg, and Y. Nir (2011b), JHEP **1110**, 124, arXiv:1107.4350 [hep-ph].

Brodsky, S. J., and X.-G. Wu (2012), Phys.Rev. **D85**, 114040, arXiv:1205.1232 [hep-ph].

Cacciari, M., G. P. Salam, and G. Soyez (2008), JHEP **0804**, 063, arXiv:0802.1189 [hep-ph].

Campbell, J. M., and R. K. Ellis (1999), Phys.Rev. **D60**, 113006, arXiv:hep-ph/9905386 [hep-ph].

Carmona, A., M. Chala, A. Falkowski, S. Khatibi, M. M. Najafabadi, *et al.* (2014), JHEP **1407**, 005, arXiv:1401.2443 [hep-ph].

Chatrchyan, S., *et al.* (CMS Collaboration) (2011a), JHEP **1107**, 049, arXiv:1105.5661 [hep-ex].

Chatrchyan, S., *et al.* (CMS Collaboration) (2011b), JHEP **1108**, 005, arXiv:1106.2142 [hep-ex].

Chatrchyan, S., *et al.* (CMS Collaboration) (2012), Phys.Lett. **B717**, 129, arXiv:1207.0065 [hep-ex].

Chatrchyan, S., *et al.* (CMS Collaboration) (2013a), Eur.Phys.J. **C73**, 2339, arXiv:1211.2220 [hep-ex].

Chatrchyan, S., *et al.* (CMS Collaboration) (2013b), CMS-PAS-TOP-12-033.

Chatrchyan, S., *et al.* (CMS Collaboration) (2013c), Phys.Rev. **D87** (5), 052017, arXiv:1301.5023 [hep-ex].

Chatrchyan, S., *et al.* (CMS Collaboration) (2013d), Phys.Rev. **D87** (11), 114015, arXiv:1302.4794 [hep-ex].

Chatrchyan, S., *et al.* (CMS Collaboration) (2013e), Phys.Rev.Lett. **110**, 141802, arXiv:1302.0531 [hep-ex].

Chatrchyan, S., *et al.* (CMS Collaboration) (2014a), Nature Phys. **10**, 557, arXiv:1401.6527 [hep-ex].

Chatrchyan, S., *et al.* (CMS Collaboration) (2014b), Phys.Rev.Lett. **112**, 182001, arXiv:1311.3924 [hep-ex].

Chatrchyan, S., *et al.* (CMS Collaboration) (2014c), JHEP **1404**, 191, arXiv:1402.3803 [hep-ex].

Cheung, K., W.-Y. Keung, and T.-C. Yuan (2009), Phys.Lett. **B682**, 287, arXiv:0908.2589 [hep-ph].

Corcella, G., I. Knowles, G. Marchesini, S. Moretti, K. Odagiri, *et al.* (2001), JHEP **0101**, 010, arXiv:hep-ph/0011363 [hep-ph].

Czakon, M., P. Fiedler, and A. Mitov (2014), arXiv:1411.3007 [hep-ph].

Degrande, C., J.-M. Gerard, C. Grojean, F. Maltoni, and G. Servant (2011), JHEP **1103**, 125, arXiv:1010.6304 [hep-ph].

Delaunay, C., O. Gedalia, Y. Hochberg, G. Perez, and Y. Soreq (2011), JHEP **1108**, 031, arXiv:1103.2297 [hep-ph].

Djouadi, A., G. Moreau, F. Richard, and R. K. Singh (2010), Phys.Rev. **D82**, 071702, arXiv:0906.0604 [hep-ph].

Dobrescu, B. A., and F. Yu (2013), Phys.Rev. **D88** (3), 035021, arXiv:1306.2629 [hep-ph].

Dorsner, I., S. Fajfer, J. F. Kamenik, and N. Kosnik (2010), Phys.Rev. **D81**, 055009, arXiv:0912.0972 [hep-ph].

Drobnak, J., A. L. Kagan, J. F. Kamenik, G. Perez, and J. Zupan (2012a), Phys.Rev. **D86**, 094040, arXiv:1209.4872 [hep-ph].

Drobnak, J., J. F. Kamenik, and J. Zupan (2012b), Phys.Rev. **D86**, 054022, arXiv:1205.4721 [hep-ph].

Duraisamy, M., A. Rashed, and A. Datta (2011), Phys.Rev. **D84**, 054018, arXiv:1106.5982 [hep-ph].

Fajfer, S., J. F. Kamenik, and B. Melic (2012), JHEP **1208**, 114, arXiv:1205.0264 [hep-ph].

Falkowski, A., M. L. Mangano, A. Martin, G. Perez, and J. Winter (2013a), Phys.Rev. **D87**, 034039, arXiv:1212.4003 [hep-ph].

Falkowski, A., G. Perez, and M. Schmaltz (2013b), Phys.Rev. **D87**, 034041, arXiv:1110.3796 [hep-ph].

Ferrario, P., and G. Rodrigo (2008), Phys.Rev. **D78**, 094018, arXiv:0809.3354 [hep-ph].

Frampton, P. H., and S. L. Glashow (1987), Phys.Lett. **B190**, 157.

Frixione, S., P. Nason, and G. Ridolfi (2007), JHEP **0709**, 126, arXiv:0707.3088 [hep-ph].

Frixione, S., and B. R. Webber (2002), JHEP **0206**, 029, arXiv:hep-ph/0204244 [hep-ph].

Gabrielli, E., and M. Raidal (2011), Phys.Rev. **D84**, 054017, arXiv:1106.4553 [hep-ph].

Gabrielli, E., M. Raidal, and A. Racioppi (2012), Phys.Rev. **D85**, 074021, arXiv:1112.5885 [hep-ph].

Giudice, G. F., B. Gripaios, and R. Sundrum (2011), JHEP **1108**, 055, arXiv:1105.3161 [hep-ph].

Gresham, M. I., I.-W. Kim, and K. M. Zurek (2011a), Phys.Rev. **D83**, 114027, arXiv:1103.3501 [hep-ph].

Gresham, M. I., I.-W. Kim, and K. M. Zurek (2011b), Phys.Rev. **D84**, 034025, arXiv:1102.0018 [hep-ph].

Gresham, M. I., J. Shelton, and K. M. Zurek (2013), JHEP **1303**, 008, arXiv:1212.1718 [hep-ph].

Grinstein, B., A. L. Kagan, M. Trott, and J. Zupan (2011a), Phys.Rev.Lett. **107**, 012002, arXiv:1102.3374 [hep-ph].

Grinstein, B., A. L. Kagan, J. Zupan, and M. Trott (2011b), JHEP **1110**, 072, arXiv:1108.4027 [hep-ph].

Grinstein, B., C. W. Murphy, D. Pirtskhalava, and P. Uttayarat (2012), JHEP **1208**, 073, arXiv:1203.2183 [hep-ph].

Gross, C., G. Marques Tavares, M. Schmaltz, and C. Spethmann (2013), Phys.Rev. **D87**, 014004, arXiv:1209.6375 [hep-ph].

Haberl, P., O. Nachtmann, and A. Wilch (1996), Phys.Rev. **D53**, 4875, arXiv:hep-ph/9505409 [hep-ph].

Hewett, J. L., J. Shelton, M. Spannowsky, T. M. Tait, and M. Takeuchi (2011), Phys.Rev. **D84**, 054005, arXiv:1103.4618 [hep-ph].

Hollik, W., and D. Pagani (2011), Phys.Rev. **D84**, 093003, arXiv:1107.2606 [hep-ph].

Hong, Z., R. Edgar, S. Henry, D. Toback, J. S. Wilson, *et al.* (2014), arXiv:1403.7565 [hep-ph].

Isidori, G., and J. F. Kamenik (2011), Phys.Lett. **B700**, 145, arXiv:1103.0016 [hep-ph].

Jacob, M., and G. C. Wick (1959), Annals Phys. **7**, 404.

Jezabek, M. (1994), Nucl.Phys.Proc.Suppl. **37B**, 197, arXiv:hep-ph/9406411 [hep-ph].

Jung, S., H. Murayama, A. Pierce, and J. D. Wells (2010), Phys.Rev. **D81**, 015004, arXiv:0907.4112 [hep-ph].

Jung, S., A. Pierce, and J. D. Wells (2011), Phys.Rev. **D83**, 114039, arXiv:1103.4835 [hep-ph].

Kagan, A. L., J. F. Kamenik, G. Perez, and S. Stone (2011), Phys.Rev.Lett. **107**, 082003, arXiv:1103.3747 [hep-ph].

Kidonakis, N. (2011), Phys.Rev. **D84**, 011504, arXiv:1105.5167 [hep-ph].

Kidonakis, N. (2013), arXiv:1304.7775 [hep-ph].

Kidonakis, N. (2015), arXiv:1501.01581 [hep-ph].

Ko, P., Y. Omura, and C. Yu (2013), Eur.Phys.J. **C73**, 2269, arXiv:1205.0407 [hep-ph].

Krohn, D., T. Liu, J. Shelton, and L.-T. Wang (2011), Phys.Rev. **D84**, 074034, arXiv:1105.3743 [hep-ph].

Kuhn, J. H., and G. Rodrigo (1998), Phys.Rev.Lett. **81**, 49, arXiv:hep-ph/9802268 [hep-ph].

Kuhn, J. H., and G. Rodrigo (2012), JHEP **1201**, 063, arXiv:1109.6830 [hep-ph].

Ligeti, Z., G. Marques Tavares, and M. Schmaltz (2011), JHEP **1106**, 109, arXiv:1103.2757 [hep-ph].

Lyons, L., D. Gibaut, and P. Clifford (1988), Nucl.Instrum.Meth. **A270**, 110.

Maltoni, F., M. Mangano, I. Tsinikos, and M. Zaro (2014), Phys.Lett. **B736**, 252, arXiv:1406.3262 [hep-ph].

Mangano, M. L., M. Moretti, F. Piccinini, R. Pittau, and A. D. Polosa (2003), JHEP **0307**, 001, arXiv:hep-ph/0206293 [hep-ph].

Manohar, A. V., and M. Trott (2012), Phys.Lett. **B711**, 313, arXiv:1201.3926 [hep-ph].

Marques Tavares, G., and M. Schmaltz (2011), Phys.Rev. **D84**, 054008, arXiv:1107.0978 [hep-ph].

Nelson, A. E., T. Okui, and T. S. Roy (2011), Phys.Rev. **D84**, 094007, arXiv:1104.2030 [hep-ph].

Schael, S., *et al.* (ALEPH Collaboration, DELPHI Collaboration, L3 Collaboration, OPAL Collaboration, SLD Collaboration, LEP Electroweak Working Group, SLD Electroweak Group, SLD Heavy Flavour Group) (2006), Phys.Rept. **427**, 257, arXiv:hep-ex/0509008 [hep-ex].

Shelton, J., and K. M. Zurek (2011), Phys.Rev. **D83**, 091701, arXiv:1101.5392 [hep-ph].

Shu, J., T. M. Tait, and K. Wang (2010), Phys.Rev. **D81**, 034012, arXiv:0911.3237 [hep-ph].

Sjostrand, T., S. Mrenna, and P. Z. Skands (2006), JHEP **0605**, 026, arXiv:hep-ph/0603175 [hep-ph].

Skands, P., B. Webber, and J. Winter (2012), JHEP **1207**, 151, arXiv:1205.1466 [hep-ph].

Valassi, A. (2003), Nucl.Instrum.Meth. **A500**, 391.

Zhu, G. (2011), Phys.Lett. **B703**, 142, arXiv:1104.3227 [hep-ph].